AN ABSTRACT OF THE THESIS OF

DINGHAN LOU for the Master of Science Degree in Physical Science (Chemistry) presented on December 05, 1995

Title : Polarographic Reduction of Aqueous-Isopropyl Alcohol Heteropolytungstate Mixtures

Abstract approved : Dr Arthur M Landis

The reduction behavior and properties of the 11-tungsto (aquocobalto(II)) silicate anion, $K_6[SiO_4W_{11}CoO_6H_2]\cdot 15\ H_2O$, and Keggin-structure 12-tungstophosphoric (V) anion, $H_3[PW_{12}O_{40}]\cdot 29H_2O$, upon addition of isopropyl alcohol (IPA), acetone and acetonitrile (ACN) in pH 4.99 buffer solution have been studied using an IBM Instruments EC/225 voltammetric analyzer with a dropping mercury electrode. Three-reduction waves for each heteropoly anion were observed. The half-wave potentials did not change as the above organic substrates were added. However, the peak height did change upon adding organic substrate. The change in peak height of the first-wave was studied in detail. At low concentration, the first-wave height initially remains essentially constant. Above threshold values, the first-peak height decreases rapidly as the concentration of IPA, acetone, and ACN increases. Threshold values increase on going from IPA to acetone to ACN for the heteropoly anions studied. Three possibilities for relationships between the decrease of the first-wave current and the increase of substrate concentration are described. The association of the heteropoly

(HPC) with organic substrate to form an association complex is considered to be the most likely possibility. The equilibrium constant (K_c) for the formation of association complexes decreases on going from IPA to acetone to ACN. The IPA, acetone or ACN molecules that form association complexes were deduced to associate at specific sites on the HPC.

Polarographic Reduction of Aqueous-Isopropyl Alcohol Heteropolytungstate Mixtures

A Thesis

Presented to

the Division of Physical Science

EMPORIA STATE UNIVERSITY

In Partial Fulfillment

of the Requirements for the Degree

Master of Science

by

Dinghan Lou

December 1995

DeWayne Backhus PhD

Approved for the Major Division

Approved for the Graduate Council

ACKNOWLEDGMENTS

I would like to express my deepest gratitude to my research advisor, Dr. Arthur M. Landis, for his idea, direction, and understanding. Without his guidance, I would have never been able to complete this thesis. I would also like to express my sincere thanks to my committee members, Dr. Charles Greenlief and Dr. Richard Schrock, for their assistance during the creation of this thesis. I would also like to express my appreciation to all of the members of the Chemistry Department for their advice during my course work and research while obtaining this degree.

I would like to thank my friends who encouraged me to finish this degree. I am greatly indebted to my parents and my sisters who have provided me with encouragement and understanding. Especially, I would like to thank my parents-in-law for their dedication to my family. I am also very deeply thankful to my wife, Yanming Chen, and son, Han Chen, who have given me their endless love and their moral and spiritual support.

TABLE OF CONTENTS

LIST OF FIGURES

LIST OF TABLES

CHAPTER I. INTRODUCTION

I-1. Definition of Isopoly and Heteropoly Acids and Anions

The compositions of numerous metal-containing oxo acids and oxo anions are suggestive of being formed by dehydration and condensation of one type of oxoanion {eq.[a]} or two or more different types of oxoanions {eq. [b]}. Each of these poly acids and poly anions consists of either one kind of oxoanion which is called an isopoly or two or more different oxoanions which is called a heteropoly [1 and 2].

$7\ MoO_4^{2-} + 8\ H^+ \text{----->} [Mo_7O_{24}]^{6-} + 4\ H_2O$ [a]

$12\ WO_4^{2-} + HPO_4^{2-} + 23\ H^+ \text{---->} [PW_{12}O_{40}]^{3-} + 12\ H_2O$ [b]

Isopoly species are characteristic of both certain nonmetals (e.g., S, P, As) and certain d-transition metals (especially V, Mo, W). Heteropoly species are characteristic of certain d-transition metals (especially V, Mo, W) in combination with one or more of over 70 different elements [3] that are called heteroatoms [1].

The iso- and heteropoly acids and anions which contain early d-transition metals are most frequently derived from molybdenum and tungsten or mixtures of these elements; and less frequently vanadium, niobium, or tantalum in their highest (d^o, d^1) oxidation states [4]. The isopoly acids and their related anions, for the case of molybdenum, contain only molybdenum along with oxygen and hydrogen. Heteropoly acids and anions contain one or two atoms of another element in addition to molybdenum, oxygen, and hydrogen [5].

The first heteropolytungstates were discovered and characterized by Marignac in 1862. Since that time, the isopoly anions and heteropoly anions were intensively investigated and hundreds of such compounds are described in the Gmelin volumes published in the 1930's [3]. Over past few years considerable interest in heteropoly (HPC) and isopoly anions or acids has been shown not only in the structure and characterization of such substances but also in those aspects of their chemistry that have given them important roles in industrial applications such as catalysts for hydrocracking, hydrogenation, isomerization, and polymerization in a variety of commercially important chemical processes [6 and 7].

The iso- and heteropoly acids and anions differ in many ways from the more classical complexes. These poly species constitute a large category of coordination-type salts and free acids. Each member contains a complex and has a high molecular weight. The general formulas of these complex anions can be represented as:

$[M_mO_y]^{p-}$ $(y \geq m)$ for isopolyanions, and

$[X_xM_mO_y]^{q-}$ $(x \leq m < y)$ for heteroployanions.

Here M is the so-called addenda atom or polyatom and usually, as stated above, is molybdenum or tungsten; and to a lesser extent, vanadium, niobium, or tantalum; or a mixture of these elements. The X is a heteroatom or a central atom that can be from all group of the Periodic Table with the exception of the rare gases [3]. Of these heteroatoms or central atoms, 69 are listed in Table I [4]. In addition some of these species also contain hydrogen.

The requirements for the central atom or polyatom of the anion appear to be much less stringent than those for the peripheral metal atom [4]. The suitability of elements as peripheral metal atoms appears to depend on the ionic radius and charge as well as the ability to form a peripheral metal-oxygen d_π-p_π bonds. While isopoly and heteropoly anions have been prepared with central atoms or heteroatoms from over 70 elements, a much smaller number of peripheral metals are known [8]. Also, there exist mixed polyoxometalates, as heteropoly anions are now known, with the general formula $[M_mM'_nO_y]^{p-}$ and $[X_xM_mM'_nO_y]^{q-}$, where M' is called a secondary addenda or polyatom and can be one of the above metals or other metals that are in high oxidation states(d^o, d^1). Here again the O represents oxygen. This polyoxometalate field is enormous because of the large range of the various possible m/x ratios and the range of different atoms M, M' and X which can participate in the formation of these anions [3 and 7].

One of the structures which can exist is called the Keggin structure. The Keggin structure has the formula, $PW_{12}O_{40}^{3-}$, and is shown in Figure 1. Four different kinds of oxygen atoms are present. Four of these atoms are called internal oxygen atoms (O_a) and are connected to the central atom (P) and to the peripheral metal atoms (W); twelve are edge-sharing oxygen atoms (O_b) and are connected to sets of three peripheral metal atoms (W's); twelve are corner-sharing oxygen atoms (O_c) and bridge the W_3O_{13} units; and twelve are terminal oxygen atoms (O_d) and are bonded only to a peripheral tungsten atom (W). These latter oxygen atoms protrude from the anion [2].

I-2. Background of Polyoxometalates

I-2-1. General Historical Perspective of Polyoxometalates

In 1826, Berzelius first reported the formation of yellow products from the reaction of molybdate with phosphate or with arsenate (now know as 12-molybdophosphate, $(NH_4)_3PMo_{12}O_{40} \bullet$ aq or 12-molybdoarsenate, $(NH_4)_3AsMo_{12}O_{40} \bullet$ aq). He reported the subsequent ready formation (which has important consequences) of the blue (mixed-valence) derivatives [9]. Svankerg and Struve in 1848 introduced this compound into analytical chemistry [4]. In 1854, Struve described the heteropoly molybdates of Cr^{3+} and Fe^{3+}, but he postulated these as double salts, not condensed structures [6]. In 1862, Marignac prepared 12-tungstosilic acid and recognized such compounds as a distinct class of compounds rather than the class of double salts. He also precisely determined the analytical compositions of such heteropoly acids. Thereafter, the field developed rapidly [4 and 6].

In 1908, Miolati made the first systematic attempt to understand the nature of heteropoly compounds by suggesting a structure for these compounds based upon ionic theory and Werner's coordination theory. Rosenheim and his co-worker further developed and applied this suggestion. This model is now called the Miolati-Rosenheim(MR) theory. According to MR theory, heteropoly acids are based upon six-coordinate heteroatoms with MO_4^{2-} or $M_2O_7^{2-}$ anions as ligands or bridging groups coordinated to the central atom. The formulas derived from this theory suggest a different acidity than expected from the modern theory. For instance, the formula $H_8[Si(W_2O_7)_6]$ is given by the MR theory, however the formula $H_4[SiW_{12}O_{40}]$ is the modern formula for this compound. It will be noticed that in the above formulae the ratios of silicon (Si) to tungsten (W) are the same, but the number of oxygen (O) atoms and the number of acidic hydrogen (H) atoms are different. However, until recently, the MR formulae were still employed to interpret some of heteropoly structures [4].

In 1929, Pauling, with his instinct for an important class of compounds, proposed a structure for the 12:1 complexes based upon an arrangement of twelve MoO_6 or WO_6 octahedra surrounding a central XO_4 tetrahedron. According to this proposal, the molybdenum (M^{6+}) and tungsten (W^{6+}) were octahedrally coordinated by oxygen, using corner-sharing (but not edge- and face-sharing) of the twelve MO_6 octahedra. These octahedra surrounded the central XO_4 tetrahedron [4 and 10]. Based on this structure the formulas required 58 oxygen atoms. For the silicon compound he proposed the formula $H_4[SiO_4W_{12}O_{18}(OH)_{36}]$ in order to conform to the observed acidities. In 1933, Keggin solved the structure of the heteropoly acid $[H_3PW_{12}O_{40}]\bullet 6H_2O$ by analysis of 32 powder X-ray crystallography lines and showed that the anion was indeed based on WO_6 octahedral units as suggested, but the importance of more compact edge- and corner-linked polyhedral arrangements was revealed [3 and 11]. This structure now is called the "Keggin structure." The general formula of Keggin is $[X^{n+}M_{12}O_{40}]^{(8-n)-}$. The structure is shown in Figure 1 using polyhedra. In Figure 1, the corners of the twelve octahedra and of the one tetrahedron represent the 40 oxygen atoms. The Keggin structure was confirmed by Bradley and Illingworth's investigation of $H_3PW_{12}O_{40}\bullet 29H_2O$ by using powder photographs in 1936 [4]. In 1948, Evans [12] reported the next new polyanion structure of $[TeMo_6O_{24}]^{6-}$ confirmed via an X-ray structure. This structure had in fact been suggested by Anderson [13] as a possibility for the 6:1 heteropolyanions and for para(hepta) molybdate anion $[Mo_7O_{24}]^{6+}$. The formula of $[X^{n+}Mo_6O_{24}]^{(12-n)-}$ is now called the "Anderson structure" [2].

Further progress was slow; in 1971, Evans [14] listed only 25 X-ray investigations, most of low quality. Subsequent developments in X-ray crystallographic hardware and software have increased the number of different structures. During the last two decades, new analytical techniques such as fast atom bombardment (FAB), mass spectrometry, and spectroscopic methods such as Raman and IR and one- and two-dimensional NMR and oxygen-17 and tungsten-183 NMR, in combination with precise electrochemical measurements, have enabled the further study of heteropoly compounds.

Hitherto, new classes of structure with often unexpected reactivity and applications are still being characterized. More than 70 different heteroatoms with "coordination numbers" ranging from 3 to 12 have been employed. Numerous stoichiometries and structures are known such as P/Mo pair and V/Mo pair species [3]. Recently electrochemical studies were done in which transition metal-substituted heteropolytungstates were examined [15]. Electrochemistry at the liquid/liquid interface offers a promising possibility for understanding the interfacial processes including extraction and phase tranfer catalysis [16 and 17]. Osakai et al. have studied the transfer of some isopoly and heteropoly anions across the water/nitrobenzene (W/NB) interface by cyclic voltammetry (CV) and normal pulse voltammetry [18]. Wang and his co-worker have also studied the transfer of some heteropoly [e.g. $[H_3PW_{11}O_{39}]^{4-}$] and isopoly [e.g.$[H_2W_{12}O_{39}]^{4-}$] anions across the W/NB interface by CV and chronopotentiometry with linear current scanning (CLC) [19]. Recently, unusually strong adsorption of highly charged heteropolytungstate anions on mercury electrode surfaces has been studied [20]. A continuing study of the roles played by delocalized "blue" electrons and by unpaired electrons in determining properties and structures of heteropoly complexes and their blue reduction products has been investigated by Baker's group [21].

I-2-2. Basic Principles of Polyoxometalates

Although new structural types of polyanions continue to be discovered, it is possible to recognize some general principles that control such structures. "Polyoxoanion formers par excellence of molybdenum(VI) and tungsten(VI) result from both a favorable combination of ionic radius and charge, and of accessibility of empty d-orbital for metal-oxygen π bonding. Other elements and oxidation states possess these attributes to a greater or lesser degree. Well known, of course, are polyoxoanions of vanadium(V), niobium(V) and tantalum(V). Hexavalent Tc, Re, Ru, Os, pentavalent Cr, Mo, W, Tc, Re, and tetravalent Ti, V, Cr, Mo, W may also be useful and interesting ingredients for cluster formation" [22].

Polyoxometalate structures are governed by two general principles, the most important one being the first. (1) Each metal atom occupies an MO_n coordination polyhedron (most commonly an octahedron or square pyramid) in which the metal atoms are displaced, as a result of MO π-bonding, towards those polyhedral vertices that form the surface. (2) The structures are generated by linking MO_n polyhedra in different ways, producing different types of faces on the surfaces.

The most well known species have a quasi-spherical structure derived from assemblies of MO_6 octahedra. These structures often are based on regular (Platonic) solids.

Four compact, highly symmetrical ("parent") clusters of MO_6 octahedra are shown in Figures 1-4 [22]. One important principle is that in most cases the cluster retains (remarkably!) the symmetry of its central oxygen polyhedron: a tetrahedron in Figures 1 and 4, an octahedron in Figure 2, and an icosahedron in Figure 3. These structures are important for the chemistry of Mo and W. The parent clusters form a convenient starting point for the discussion of many other polyoxometalate structures, which can be regarded as "derivatives."

The important polyhedra in the present context are mostly Platonic (all vertices are equivalent and all faces are of the same type), or Archimedean (only the first condition is retained). Polyoxometalate chemistry is governed by these types of polyhedra with vertices defined by oxygen and/or metal atoms. Such "global" polyhedra may be distorted due to the influence of a lower-symmetry, fundamental central unit as in the Keggin-type species.

I-2-3. Structure of Polyoxometalates

Although a variety of polyanion structures are known, and new structural types of polyanions continue to be discovered, the following five broad groups which have been structurally characterized can be conveniently classified for heteropolyanions, based upon the heteroatom, parent atom stoichiometry, and upon the coordination number of the heteroatom [23]. A brief description of these classifications follows.

Group I. 1:12 and 1:11 heteropolyanions, containing a tetrahedrally coordinated heteroatom (Keggin structure). A typical example of the former is $[SiW_{12}O_{40}]^{4-}$. Related heteropolyanions containing more than two metal atoms are also contained in this group.

Group II. 2:18 and 2:17 heteropolyanions, which also contain tetrahedrally coordinated heteroatoms and are structurally related to the first group (Dawson structure). A typical example of a 2:18 anion is $[As_2W_{18}O_{62}]^{6-}$. Related heteropolyanions containing more than two metal atoms are also known.

Group III. 1:6 heteropolyanions which contain an octahedrally coordinated heteroatom (Anderson structure). A typical example is $[TeMo_6O_{24}]^{4-}$.

Group IV. 1:9 heteropolys which also contain an octahedrally coordinated heteroatom (Waugh structure). One example is $[MnMo_9O_{32}]^{6-}$. These are unrelated to the 2:18 anions of Group II, above, but they are related to the 1:6 anions in Group III, and possibly also with the 1:12 heteropolyniobate of unconfirmed structure which is also in this group.

Group V. 1:12 heteropolyanions such as $[CeMo_{12}O_{42}]^{8-}$(Silverton structure). These contain an icosahedrally coordinated metal atom, in which the parent MO_6 octahedra share faces and corners with each other, compared with the edge-sharing or corner-plus-edge-sharing of the first four groups.

Of present interest is the heteropoly anions or acids with the 1:12 heteropoly of Group I and 1:1:11 heteropoly. The former is the so-called Keggin structure and the latter is a modification of Keggin structure.

1. Keggin Structure, 1 : 12, Heteropoly Anions

Three compact symmetrical clusters of MO_6 exist: (1) a tetrahedron(T_d), (2) an octahedron (O_h), and (3) an icosahedron(I_d) [3]. The Keggin structure has a tetrahedron (T_d) and has an overall T_d symmetry that is composed of a central XO_4 tetrahedron surrounded by twelve MO_6 octahedra. The central atom or heteroatom, X, can be P, As, Si, Ge, B, etc., and most of the peripheral atoms which are called poly or addenda atoms (M), are W or Mo. A few of the addenda atoms can be substituted by V, Co, Fe, etc. These 12 octahedra are organized into four groups of three sets of MO_6 octahedra (written as M_3O_{13}). The MO_6 units are joined to members of the same group through shared edges and to the MO_6 units of other M_3O_{13} groups and to the XO_4 tetrahedron through shared corners. The bonds in the 1:12 Keggin series have been distinguished as twelve quasilinear M-O-M bonds, twelve M-O-M angular bonds, four X-O-M, and twelve M-O bonds (with terminal O atoms).

In addition to the Keggin structure referred to as α-type (shown in Figure 1) there are geometrical isomers (ß-, and γ-type). The general formula of the Keggin structure is $[X^{n+}M_{12}O_{40}]^{(8-n)-}$ as previously mentioned. Some common examples of heteropoly anions having the Keggin structure are $[PW_{12}O_{40}]^{3-}$, $[SiW_{12}O_{40}]^{4-}$, $[BW_{12}O_{40}]^{5-}$, $[PMo_{12}O_{40}]^{3-}$, and $[SiMo_{12}O_{40}]^{4-}$. A typical example, $H_3PW_{12}O_{40} \cdot 29\ H_2O$, of a 12-heteropoly anion ($XM_{12}O_{40}$), has been studied in this paper. Within each octahedron, the longest W-O distance of 2.49 Å occurs between the tungsten and an oxygen atom in the interior of the complex; whereas, the W-O distance involving the peripheral oxygen atoms which are not shared by other tungsten atoms is only 1.43 Å [24].

The second type of symmetrical clusters of MO_6 octahedra (O_h) has not been observed for a discrete polyoxometalate. However, several derivatives, such as the mixed-valence mineral sherwoodite, $[AlV_{14}O_{40}]^{9-}$, are known [3]. This cluster is based upon edge sharing MO_6 octahedra and may be considered as fragments of a cubic closest packing of oxygen atoms [25].

The icosahedron, the third type of cluster, has I_d symmetry. This structure is known only for a handful of heteropoly molybdates of tetravalent lanthanide and actinide cations [3].

The 1: 12 heteropoly anions with Keggin structure are the most easily formed, and have been the most thoroughly studied [26]. It is well-known that the tungsten-oxygen frameworks of Keggin-type heteropoly anions are excellent conductors of electrons [27].

2. Heteropoly Anions, 1 : 1 : 11, with Modification of Keggin Structure

Simmons [28] and Baker discovered that one or more of the addenda atoms can be replaced by a second kind of octahedrally-coordinated heteroatom and prepared the first heteropoly anion which contained two different heteroatoms, cobalt and silicon, in combination with tungsten in 1962. The structure was shown to be a modification of the well-known 12-tungsto "Keggin" structure. Octahedrally-coordinated M^{m+} replaces just one of the 12 octahedral W atoms of the conventional Keggin structure, and X^{x+} occupies the Keggin unit's central tetrahedral cavity. This was formulated as

$[H_hM^{m+}O_5X^{x+}O_4W_{11}O_{30}]^{(14-m-x-h)-}$. In Figure 5 the heteroatom, X^{x+}, is within the central hatched tetrahedron. Each of the 12 octahedra contains a W atom or the heteroatom M^{m+}(hatched octahedron in Figure 5). The circled vertex in Figure 5 locates the center of the donor atom of a ligand, H_2O or NH_3, which is coordinated to M^{m+}. All of the other vertices locate the centers of close-packed O atoms. The representations show regular polyhedra. In actual anionic complexes, the W octahedra, which share corners and edges, are all considerably distorted by movement of the metal atoms far off-center in the octahedra, toward the unshared vertices. The distorted W octahedra severely distort the M^{m+} octahedra, removing its center of symmetry, as revealed by spectra. The X^{x+} to M^{m+} distance is about 3.3 Å and the X^{x+}-O-M^{m+} angle is about 125° in a model built with regular polyhedra [29]. In 1970, Figgis and Baker confirmed that the species of Simmons really was a 1:1:11 heteropoly anion [30]. Their heteropoly anion was shown to contain two non-acidic hydrogen atoms and was formulated as $K_6[SiW_{11}O_{39}CoH_2O]$, not as $K_6H_2[SiCoW_{11}O_{40}]$ as had Simmons. Figgis further formulated this anion as $[H_2OCoO_5W_{11}O_{30}SiO_4]^{6-}$ to imply water as a ligand. Following this paper, other researchers reformulated their results using the 1:1:11 formula.

Landis substantiated the 1:1:11 formulation for analogous "dumbbell" complexes with bridging pyrazine which bonds in a very particular way (synergic bonding) to the Co(III) in 1977 [31]. The heteroatom could be B, Co, Zn, Fe, Ge, etc. He further studied the octahedral "trans effect" of cobalt in a series of these 1:1:11 diheteropoly tungstate salts. Also, he analyzed and characterized 32 potassium salts of dihetero-11-tungsto anions. For instance, typical formulae of these dihetero-11-tungsto anions are the pyrazine cobalt(III)-11-tungstogermanate,$[N_2C_4H_4CoO_5W_{11}O_{30}GeO_4]^{5-}$ and $[N_2C_4H_4(CoO_5W_{11}O_{30}GeO_4)_2]^{10-}$. In 1980, Kazanskii [32] and co-workers studied the magnetic susceptibility of $K_6[SiM_{11}Fe^{III}(OH)O_{39}]\bullet H_2O$ and determined that the iron was in a low spin Fe^{III} state for the molybdate anion and a high spin Fe^{III} state for the tungstate anion.

I-3. Heteropoly Blues and Redox Chemistry of Polyanions

I-3-1. Heteropoly Blues

Many heteropoly anions or acids yield, upon reduction by addition of various numbers of electrons, products which typically retain the general structures of their oxidized parents and are frequently deep blue in color [33]. These blue reduction products of heteropoly anions or acids are called heteropoly blues (HPB). Heteropoly blues which are obtained by reduction of isopoly- and heteropoly-molybdates, tungstates and vanadates are a class of mixed valence complexes that are restricted to well-defined crystalloidal molecular or ionic species [34]. The anions or acids of the Keggin ($XM_{12}O_{40}$), Dawson ($X_2M_{18}O_{62}$), hexametalate (M_6O_{19}), decatungstate ($W_{10}O_{32}$) and related structures can be reduced to blue mixed-valence species without loss of structure. The formation of the heteropoly blue is a rapid and reversible reduction process. This process is reversible to at least the brown-violet stage (i.e. six-electron reduction), but further reduction may involve isomerization and be irreversible [4]. Polyanions or acids which form heteropoly blues have polarograms with several reversible diffusion-controlled waves. This means that reduction must be accompanied by only minor structural changes. The added ("blue") electrons are usually delocalized, according to various times scales, by means of very rapid hopping between specific "addenda" atoms (i.e. W, Mo, V, etc.) in certain regions of structure. But the role of the central heteroatom is generally insignificant [4, 5, 33, and 34].

Heteropoly blues are used in analytical chemistry in the colorimetric determination of several elements such as phosphorus (P), silicon (Si), arsenic (As), and germanium (Ge). These blues are also used in the biochemical determination of compounds such as uric acid, adrenalin, phenol, and sugar [35 and 36].

For crystalline solids, migration of the electrons within the crystal lattice can be influenced by applying an external potential [7]. For example, when a heteropoly compound is oxidized in an externally applied electric field, the heteropoly compound becomes blue. The blue color disappears when the polarity is reversed. Hence the electrochromism of the heteropoly compounds is of interest in industry because of the possibility of use in digital display devices [37].

I-3-2. Reducibility of Polyanion

1. Structural Considerations

Lipscomb [38] first noted that no reduced isopoly- or heteropolyanion structure contained addenda MO_6 octahedra with more than two unshared oxygen atoms and proposed that this might be a general feature of all polyanion structures. Pope [39] drew attention to the analogy between MO_6 octahedra in polyanions and the mononuclear oxocomplexes MOL_5 and MO_2L_4. Two kinds of metal atom displacement are observed in polyanions: type I, towards one, always terminal, oxygen atom; and type II, towards two cis, usually but not always, terminal oxygen atoms. The reducibility of isopoly- and heteropolyanions appear to depend upon these types of structures.

In 1972, Pope [39] further proposed, and later observations proved, that only polyanions with one terminal oxygen per metal (type I structure) would undergo reversible one-electron reductions to form heteropoly blues (e.g. $WOCl_5^-$, $VO(H_2O)_5^{++}$). Pope's proposal implies that the electron is added to a metal orbital (d_{xy} or b_2 in C_{4v} symmetry) which is formally non-bonding or weakly π-antibonding (see Figure 6). In the absence of in-plane π-bonding, the LUMO for type I octahedra is a nominally nonbonding, mainly metal-centered ("d_{xy}") orbital [3]. Thus addition of an electron will not cause much structural change.

In some other poly anion structures (type II) the MO_6 octahedra have two (cis) terminal oxygens as in $MoO_2F_4{}^{2-}$. The facts are that cis dioxo complexes are known only for d^o metal ions, whereas monooxo(C_{4v}) complexes may contain d^o, d^1, or d^2 central atoms. The LUMO for type II octahedra is strongly antibonding with respect to the terminal M-O bonds. Thus, in a type II polyanion, each metal has two terminal oxygens and the added electron must fill an anti-bonding orbital and will result in large structural changes. These considerations account for the lack of cis MO_2L_4 complexes with other than d^o metal ions, and for the observation that only type I polyanions seem to form heteropoly blues[39].

Polyanions constructed of type I octahedra, of which the Keggin structure is a prime example, are therefore easily reduced to mixed-valence species (heteropoly "blues" and "browns") which retain the overall architecture of the oxidized anions. The result can also be understood from extended Huckel and X_α calculations, which show that, as expected, the density of states in the LUMO (a "d_{xy} band" that has some oxygen contribution and is responsible for the intervalence charge-transfer (IVCT) transitions) increases, and the HOMO-LUMO gap decreases, with aggregation of MO_6 octahedra [3]. On the other hand, type II polyanions are reduced irreversibly and with more difficulty to complexes that have not yet been identified.

According to the above criterion, some other (type I structure) polyanions should also have polarograms with reversible waves. Examples are (a) α-$X_2M_{18}O_{62}^{6-}$, i.e. the Dawson structure (the ß-isomer has one edge-shared M_3O_{13} group rotated by 60°); (b) the hexametalate ($M_6O_{19}^{2-}$); (c) $MnV_{13}O_{38}^{7-}$; and (d) $XW_{10}O_{36}^{8-}$. In contrast, type II polyanions, such as the Anderson structure (XMo_6O_{24}), are either polarographically inactive or show irreversible multielectron reductions [4, 34].

2. Stoichiometry

In 1943, Souchay was the first to study polyanion solutions by using polarography [40]. He identified two- and four- electron reduction steps for poly-tungstophosphate, tungstosilicate, and metatungstate [41]. Thereafter, the electrochemistry of several Keggin and Dawson molybdates and tungstates have been studied in some detail.

Numerous electrochemical studies have been performed to study the redox chemistry of polyanions. The Keggin-structure heteropolyanions (both alpha and beta forms) have been the most intensely studied. As in all polyanion structures the M-atoms are strongly displaced from the centers of their MO_6 octahedra towards the terminal unshared oxygen atoms. The α-Keggin structure has overall T_d symmetry. A ß-isomer, of C_{3v} symmetry, in which one M_3O_{13} group has been rotated by 60° is also known and this isomer appears to be stabilized upon reduction [42 and 43].

Pope [3] has used the behavior of α- and ß- $SiMo_{12}O_{40}^{4-}$ to illustrate the general pattern of reductions for Keggin-structure anions which had been studied in some detail by Massart [44, 45, 46, and 47] and Launay [48]. In the scheme [4] below for α-$[SiMo_{12}O_{40}]^{4-}{}_{(O)}$, the Roman numerals denote the number of electrons added to the oxidized anion (O), double-headed arrows denote polarographically reversible electron transfer processes and single-headed arrows denote irreversible chemical and redox processes. Primes are used to indicate "isomeric" series and those which in contrast to the tungstate are much less stable than the initial "blue" series.

$$\begin{tikzcd}
0 \arrow[r, leftrightarrow] & \mathrm{I} \arrow[r, leftrightarrow] & \mathrm{II} \arrow[r, leftrightarrow] & \mathrm{III} \arrow[r, leftrightarrow] & \mathrm{IV} \arrow[r, leftrightarrow] & \mathrm{V} \arrow[r, leftrightarrow] & \mathrm{VI} \arrow[r, leftrightarrow] & (\mathrm{VIII}) \arrow[d, shift left] & & \\
& & & & & & (\mathrm{VI'}) \arrow[u] \arrow[r, leftrightarrow] & (\mathrm{VIII'}) \arrow[u, shift left] \arrow[r, leftrightarrow] & \mathrm{X'} \arrow[r, leftrightarrow] & \mathrm{XII'} \arrow[d] \\
& & & & & & & & & (\mathrm{XVIII})
\end{tikzcd}$$

Polarograms of both α and ß isomers in acidic solutions show a group of three two-electron reversible waves, O ↔ II, II ↔ IV and IV ↔ VI (see Table II). The half-wave potentials vary with pH in such a way as to correspond to the addition of a proton for each electron. The reduced species H_6SiMo_{12}(II) and H_8SiMo_{12}(IV) can be readily isolated by controlled potential electrolysis or by careful chemical reduction, e.g., with ascorbate. Reduced species VIII, VI' and VIII' are detectable only by rapid scan cyclic voltammetry, and XVIII rapidly decomposes even at 0 °C. The two series of related redox potentials are shown in Figure 7 and these show reduction of IV leads directly to XII' (which has been partially characterized and isolated as a potassium salt).

For the tungstates, the polarographic waves, as compared to $SiMo_{12}$, are shifted to more negative potentials. As the pH increases each of the three waves splits into two one-electron waves -- the first wave above pH 2.4, the second above pH 9.5, and the third above pH 13. Rates of reduction are pH-dependent and intermediate reduction species are prone to disproportionation for all of the reduced molybdate species. The odd reduction states I, III, V disproportionate via protonation, e.g.,

2 I + 2 H^+ -----> O + II H_2 below pH 2.4

and at high pH, equilibria such as

2 II <--------> IV + O   and

3 II <--------> 2 III + O

are displaced toward the right by the hydrolysis of O into SiO_2 + $MoO_4{}^{2-}$. However, the suitable choice of pH or mixed solvents can stop both acid- and base-driven disproportionations [4].

Analogous polarographic behavior of other Keggin anions, molybdates and tungstates are known. Waves corresponding to the reversible addition of one or two electrons (depending upon pH), and of four or six electrons occur. Differences between individual anions arise because (a) tungstates have more negative reduction potentials than molybdates; (b) tungstates are less strongly protonated than analogous molybdates and splitting of the two-electron waves occurs at lower pHs, e.g. SiW_{12} undergoes 1, 1 and 2 electron reductions at pH 0; and (c) there is an electrostatic effect of the anion charge on the reduction potentials (see Figure 8) [34].

Reduction of Keggin anions beyond the six-electron level results in a modification of the anion structure. This behavior has been observed for SiW_{12}, BW_{12}, H_2W_{12}, and $SiMo_{12}$. The case of H_2W_{12} has been most completely studied (the two H atoms in this anion are located in the central interior tetrahedral cavity of the anion). In one case studied, reductions of up to 26 more electrons resulted in polarographically irreversible multielectron steps. The resulting species, generally brown or red, are still quantitatively oxidizable to the original Keggin structures [49]. Launay [49] has concluded that the initially formed six-electron blue undergoes valence-isomerization:

$H_2W_6^{V}W_6^{VI}{}_{\text{(blue)}}$ ------> $H_2W_3^{IV}W_9^{VI}{}_{\text{(brown)}}$

Launay has proposed that the brown complex contains three W(IV) atoms in an edge-shared W_3O_{13} group of the Keggin structure, the three terminal oxygens of this group being converted to OH groups and the tungstens participating in metal-metal bonds. The brown six-electron products may be further reduced to twelve-, eighteen-, and twenty-four-electron species, each group of the Keggin structure being in turn reduced to $W_3^{IV}O_{13}$. Oxidation of the amphoteric 24-electron product restores the original polyanion without decomposition. The 24-electron product, isolated from 1 M HCl as a cation, undergoes a slow transformation to an isostructural species with one proton (instead of two) in the central tetrahedral cavity of the Keggin structure. The new complex may be reoxidized to give $HW_{12}O_{40}{}^{7-}$ which is slowly converted to $H_2W_{12}O_{40}{}^{6-}$; both species have been characterized by ^1H NMR [50].

Cotton [51] has elucidated a molecular orbital (M.O.) scheme for an M_3L_{13} metal-metal bonded cluster. Three bonding orbitals, one non-bonding orbital, and five antibonding orbitals were obtained from the nine t_{2g} orbitals of the metals. In $W_3{}^{IV}O_{13}$ groups, the bonding levels are filled, and Launay has shown that the 24-electron product of H_2W_{12} can accept eight more electrons which presumably fill the non-bonding levels of the four W_3O_{13} groups.

I-4. Problem of Nomenclature

Various methods of nomenclature for heteropoly compounds have appeared in the literature [6]. These have not been used consistently. The names "isopoly" and "heteropoly" for species such as those formed in equations [a] and [b] in section I-1, respectively, are unsatisfactory for at least two reasons: not only is "homo" a more usual antonym for "hetero", but the distinction between the two groups is wholly artificial and could lead to solecisms such as "mixed isopolyanion" to describe species such as ß-$[Mo_6V_2O_{26}]^{6-}$ (isostructural with the isopoly molybdate ß-$[Mo_8O_{26}]^{4-}$)and the consideration of $[(H_2)W_{12}O_{40}]^{6-}$ (which is chemically and structurally equivalent to a heteropolyanion like $[SiW_{12}O_{40}{}^{4-}]$) as an isopolyanion [3].

More recently, names such as "polyoxoanions" and "polyoxometalates" have been used. But it is important with a field as venerable as this, with a vast early literature, that changes in nomenclature not be made lightly. However, a name such as "metal-oxygen clusters" has been introduced by Pope [3], which can be used for the field as a whole and which emphasized the presence of metal centers. The word cluster in inorganic chemistry has hitherto been applied to species in which there are strong as well as weak metal-metal interactions (cf. "iron-sulfur clusters"). This seems appropriate for the present field, since polyoxometalates exhibit the whole range of metal-metal interactions, from extremely weak to very strong.

The question of systematic nomenclature has been addressed by the IUPAC in order to be able to retrieve important information [52]. A labeling system must be used for the metal atoms and may be used for the oxygens in case of ambiguity. However, the resulting names are almost never used in normal scientific intercourse, since they are very long and cumbersome [3]. But during the last several decades, the IUPAC has used a different system. Heteropoly anions are names with an Arabic numeral designating the simplest ratio of molybdenum or tungsten atoms to the central atom. This is followed by the prefix "molybdo" or "tungto" and then by the name of the simple anion (or acid) which contains the central atom in the corresponding oxidation state. In case of ambiguity, Roman numerals may be used to designate the oxidation state of the central atom. For example, $H_3[P^{5+}W_{12}O_{40}]$ is named 12-tungstophosphoric(V) acid and the shorthand notation which is used is $HW_6 + P$; $K_6[SiO_4W_{11}O_{30}CoO_5H_2]$ is named potassium aquocobalto(II)-11-tungstosilicate and the notation is $KCo_2W_6 + Si$.

I-5. Properties of Polyoxometalates

The following are the general properties of polyoxometalates [2, 4, 6 and 7].

1. Polyoxometalates generally have very high molecular weights (oxide clusters with molecular weights of 2000 - 7000).

2. Polyoxometalates with small metal counter cations are very soluble in water and polar solvents.

In water, most free acids are extremely soluble. For salts, usually the larger the cation, the less soluble is its salt with a given heteropoly anion. Salts with large counter cations such as with Cs^+, Ag^+, Tl^+, Hg^{++}, Pb^{++}, and the large alkaline earth cations are often insoluble. However, the NH_4^+, K^+, and Rb^+ salts of some of the most important heteropoly anions are insoluble, but these three cations form other soluble heteropoly salts.

In organic solvents, many of the free acids and a few of the salts are very soluble, especially if the solvents contain oxygen. Ethers, alcohols, and ketones, in order, are generally the best solvents. The dehydrated salts sometimes dissolve readily in organic solvents; the hydrated salts are insoluble.

3. In aqueous solution, polyoxometalates are stable at low pH, but tend to be hydrolyzed at a high pH. The stability is higher in organic media.

4. The crystalline free acids and salts of polyoxometalates are almost always highly hydrated. Several solid hydrates will be formed from a given acid or salt of heteropoly anions.

5. Many polyoxometalates are highly colored. The colors range through the spectrum and occur in many shades.

6. Many polyoxometalates are multi-electron oxidants, and those having Mo and V as polyatoms are strong oxidants. The reduction products are colored an intense, deep blue or brown-red. In solution, the blue substances obey Beer's Law. The reduced products can in turn act as reducing agents, and the original colors of the anions are restored upon oxidation.

7. Free acids of polyoxometalates are strong Bronsted acids. They are much stronger than the oxoacids of their constituent elements and ordinary mineral acids. The strong acidity is caused by: (a) dispersion of the negative charge over many atoms of the polyanion and (b) the fact that the negative charge is less distributed over the outer surface of the polyanion due to the double-bond character of the addenda atom (M) and of the terminal oxygen bond, which polarizes the negative charge of terminal oxygen (O) to addenda atom (M).

The acid strengths estimated from the formation constants for complexes of polyanions with chloral hydrate, 2, 2, 2-trichloro-1, 1, 1-ethandiol, are in the order [53 and 54]:

$$PW_{12} > PMo_{12} > SiW_{12} \approx GeW_{12} > SiMo_{12} \approx GeMo_{12}$$

The acid strength has been measured by various methods and the general trends of the acid strength are $W^{6+} > Mo^{6+} > V^{5+}$ (for polyatom) [55] and $P^{5+} > Si^{4+}, Ge^{4+}$ (for heteroatom or the charge of polyanion) [53 and 54]. For example, the acid strength in acetone (the pK, values in parentheses) decreased in the following order,

$PW_{12}{}^{3-}(1.6) > PVW_{11}{}^{4-}(1.8) > SiW_{12}{}^{4-}(2.0) \approx PMo_{12}{}^{3-}(2.0) > SiMo_{12}{}^{4-}(2.1)$ [56], where $PW_{12}{}^{3-}$, etc. denotes the acidic $H_3PW_{12}O_{40}$, etc. These two orders of the acid strengths almost agree. The acid strength tends to decrease upon reduction or partial substitution of Mo^{6+}, W^{6+}, by V^{5+} due to an increased negative charge.

The acidic properties of heteropoly compounds in the solid state are very sensitive to counter cations as well as the constituent elements of the polyanions. In the case of metal salts, five likely mechanisms are possible for the origins of the acidity: (a) protons in the acidic salts, (b) partial hydrolysis during the preparation process, (c) acidic dissociation of coordinated water, (d) Lewis acidity of metal ions, and (e) protons formed by the reduction of metal ions [2].

8. All heteropolymetalate anions are decomposed by strongly basic solutions. For instance, the final products are simple molybdate or tungstate ions and either an oxyanion or a hydrous metal oxide of the central atom. Two examples of heteropoly molybdates and heteropoly tungstates are:

$$[PW_{12}O_{40}]^{3-} + 23\ OH^- \text{----->} HPO_4^{2-} + 12\ WO_4^{2-} + 11\ H_2O$$

$$[P_2Mo_{18}O_{62}]^{6-} + 34\ OH^- \text{----->} 2\ HPO_4^{2-} + 18\ MoO_4^{2-} + 16\ H_2O$$

Heteropolytungstates are more stable in acid solutions than the corresponding molybdates. As a rule, heteropolytungstates are hydrolytically more stable than the heteropolymolybdates. A few heteropoly molybdates exist only in very acidic solutions.

9. The redox chemistry of polyoxometalates is characterized by their ability to accept and subsequently release a certain number of electrons in distinct redox steps without decomposition. Reduction-oxidation reaction of polyoxometalates has been shown by

various methods such as potentiometric titrations (using Cr^{2+}, Fe^{2+}, Eu^{2+} etc.), polarography, photoredox reactions, and high energy radiation through formation of reducing free radicals. The following is typical of redox properties of polyoxometalates. (a) Reduction of polyoxometalates proceeds without substantial change of their structure with addition of a certain characteristic number of electrons. On reduction they are colored mainly blue, producing the HPB which have a broad absorption at about 700 nm [7]. (b) Reduction is often followed by protonation that makes the corresponding potential pH-dependent. A pH increase shifts the redox potential to more negative values and often splits the two-electron polarographic waves into two one-electron pH-independent waves [57 and 58]. (c) The reduction potentials shift to more negative values with increasing negative charge on HPC [57]. (d) Molybdates are reduced more easily than the corresponding tungstates [59]. (e) The 2:18 HPC are reduced at slightly more positive potentials and retain their structure upon addition of more electrons than the corresponding 1:12 compounds. (f) The reduced HPC are more stable in basic solutions than the corresponding non-reduced compounds [57, 58]. However, in some mixed HPC the reverse has been observed [60 and 61]. (g) Addition of electrons beyond a certain number results in distortion of structure, formation of d^2 electronic configuration, and increased metal-metal bond character [62 and 63]. (h) In mixed HPC, the added electron is localized on the more electronegative metal [27, 64, and 65]. (i) The electrochemical reduction of 1:12 (XM_{12}) heteropolyanions with Keggin structure generally proceeds reversibly by the addition of one to six electrons, depending upon the applied potentials, solvent, etc.

I-6. Applications of Polyoxometalates

The applications of polyoxometalates are mainly based upon their unique properties: molecular weights, size, electrochemical activity and reducibility to form colored species, electron- and proton-transfer/storage abilities, thermal stability, Bronsted acidity of the corresponding acids, and lability of lattice oxygen. An additional advantage is the fact that heteropoly acids can be separated and enriched by extraction into organic solvents. In this section, the major applications of polyoxometalates are described in two areas: (a) analytical chemistry and biology, and (b) catalysis and photocatalysis.

I-6-1. Analytical and Biochemical Applications

Analytical applications have been based upon the properties of polyoxometalates such as: (1) their high molecular weights, (2) their electrochemical activity and reducibility to form colored species, and (3) the variety of elements that can be incorporated. Gravimetric methods and physical (e.g. colorimetric) methods have been widely used to determine P, As, Si, or Ge, either separately or in combination after reduction to heteropoly blues [66 and 67]. Analytical determinations of elements such as Ti, Zr, Hf, Th, Nb, Ce, and Sb are based on structurally undefined complexes of these elements with $[PMo_{12}O_{40}]^{3-}$ or $[SiMo_{12}O_{40}]^{4-}$ [68, 69, and 70]. Recent examples include the simultaneous determination of P, Si, Ge, and As by differential-pulse anodic voltammetry [71], chromatographic (HPLC) separation [72], and measurement of nanomolar concentrations of silica in seawater [73].

Polyoxometalates have been used to routinely analyze many pharmaceuticals and biological samples [74]. The ability of polyoxometalates to coagulate proteins and to precipitate organic molecules like alkaloids is an important use in the analysis of biologically active molecules, drug preparations, and pesticides and in clinical chemistry [74]. Reduction to mixed-valence blues of polyoxometalates is involved in uric acid determination [75], Lowry protein determination [76], and selective precipitation such as cholesterol and low-density lipoprotein (LDL) and high-density lipoprotein (HDL) separations [77]. The use of polytungstates for electron microscopy has recently been developed with organic derivatives of these anions which permit highly selective labeling [78 and 79].

I-6-2. Catalysis and Photocatalysis

Attempts to utilize polyoxometalates for catalysts has a long history; but systematic basic study only started in the 70's [2 and 80]. Polyoxometalates are widely used as oxidation catalysts as well as acid catalysts. Various types of catalysis have been reported for heteropolyacids (HPA) [81]. Three different types are for solid HPA catalysts and two types are for solution HPA systems. The types of solid HPA catalysts are surface, bulk-type(I) (=pseudoliquid), and bulk-type(II) catalysts, both in gas-solid and liquid-solid systems. The two types for solution HPA systems are homogeneous and phase-transfer catalysis.

The basic reversible redox reactions involved in substrate oxidation are presented in Equations (c) and (d) [3]:

$$[HPA]_{ox} + S + (n/2).\ H_2 \longleftrightarrow H_{n/2}[HPA]_{red} + Ox.S \qquad (c)$$

$$H_n[HPA]_{red} + n/4\ O_2 \longleftrightarrow [HPA]_{ox} + n/2\ H_2O \qquad (d)$$

Where $[HPA]_{ox}$ and $[HPA]_{red}$ are the oxidized and reduced forms of the heteropoly anions, respectively. The S is substrate, and the Ox.S is oxidized substrate. Such catalysts can be used, for example, in the formation of carboxylic acids from the corresponding aldehydes, as well as in the dehydrogenation of alcohols, aldehydes, and carboxylic acids to form C=C and C=O bonds.

Heterogeneous catalytic oxidation processes involving well-characterized polyoxometalates are known. Some of the more important processes are in the commercial vapor-phase oxidation of methacrolein to methacrylic acid [82] and methane oxidation [83]. Recently, synthesis of new bifunctional catalysts from polyoxometalates has been developed. For example $[(Ph_3P_2)Rh(CO)]_4[SiW_{12}O_{40}]$ is used for sequential hydroformylation and oxidation of olefins [84 and 85].

Homogeneous oxidative catalytic activity [86] has been studied in both the thermal [87] and photochemical dehydrogenation of H_2 from RX-type species (e.g., X= CH_2OH, COOH) and from water-splitting processes [7, 88, and 89]. Homogeneous catalysis of oxygen transfer to alkanes has been reported [90]. Recently, heteropoly compounds have been used in the sensitization of semiconductors [91] and sensitization of electrodes [92].

I-7. The Goals of the Research

The purpose of this research was to study the affect of the concentration of organic substrates on the magnitude of the reductive current of the heteropoly anion (HPC) and on the ease of reduction of the HPC. Two different heteropoly anions and three different organic substrates were used to investigate the reduction potentials of the HPC.

Since this research focused on two typical heteropoly anions and several organic substrates, this paper is generally divided into four areas: (1) results for HPC, $K_6[SiW_{11}CoO_{40}H_2]\bullet 16\ H_2O$, at a concentration of 9.33×10^{-4} M with several concentrations of IPA, acetone, and ACN; (2) results for HPC, $K_6[SiW_{11}CoO_{40}H_2]\bullet 16H_2O$, at a concentration of 5.23×10^{-4} M with several concentrations of IPA; (3) results for HPC, $H_3[PW_{12}O_{40}]\bullet 29\ H_2O$, at a concentration of 9.17×10^{-4} M with several concentrations of IPA, acetone, and ACN; and (4) results for cadmium nitrate, at a concentration of 1.056×10^{-3} M, with several concentrations of IPA.

CHAPTER II. EXPERIMENTAL

II-1. Apparatus

II-1-1. EC/225 Voltammetric Analyzer

An IBM Instruments EC/225 voltammetric analyzer was used to record the dropping mercury polarograms. The EC/225 can perform the following types of electrochemical analysis: DC polarography, sampled DC (TAST) polarography, normal pulse polarography (NPP), differential pulse polarography (DPP), constant potential pulse polarography (CPPP), alternate drop pulse polarography (ADPP), and linear sweep voltammetry (LSV), cyclic voltammetry (CV), and stripping voltammetry (SV). All samples were recorded using DC polarography. The dropping mercury electrode (DME) assembly consisted of a leveling bulb partially filled with triply distilled Bethlehem Instrument mercury connected with Tygon tubing to a 20.5 cm piece of capillary tubing which has a 0.076 mm internal diameter. Typical capillary characteristics were: mercury height equal to 66.5 cm, dropping interval equal to 1.0 second, mass of the falling drop using a timer setting of 1.0 second, and a standard cell which contained the reference electrode, the DME and a working electrode. The DC polarograms were record on a Fisher Recordall series 5000 recorder (Houston Instrument, Austin, Texas U.S.A). Potentials were measured and reported versus saturated calomel electrode (SCE) as the reference electrode.

II-1-2. Nitrogen De-oxygenation Device

Oxygen was removed by reaction with vanadium solution. The device and the solution preparation was basically as described by Landis [31]. Traces of oxygen were removed from the nitrogen by passing the tank nitrogen through scrubbing towers of 0.1 M vanadium(II) in 0.5 M sulfuric acid containing amalgamated zinc, next through an empty flask, then through a scrubbing tower of distilled water, and finally another empty flask. The empty flasks were used to prevent the solutions from mixing or being eluted (as an error) with the nitrogen gas. A sketch of the scrubbing tower system is given in Figure 9.

Mossy zinc was amalgamated by stirring the metal in a mixture of 0.8 g mercuric chloride and 20 mL hydrochloric acid for about one-half hour. The vanadium(II) solution was prepared by dissolving 3.990 g of vanadyl sulfate dihydrate in water, adding 5.60 mL of concentrated sulfuric acid, and finally diluting to 200 mL in a 250 mL beaker.

The solutions to be measured were deaerated in the standard sample cell prior to use by slowly bubbling oxygen-free moist nitrogen through the standard sample cell top-arm. After deaeration, a gentle stream of moist nitrogen was slowly passed over the surface of the solution.

II-1-3. Balance

Masses of the heteropoly compounds were determined using a Sartorius 1207 MP 2 electronic balance. The sensitivity of the balance is given as 1 x 10^{-4} g. Masses of the other solid chemicals were determined using Sartorius 1265 MP and Denver Instrument DI-400D electronic milligram balances.

II-1-4. Measurements of pH

The pH of all solutions were determined using a pH meter after preparation. The pH meter, from Hanna Instruments, was calibrated by using standard buffers of pH 4.00 and pH 7.00. The sensitivity of the pH meter is given as 0.01.

II-1-5. Glassware and Other Apparatus

In order to decrease the error, a mortar and pestle were used to grind the HPC. A plastic spatula was used to handle the HPC to prevent reduction of the HPC by reaction with the metal of the spatula.

Eppendorf micropipettes used were 5, 10, 20, 50, 100, 200, 500, 1000 mL. Volumetric and graduated pipettes of 1.0, 2.0, 5.0, 10.0, 25, and 50 mL were used and were obtained from Alpha, Fisher, Kimax, and Pyrex, respectively. Class A volumetric flasks purchased from Kimax and Pyrex were used. Other standard general laboratory apparatus and glassware were used as needed.

II-2. The Measurements of the Wave Heights and Half-wave Potentials

The wave heights and half-wave potentials were measured using a graphical method [31] illustrated in Figure 10. The lines are constructed in alphabetical sequence. The linear portions of the polarographic curve before and after the wave (along the maxima of the current oscillations) are extrapolated (lines AA' and BB'). The best straight line along the maxima of the current oscillations of the curve through the approximate half-wave potential is drawn (line CC') and extended across both of the previous two lines. This line is to be one diagonal of a rectangle. At the two intersections of these lines are constructed two lines parallel to the voltage axis (lines DD' and EE') and two lines parallel to the current axis (lines FF' and GG'), thus forming a rectangle (MNOP). Next the remaining diagonal of the rectangle is drawn (line HH'). The intersection of the two diagonals (L) is taken as the half-wave potential. If a line is constructed through the intersection of the diagonals and perpendicular to the voltage axis (line JJ'), the limiting current can be measured as the distance between the first two extrapolated lines (lines AA' and BB') of the linear portions of the polarographic curve. This method was chosen especially because it is suitable [93] for cases which have less well-defined waves and when the plateaus before and after the wave are not parallel.

II-3. Procedure and Instrument Settings

1. Procedure

a). Preparation

For all of the measurements, each trial solution was prepared using pH 4.99 stock solution of buffer. The stock buffer solution contained sodium acetate and acetic acid (0.1 molar total acetate concentration) which had been dissolved in 1.0 M sodium sulfate solution. This was used in order to maintain a nearly constant high ionic strength to swamp any changes of activity coefficients of the HPC species, and also to act as the supporting electrolyte. Two large batches of stock buffer were prepared and used for all measurements.

Basically, solutions to be measured were prepared in 50.00 mL volumetric flasks by adding (in the following order) 45.00 mL pH 4.99 buffer solution, HPC, "X" mL organic substrate, and then about (5-X) mL of distilled, deionized water to fill the flask to the mark.

b). The sample cell was rinsed several times with deionized distilled water before use and then was rinsed with and filled with the heteropoly solution.

c). The pH was measured.

d). Next the sample, after placing into the polarographic cell, was deaerated.

e). Then the voltage was scanned versus the SCE and the current was recorded.

f). From the polarograms the half-wave potential ($E_{1/2}$) and wave heights were determined.

g). A spreadsheet program (Quattro Pro) was used to make the graphs and calculate the data. For some calculations, a peak fitting program (Peakfit) was used to find best fit. Alchemy III was used to estimate the surface areas of organic substrates.

2. Instrumental Settings

a). For the first and the second reduction waves:

* Mode : DC
* Sweep range : Initial -0.60 V;
  Final -1.150 or - 1.200 V
* Current range : 0.2 μA

* Sweep rate : 5 x 1 mV/sec
* Drop Knocker Timer : 1.0 sec
* Recorder : 2.5 cm/min
* Filter Time Constant (sec) : 1+0.3
* Pulse Amplifier (mV) : 40
* Sweep Waveform : _/_

b). For the third reduction wave:

The settings, except for the current range and sweep rate, were the same as above.

* Current range : 2 μA
* Sweep rate : 10 x 1 mv/sec

II-4. Chemicals

HPLC grade 2-Propanol and acetonitrile were purchased from Fisher. All other chemicals, except for sodium silicate, were either ACS grade or analytical reagent grade and were purchased from Fisher or Mallinckrodt. Technical grade sodium silicate solution from W. M. Welch was used in the preparation of the aquocobalto(II)-11-tungstosilicate.

II-5. Preparation of the Heteropoly Compound

1. Potassium Aquocobalto(II)-11-tungstosilicate

Potassium aquocobalto(II)-11-tungstosilicate was prepared and recrystallized following the procedure described by A. M. Landis [31]. This method is as follows. A slurry of 0.01 mole of sodium silicate pentahydrate (2.544 g), 0.11 mole of tungstic acid (27.487 g), and 0.22 mole of sodium hydroxide (8.822 g) was dissolved in 80 mL of water. To the slightly cloudy solution, about 10 mL of glacial acetic acid were added dropwise to adjust the pH to 6.2 and to allow the assembly of the heteropoly anions. The solution was heated to boiling. A hot solution of a 0.01 mole of cobalt acetate tetrahydrate (2.493 g) in 25 mL of water containing 0.2 mL of glacial acetic acid was slowly added. The solution turned wine red, was boiled five minutes, and then filtered, while hot, through Whatman #50 filter paper. The filtered solution was reheated to boiling and a hot solution of 0.33 mole of potassium acetate (32.390 g) in 16 mL of water containing enough glacial acetic acid to adjust the pH to about 6 was added. The solution was allowed to cool. Wine-red crystals and fine pink solid precipitated.

The red crystals were recrystallized by dissolving them in a minimum amount of boiling 1% (by volume) acetic acid solution. The solution was then slowly cooled until it reached 62 °C. Filtration through Whatman #50 filter paper removed most of the fine pink precipitate by repeating the procedure three times. Upon cooling slowly to room temperature, wine-red crystals were formed which appeared free of impurity when viewed under the microscope. These crystals are the material labelled as potassium aquocobalto(II)-11-tungstosilicate.

2. 12-Tungstophosphoric(V) Acid

The 12-tungstophosphoric(V), $H_3[PW_{12}O_{40}]\bullet 29H_2O$, acid used had previously been prepared by A. M. Landis.

II-6. Conditions in the Laboratory

During these studies the mixtures were at ambient laboratory temperature. The laboratory temperature was generally between 23.5 and 26.0 °C. The temperatures of individual solutions were measured and are given in corresponding tables.

CHAPTER III. RESULTS

This chapter is divided into four parts. These are: (1) general results from polarography for two types of heteropoly compounds; (2) the measurements of the first-wave reduction currents in different mixtures with 9.326 x 10 $^{-4}$ M $K_6[SiW_{11}CoO_{40}H_2]\bullet15H_2O$ (FW 3256.20) upon changing the concentration of IPA, acetone, and ACN and with 5.227 x 10^{-4} M $K_6[SiW_{11}CoO_{40}H_2]\bullet15H_2O$ upon changing the concentration of IPA; (3) the measurements of the first-wave reduction currents in different mixtures with a constant concentration of $H_3[PW_{12}O_{40}]\bullet$ $29H_2O$ (FW 6682.26) upon changing the concentration of IPA, acetone, and ACN respectively; and (4) the reduction properties of cadmium nitrate upon addition of several concentrations of IPA.

All mixtures used were one phase (e.g., true solutions). For cadmium nitrate solutions more than 5.0 mL were required to cause separation into two phases.

III-1. Polarography of a 1:1:11 and a 1:12 Heteropoly Compound with pH 4.99 Buffer.

The polarography of two compounds was determined using a EC/225 Voltammetric Analyzer. The sweep rate did not affect the peak height. No effect on the peak heights was noted upon changing the sweep rate from 5, to 10, to 15 mV/sec. A sweep rate of 5 mV/sec and a current range of 0.2 μA were employed for the first and the second waves. A sweep rate of 10 mV/sec and a current range of 2 μA were employed for the third and fourth waves. The instrument settings for all "sketches" of the DME polarograms of HPC are given in the corresponding figures. Unless otherwise indicated in the particular figures or for particular purposes, the half-wave potentials and currents were measured in mixtures prepared using 50 mL volumetric flasks with 45 mL of pH 4.99 buffer, "X" mL of organic substrate, and approximately (5-X) mL of water. As noted in the experimental section, the buffer was sodium acetate/acetic acid in which the sum of the molarities of the acetate ion plus acetic acid was 0.1 M and which also combined 1.00 M sodium sulfate. This buffer system had a useful polarographic range of +0.214 to -1.65 volts versus the SCE. No waves were observed within this region at a sensitivity setting of 0.1 μA after oxygen-free nitrogen bubbled for five minutes (Figure 11).

For 9.326 x 10 $^{-4}$ M aquocobalto(II)-11-tungstosilicate at pH 5.08, three well-resolved waves at -0.793 V, -0.947 V, and -1.296 V were observed. The first and the second waves, without any added organic substrates, were similar in height and the third wave was huge relative to the first two waves. This phenomenon had been observed before by Landis [31]. The current ratio of the first, second, and third waves are approximately one to one to thirty-two (1:1:32). Sketches of DME polarograms of the aquocobalto(II)-11-tungstosilicate with 0.050 mL IPA at pH 5.07, with 0.050 mL acetone at pH 4.99, and with 0.20 mL ACN at pH 4.97 are given in Figures 12, 13 and 14.

The $E_{1/2}$ for these three waves did not change for the 9.326 x 10^{-4} M $K_6[SiW_{11}CoO_{40}H_2]\bullet 15H_2O$ with various concentrations of IPA, acetone, and ACN. However, the peak heights changed upon addition of various concentrations of these organic substrates. The first wave is of interest and the details will be described in the next section. Basically after the addition of some organic substrate, the first wave disappeared. The second wave becomes less resolved and was difficult to measure. In general, the second-wave height increased upon addition of more organic substrates. The third wave just slightly decreased upon addition of organic substrate. This decrease does not appear to follow any particular relation. Just after -1.750 volts, a huge wave (fourth wave) begins and does not reach its maximum before going off scale on the 2 μA sensitivity setting (hereafter called going off scale). In all solutions containing heteropoly, a fourth peak appears. This peak is also huge and does not reach its maximum before going off scale. The buffer solution without any heteropoly does not exhibit this huge peak, but does exhibit a small peak at $E_{1/2}$ of -1.650 V.

For the polarogram of 5.227 x 10^{-4} M aquocobalto(II)-11-tungstosilicate without any organic substrate at pH 4.87 (Figure 15), two well-resolved waves were observed at -0.802 V, and -1.309 V. The characteristics of these two waves were similar to those observed at a concentration of 9.33 x 10^{-4} M. The second wave was not well-resolved and was difficult to measure, even without IPA. A sketch of DME polarogram of 5.227 x 10^{-4} M aquocobalto(II)-11-tungstosilicate with 0.050 mL IPA at pH 4.87 for the first wave is given in Figure 16.

For 9.17 x 10^{-4} M 12-tungstophosphoric(V) acid, $H_3[PW_{12}O_{40}]\cdot 29H_2O$, at pH 4.88 without organic substrate, there are also three well-resolved waves at -0.771 V, -0.881 V, and -1.217 V. The current ratio of the first, second, and third waves are approximately one to one to thirty-three (1:1:33). Sketches of the DME polarogram of the 12-tungstophosphoric(V) acid with 0.075 mL IPA at pH 4.84, with 0.075 mL acetone at pH

4.84, and with 0.075 mL ACN at pH 4.86 are shown in Figures 17, 18 and 19. The characteristics of these three waves were similar to aquocobalto(II)-11-tungstosilicate obtained at concentration 9.326 x 10^{-4} M.

III-2. Measurements of the First-wave Reduction Currents at Several Concentrations of IPA, Acetone, and ACN with Constant Concentration of $K_6[SiW_{11}CoO_{40}H_2]\bullet 15H_2O$

Aqueous-mixtures of various concentrations of organic substrates with 9.326 x 10^{-4} M $K_6[SiW_{11}CoO_{40}H_2]\bullet 15H_2O$ were prepared as given in Table III for IPA, in Table IV for acetone, and in Table V for ACN. Three reduction waves, in addition to the huge peak near -1.750 V were observed upon addition of various concentrations of the organic substrates. Currents for the first peak, measured as peak height, do exhibit changes upon addition of IPA, acetone, and ACN after a threshold value. Plots of these peak heights of the first wave versus concentration for each organic substrate exhibit three regions. At low concentrations of organic substrate, the peak heights are essentially independent of the concentrations. At larger concentrations, the peak height decreases in a linear manner. At even larger concentrations, the peak heights are immeasurable (i.e. zero). The peak heights of first wave versus concentration of organic substrates are shown in Figure 20 with IPA, in Figure 21 with acetone, and in Figure 22 with ACN.

Aqueous-mixtures of various concentrations of the organic substrates with 5.227 x 10^{-4} M $K_6[SiW_{11}CoO_{40}H_2]\bullet 15H_2O$ were prepared as given in Table VI for IPA. The peak height of the first wave versus concentration for IPA exhibits three regions. At low concentrations of IPA, the peak heights are essentially independent of the concentrations. However, fluctuations in the data do occur. At larger concentrations, the peak height decreases in a linear manner. At even larger concentrations, the peak heights are immeasurable (i.e. zero). Currents for first peak, measured as peak height, do exhibit changes upon addition of IPA after a threshold value. The peak heights of first wave versus concentration of IPA is shown in Figure 23.

III-3. Measurements of the First-wave Reduction Current at Several Concentrations of IPA, Acetone, and ACN with Constant Concentration of $H_3[PW_{12}O_{40}]•29H_2O$

Aqueous-mixtures of various concentrations of organic substrates with $H_3PW_{12}O_{40}•29H_2O$ were prepared as given in Table VII for IPA, in Table VIII for acetone, and in Table IX for ACN. As with the 1:1:11 heteropoly, for this 1:12 heteropoly, three reduction waves were observed upon addition of various concentrations of organic substrates. The peak height of the first wave versus concentration for each organic substrate exhibits three regions. At low concentrations of organic substrate, the peak heights are essentially independent of the concentration. At larger concentrations, the peak heights decrease in a linear manner. At even larger concentrations, the peak heights are immeasurable (i.e. zero). The peak heights of first wave versus concentration of organic substrates are shown in Figure 24 with IPA, in Figure 25 with acetone, and in Figure 26 with ACN.

III-4. The Reduction Properties of Cadmium Nitrate upon Addition of Several Concentrations of IPA

Aqueous-mixtures of various concentrations of IPA with 1.056 x 10^{-3} M $Cd(NO_3)_2 \cdot 4 H_2O$ were prepared as given in Table X. The half-wave potentials and currents were measured in the same manner as with the heteropoly solutions.

One reduction wave was observed without addition of IPA (Figure 27). The half wave potential was -0.6452 V and the peak height was 0.036 μA. The half wave potentials and peak heights did not change upon addition of 0 to 1.00 mL of IPA. The data are given in Table XI. Upon addition of 5.00 mL of IPA the current decreased to 0.026 μA. Upon addition of additional IPA a second phase appeared.

CHAPTER IV. DISCUSSION

This chapter is divided into five sections. These sections are: (a) interpretation of the results for reduction of the two types of heteropoly compounds upon addition of organic substrates; (b) interpretation of the results for the first-wave reduction of the two types of heteropoly compounds upon addition of organic substrates using a model based on the adsorption on mercury drop of the electrode; (c) interpretation of the results for the first-wave reduction of the two types of heteropoly compounds upon addition of organic substrates using a model based on surface area of a sphere; (d) interpretation of the results for the first-wave reduction of the two types of heteropoly compounds upon addition of organic substrates using a model based on association complexes; and (e) overall conclusion and summary.

IV-1. Interpretation of the General Results of the 1:1:11 and 1:12 Heteropoly Compounds

IV-1-1. Interpretation of General Results

Reduction behavior and properties of the 11-tungsto(aquocobalto(II)) silicate anion and Keggin-structure 12-tungstate anions are, in general, similar. These similarities have also been observed in the literature [30]. These features provide the best evidence available that the added electrons do not reduce the Co(II) atom of the 11-tungsto(aquocobalto(II)) silicate anion, nor do they become localized in the vicinity of that ion. In addition, these investigators report that the cobaltous ion can be separated from a solution of the 2-electron blue derivative of $[(H_2O)CoO_5SiO_4W_{11}O_{30}]^{6-}$ in strongly acid solutions, just as it can be separated from the oxidized anion in a similar medium. The resulting tungstosilicate species remain blue. This blue color is taken to indicate that the matrix retains the extra electrons.

In the work reported herein, the polarograms of 11-tungsto(aquocobalto(II))silicate anion and 12-tungstophosphoric(V) acid were strikingly similar. For both HPC anions, three waves were observed and the half-wave potentials did not change upon addition of organic substrates. The second-waves in both sets of HPC polarograms became less resolved as organic substrate was added. The third-wave height essentially remained constant upon adding the organic substrate and was well-resolved in each case.

The electron distribution of the heteropoly blue compounds is one of the most interesting features. Various speculations and supporting evidence on the extent of charge delocalization in aqueous solution were studied by Varga [94], Papaconstantinou [95], and Kozik [21] . The arguments include data from ESR measurements, the intensity of the "blue" bands in the spectra, and molecular orbital calculations on the cubic tungsten bronzes. Although no unambiguous proof exists at the present time, it is generally believed that the addition of electrons to structure of a heteropoly anion does not result in the formation of unique, non-interacting W(V) atoms in a matrix of W(VI) atoms. Either the electron hops from W to W or the electron is delocalized.

The behavior of the 11-tungsto(aquocobalto(II)) silicate ion with respect to reduction is similar to the reduction properties of the 12-tungstate compounds studied by Pope and co-workers [57, 58, and 59] and Souchay [96]. Pope has remarked that, in various pH ranges, there is a maximum negative charge which each anion can accommodate. The Keggin structure 12-tungstate ions never acquire a charge more negative than -6 units in the pH range 0 to 5 and of -8 in the range of 5 to 7. If further reduction would increase the anionic charge above these values, addition of electrons is accompanied by protonation of the anion. An examination of the pH-dependence of the polarographic half-wave potential for the two reversible reduction steps of the $[SiW_{11}CoO_{40}H_2]^{6-}$ ion suggests that the 11-tungstate anion cannot carry a charge more negative than -6 units at pH values below 9.

Pope and coworkers [57, and 97] have compared the reduction properties of many 12-tungstate Keggin-structure heteropoly anions. They find that the differences among the half-wave potentials of the initial one-electron reduction step can be largely accounted for by the value of the charge of the oxidized anions, and they constructed a linear plot of $E_{1/2}$ vs. anionic charge (see Figure 8). Not surprisingly, the half-wave potential of the first 1-electron reduction step of the 11-tungsto(aquocobalto(II)) silicate ion (-0.947 vs. SCE) does not fall on that line. (According to the graph, the half-wave potential, -0.947 V vs. SCE, corresponds to a charge of -9 units on the oxidized heteropoly tungstate ion.) It is to be expected that the electron-acceptor orbital(s) of the 11-tungsto(aquocobalt(II) silicate anion is at least somewhat different from the orbital(s) in the 12-tungstate anions.

The reduction limiting current reflects the amount of species to be reduced at that voltage. The reducibility of any species depends upon the ease of adding an electron. The iso-structural polytungstates have accepted two electrons without decomposition. These conclusions were determined by polarography and potentiometric titrations of others [57]. The reduction of HPC requires the addition of an electron into an addenda atom. The more organic substrate added, the more the HPC associates with the organic substrate. The more associated complex formed, the lower the concentration of the reducible species and the lower reduction current observed.

The third wave reported in this paper for the 11-tungsto-(aquocobalto(II))silicate anion and 12-tungstophosphoric(V) acid has not been previously reported. Figgis [30] did report what here is referred to as the fourth wave. The most likely reason is that, at lower voltages, the associated complex remains intact. The surface of the association complex, which is most likely covered by organic substrates around the surface of HPC, hinders the electron access into the addenda atom of HPC. This results in a decrease in the effective concentration of the reducible species. But at a larger applied voltage, the association complex decomposes into several smaller species similar in size to the cadmium and nitrate ions. These smaller species do not associate with the organic substrate. Therefore, these smaller species are reduced and a huge wave (i.e. third wave) occurs.

The fourth wave observed in both of the HPC anions studied was also reported by Figgis [30]. She has suggested that this polarographic wave, which here appears after the third wave reduction step of $[(H_2O)CoO_5SiO_4W_{11}O_{30}]^{6-}$, does not correspond to the addition of more electrons to the anion, but rather is related to the reduction of hydrogen. A similar postulate has been made by Ripan et al. [98] for some 12-tungstate anions. The wave near -1.750 V (fourth wave) does not appear as a huge peak when only the buffer and organic substrate are recorded (without HPC). Hence the heteropoly anions must be in some way involved in this wave (solvent reduction).

The half-wave potentials were evaluated at the points at which the current was precisely half the limit current (see Figure 10 at "L" intersection point). The confidence of potentials was checked by determining the polarographic half-wave potential of 1.036 x 10^{-3} M solution of $Cd(NO_3)\bullet 4H_2O$ in pH 4.99 buffer solution. The measured half-wave potential of Cd^{2+} was -0.6452 V vs. SCE. The values of E_{cd2+} and E_{sce} at 25.58 °C are -0.6812, + 0.2412 V respectively. Therefore, the absolute difference was 0.036 V. This error was considered as constant. From literature [31], the half-wave potentials of $K_6[SiW_{11}CoO_{40}H_2]\bullet 15H_2O$ were -0.757 V , -0.928 V , and -1.25 V for first-, second-, and third-wave respectively. The measured half-wave potentials of $K_6[SiW_{11}CoO_{40}H_2]\bullet 15H_2O$ versus SCE are -0.793, -0.947, and -1.296 V for the first-, second-, and third-waves. In the experiments under consideration here, the absolute error of the first-wave is zero. The absolute error of the second-wave is 0.017 V. The absolute error of the third-wave is 0.01 V. The relative error of the first-, second- and third-waves are 0%, 1.83%, and 0.8 % respectively. This error most likely is an instrumental error. The half-wave potentials of $H_3[PW_{12}O_{40}]\bullet 29H_2O$ in pH 5 buffer are not available from literature. If the difference 0.036 is constant, the corrected half-wave potentials are -0.735, -0.845, and -1.181 V for the first-, second-, and third-waves.

No affect was noted on peak height upon changing the sweep rate from 5, to 10, to 15 mV/sec. This indicates that the diffusion rate of reducible species is fast enough to be reduced even under a sweep of rate 15 mV/sec.

Two separate large volumes of stock buffer solution were prepared. The heteropoly $K_6[SiW_{11}CoO_{40}H_2]\bullet 15\ H_2O$ at 9.326 x 10^{-4} M with IPA acetone, and ACN and the heteropoly $H_3[PW_{12}O_{40}]\bullet 29H_2O$ at 9.17 x 10^{-4} M with IPA, acetone, and ACN were run using the same buffer. The measured pH of the buffer just after preparation was 4.99. However, during aqueous-organic mixtures preparation, the measured pH was 5.04 for $K_6[SiW_{11}CoO_{40}H_2]\bullet 15\ H_2O$ preparation at 9.326 x 10^{-4} M with IPA, acetone, and ACN. After dissolving the HPC, the pH changed by ± 0.04 unit (see Tables III, IV, and V). This change may be caused by the presence of the organic solvent. The measured pH was 5.02 for $H_3[PW_{12}O_{40}]\bullet 29H_2O$ preparation at 9.326 x 10^{-4} M with IPA, acetone, and ACN. After dissolving the HPC, the pH decreased and the lowest value was 4.84 (see Tables VII, VIII and IX). It appears that the $H_3[PW_{12}O_{40}]\bullet 29H_2O$ changes the pH of the stock buffer. The most likely reason for this is that the $H_3[PW_{12}O_{40}]\bullet 29H_2O$ is a very strong acid and at pH 4.99, 0.01 M sodium acetate-acetic acid buffer was not sufficient. The mixtures of $K_6[SiW_{11}CoO_{40}H_2]\bullet 15\ H_2O$ at 5.227 x 10^{-4} M with IPA were run using the second buffer preparation.

IV-1-2. The Parameters from the Peak Heights of First-wave Versus Concentration of Organic Substrate with Constant Concentration of HPC Using the Quattro Pro Program

1. For $K_6[SiW_{11}CoO_{40}H_2]\cdot 15H_2O$ at 9.326×10^{-4} M

A linear least square fit of the data yields intersection points (hereafter called threshold values) of 0.0294 M with IPA, 0.0876 M with acetone, and 0.457 M with ACN. Threshold values increase on going from IPA to acetone to ACN. Above the threshold values, the first-peak height decreases linearly as the concentration of IPA, acetone, and ACN increase. In this portion of plot, the X-coefficients are -0.1876 with IPA, -0.0623 with acetone, and -0.017 with ACN and the standard error of coefficients are 0.0073 with IPA, 0.00134 with acetone, 0.00043 with ACN, from regressions shown in Table XII for IPA, in Table XIII for acetone, and in Table XIV for ACN. The data were divided into two sets for calculations of the low concentration and the high concentration data. These are indicated in these tables and all other tables by off setting the data. The linear least squares fit data are reported by Quattro Pro as Regression Output. The "Constant" is the intercept. The " Std Err of Y Est" is the standard error in this intercept. The "R Squared" is a measurement of the fit. The closer to 1.00, the better is the fit. The "X Coefficient(s)" is the slope of the straight line and the "Std Err of Coef." is the standard error in the slope. The effect of organic substrates on the reduction current decrease on going from IPA to acetone to ACN after threshold values. Below threshold values, the first-peak height increases slightly as the concentration of IPA, acetone, and ACN increase. In this portion of the plot, the X-coefficients are 0.01222 with IPA, 0.00185 with acetone, and 0.00123 with ACN and the standard error of coefficients are 0.02816 with IPA, 0.00735 with acetone, and 0.00063 with ACN. Hence, the increase coefficients might not be real and the slopes might really be zero.

2. For $K_6[SiW_{11}CoO_{40}H_2]\cdot 15\ H_2O$ at 5.227×10^{-4} M

A linear least square fit of the data yields threshold values of 0.01249 M. Above the threshold values, the first-peak height decreases linearly as the concentration of IPA increases. In this portion, the X-coefficient is -0.0855 with IPA, and the standard error of coefficient is 0.00808 with IPA as obtained from regressions shown in Table XV for IPA. Below the threshold values, the first-peak height decreases slightly as the concentration of IPA. In this portion of the plot, the X-coefficient was -0.0076 with IPA, and the standard error of coefficient was 0.00441.

3. For $H_3[PW_{12}O_{40}]\cdot 29H_2O$ at 9.17×10^{-4} M

A linear least square fit of the data yields threshold values of 0.02685 M with IPA, 0.05657 M with acetone, and 0.080 M with ACN. Threshold values increase on going from IPA to acetone to ACN. Above threshold values, the first-peak height decreases linearly as the concentrations of IPA, acetone, and ACN increase. In this portion of the plot, the X-coefficients are -0.2537 with IPA, -0.02434 with acetone, and -0.017 with ACN and the standard error of coefficients are 0.00473 with IPA, 0.00135 with acetone, 0.008 with ACN from regressions shown in Table XVI for IPA, in Table XVII for acetone, and in Table XVIII for ACN. The effect of organic substrates on the reduction current decreases on going from IPA to acetone to ACN after threshold values. Below threshold values, the first-peak heights increase slightly as the concentration of IPA,

IV-2. Interpretation of the Results for the First-wave Reduction of the Two Types of Heteropoly Compounds upon Addition of Organic Substrates Using a Model Based on the Adsorption on Mercury Drop of the Electrode.

One possible explanation for the decrease in current is the adsorption of the organic substrate on the surface of the mercury drop. As the concentration of substrate increases, the drop becomes partially covered and decreases the current because the Keggin anion cannot reach the electrode. Therefore, a threshold area should be reached at which the ratio of surface area of the drop to the total surface area of the organic substrate is constant for one organic substrate to the next. Because the capillary used for these experiments was broken before the mass of mercury drop was measured, the drop was assumed to be a sphere. The size of the drops were experimentally controlled with a device to knock the drop from the electrode. The size of the drop was approximately the diameter of the internal capillary diameter. The capillary tubing was 0.076 mm internal diameter. Therefore, the surface area of the drop equals $4\pi r^2 = 0.01815\ \text{mm}^2 = 1.815 \times 10^{12}\ \text{Å}^2$. The total surface areas of the organic substrate were calculated by multiplying the surface area on one side of one organic molecule by the concentration of the organic substrate.

To obtain the surface area of IPA, acetone, and ACN, the assumption that the surface of these molecules is similar to the largest triangular area was made. Alchemy III (version 3.0) was used to calculate the length between various external atoms of IPA, acetone, and ACN and to find the largest distance between atoms. The results of surface area of IPA, acetone, and ACN are 4.564, 3.6464, 2.3219 (1.3967) Å^2 respectively (see Table XIX). The value in parentheses for ACN represents the end-on area, whereas the other area will be side-ways area.

The threshold values should be independent of the HPC concentration. This is not the case (see IPA data). The total surface areas for the substrates also are not constant. Thus one would suspect that adsorption on the drops is not the major factor. Additionally, the half-wave potentials and peak heights of cadmium nitrate do not change upon the addition of several concentrations of IPA. From this result one can conclude that the bulk properties of the water-organic mixture do not cause the phenomena observed with the heteropoly anions.

IV-3. Interpretation of the Results for the First-wave Reduction of the Two Types of Heteropoly Compounds upon Addition of Organic Substrates Using a Model Based on Surface Area of a Sphere

Another possible explanation for the decrease in current is that the organic substrate adsorbs onto the surface of the Keggin anion. This adsorbed layer prevents transfer of electrons to the Keggin anion. If the Keggin anion is not completely covered, electrons can be transferred. Hence the current initially does not decrease. After a specific amount of organic substrate has been added, the number of Keggin anions which are only partially covered decrease, thus the addition of more organic substrate decreases the current because fewer Keggin anions which are not covered are present in solution. If the above hypothesis is correct, then the surface area of all the Keggin anions divided by the surface area of all the organic substrate in solution should yield a ratio which is less than 1.0, and the ratio would be the same for all of the organic substrates.

The total surface areas of the Keggin anion in solution were approximated by calculating the surface area of the Keggin anion and multiplying by the concentration of HPC. The total surface areas of the organic substrate were calculated as in section IV-2.

The molecular volume of a typical Keggin anion ($[XM_{12}O_{40}]^{n-}$) has been reported as 685 Å^3 [4]. If it is presumed that the molecule is a sphere and the volume is $4/3\pi r^3$, then the surface area is $4\pi r^2$. From this calculation, the surface area of the Keggin anion $[PW_{12}O_{40}]^{-3}$ is 376 Å^2. The radius of the 1:1:11 heteropoly anion has been reported as about 5.6Å [30]. Hence, the surface area of the heteropoly anion is 394 Å^2.

The total surface areas at threshold values of IPA, acetone, and ACN for $K_6[SiW_{11}CoO_{40}H_2]\bullet 15\ H_2O$ at 9.326 x 10^{-4} M are 4.04, 9.62, and 31.94(19.21) x 10^{21}Å^2 respectively. The total surface areas at threshold values of IPA for $K_6[SiW_{11}CoO_{40}H_2]\bullet 15\ H_2O$ at 5.227 x 10^{-4} M are 1.72 x 10^{21} Å^2. The total surface area of IPA, acetone, and ACN for $H_3[PW_{12}O_{40}]\bullet 29H_2O$ at 9.326 x 10^{-4} M are 3.69, 6.21, and 5.59 (3.37) x 10^{21} Å^2 respectively. The ratios of total surface area of HPC to total surface area of organic substrates are shown in Table XIX.

The ratios are greater than 1.0 except for two cases of ACN and acetone with $K_6[SiW_{11}CoO_{40}H_2]\bullet 15H_2O$. Additionally, the ratio of the threshold values are not one (with the exception of acetone and ACN with $K_6[SiW_{11}CoO_{40}H_2]\bullet 15H_2O$) and these values are all different. Hence this model was discarded.

IV-4. Interpretation of the Results for the First-wave Reduction of the Two Types of Heteropoly Compounds upon Addition of Organic Substrates Using a Model Based on Association Complexes.

IV-4-1. The Evidence for Formation of Association Complexes of HPC with Organic Substrates

The half-wave potentials and peak heights of cadmium nitrate do not change upon addition of several concentrations of IPA. From this result one can conclude that the bulk proprieties of the water-organic mixture does not cause the phenomena observed with the heteropoly anions. Also, one can conclude that the organic substrate probably must associate with the heteropoly anion rather than coating the mercury drops. Otherwise the cadmium reduction current should also decrease since the reduction wave of the heteropoly anion changes upon the addition of organic substrate. The association complex does not appear to be reduced at a lower voltage near the first wave since the reduction current of the first wave decreases as the concentration of organic substrate increases.

Half-wave potentials ($E_{1/2}$) of 1:1:11 and 1:12 HPC, used at different concentrations, for the three waves do not change upon adding various concentrations of IPA, acetone, and ACN. This implies that the species which are reduced are the same in water and in the solutions. However, the peak heights do change upon addition of various concentrations of these organic substrates. This supports the idea that HPC must associate with these organic substrates and these association complexes are not able to be reduced under the experimental conditions.

relating peak height and organic substrate concentration can be derived. Recall that the peak height (i.e. the diffusion current) is directly proportional to the bulk species equilibrium concentration, not to the concentration at the electrode surface.

The heteropoly anion can be in its oxidized (ox) or reduced (red) form or can occur as the complexed (cplx) form.

ox + ne <--------> red

ox + q alc <--------> {ox.q alc} = {cplx}

In these chemical equations, ox and red are the oxidized and reduced forms of the HPC anion, n is the numbers of electrons added per HPC anion, and e is the electron. The complex or aggregate is represented as {ox.q alc} where alc is an organic substrate such as isopropyl alcohol and q is the number of alcohol molecules in the complex. Both of these reactions are considered to be in rapid equilibrium and hence have respective equilibrium expressions of:

$$K_R = [red]/[ox] \qquad (1)$$

$$K_C = [cplx]/[ox][alc]^q \qquad (2)$$

Here the square brackets represent molar equilibrium concentrations expressed in mol/L of the bulk solution and cplx is the complex or aggregate {ox.q alc}

A mass balance for the tungsten heteropoly is:

$$C_w = [ox] + [red] + [cplx] \qquad (3)$$

Here C_w is the analytical concentration of heteropoly anion in all forms and cplx is assumed to be per mole of anion.

The response of the DME is just the Ilkovic equation [99]:

$$I_d = (7.08 \times 10^{7})\, n\, D^{1/2}\, m^{2/3}\, t^{1/6}\, C$$

where I_d is the diffusion current in μA, n is the number of electrons, D is the diffusion coefficient of the oxidized form of the HPC anion in m^2/sec, m is the mercury flow rate in mg/sec, t is the drop time or drop interval in second and C is the concentration of the oxidized HPC anion in mol/L. The constant $7.08 \times 10^{+7}$ adjusts for the units. This equation under the experimental conditions reduces to:

$$\text{PkHt} = k[\text{ox}] \qquad (4)$$

where PkHt is the diffusion current in μA, k is the proportionality constant in μA•L/mol, and [ox] is bulk equilibrium concentration in mol/L.

These four equations were solved to yield a function for peak height in terms of alcohol concentration. First solve for [red] in equation 1 and for [cplx] in equation 2, then substitute into equation 3, to yield:

$$C_w = [\text{ox}] + K_R[\text{ox}] + K_c\, [\text{ox}][\text{alc}]^q$$

This equation was solved for [ox] and then substituted into equation 4 to yield the final equation:

$$\text{PkHt} = kC_w/\{1+K_R+K_C[\text{alc}]^q\} \qquad (5)$$

Note that at low alcohol concentration, $K_C[\text{alc}]^q << 1+ K_R$ and the denominator reduces to $1+ K_R$. Hence

$$\text{PkHt} = kC_w/[1+K_R] \qquad (6)$$

which is independent of the added alcohol and depends only upon the total amount of HPC in the solution. At high alcohol concentrations, $K_C[\text{alc}]^q >> 1+K_R$ and the denominator reduces to $K_C[\mathrm{alc}]^q$. This yields

$$\mathrm{PkHt} = kC_w/\{K_C[\mathrm{alc}]^q\} \qquad (7)$$

which is an exponential decrease. The logarithmic form of this high alcohol equation is:

$$\log(\mathrm{PkHt}) = \log(kC_w/K_C) - q \log[\mathrm{alc}] \qquad (8)$$

Hence if log(PkHt) is plotted versus log[alc] at sufficiently large alcohol concentrations, then a straight line should result in which the negative of the slope is q, the number of alcohol (or organic substrate) molecules in the complex per HPC anion.

Rewriting Equation 5 in logarithmic form, we have:

$$\log(\mathrm{PkHt}) = \log(kC_w) - \log\{1 + K_R + K_C[\mathrm{alc}]^q\} \qquad (9)$$

Note that at low alcohol concentration this reduces to:

$$\log(\mathrm{PkHt}) = \log\{kC_w/[1 + K_R]\}$$

At high alcohol concentration, Equation 9 reduces to Equation 8 as indeed it should.

Since C_w is a known constant value, if the constant k is known, a value for K_R can be experimentally determined from low alcohol concentration data using either Equation 6 or 10. Values for K_C and q can be obtained from Equation 8 using the high alcohol concentration data. The slope yields -q and the hypothetical intercept obtained by extrapolation yields a value which can be used to calculate K_C (refer to Figure 29-35).

Note that even though a plot of peak height versus alcohol concentration is exponential, the change in curvature immediately after the threshold value is essentially zero. Hence a good straight line best fit can be obtained.

IV-4-3. Comparison of Parameters Calculated Using the Quattro Pro and Peakfit Programs

1. Quattro Pro for Windows (Version 6.0)

For the data at the lower organic concentrations, the limiting current of the HPC anion remains essentially constant upon addition of small volumes of added organic substrates. For this portion of the plot, since the limiting current of HPC without organic substrates and the analytical concentration of heteropoly anion are known, the proportionality constant k can be calculated from Equation 4.

For slightly greater organic concentrations (which start just after the first portion) the data for slightly greater volumes of IPA result in the current rapidly decreasing (e.g., see Figure 20). The results of the logarithmic forms of the limiting currents and concentrations of organic substrate are shown in Figures 29, 30, and 31 for $K_6[SiW_{11}CoO_{40}H_2]\cdot 15H_2O$ at 9.326×10^{-4} M with IPA, acetone, and ACN in order; in Figure 32 for $K_6[SiW_{11}CoO_{40}H_2]\cdot 15H_2O$ at 5.227×10^{-4} M with IPA; in Figures 33, 34, and 35 for $H_3[PW_{12}O_{40}]\cdot 29\ H_2O$ at 9.17×10^{-4} M with IPA, acetone, and ACN in order. From these plots, the slope and intercept of Equation 8 were obtained and the K_c and q values were calculated from these data. These parameters are tabulated in Table XX.

The disadvantages of using the Quattro Pro Program are that just a few data points were used to calculated the K_c and q values, and also one of the parameters (K_R) CANNOT be deduced. Hence, the confidence in these results is low.

2. Peakfit Program(Version 3.0)

The user function Y = $\#A_0/(1+\#A_1+\#A_2*X\wedge\#A_3)$ was entered into this program. This function is based upon Equation 5, where Y is the peak height, $\#A_0$ is kCw, $\#A_1$ is K_R, $\#A_2$ is K_C, $\#A_3$ is q, and X is concentration of organic substrate. This program finds the best fit for the four "#A" parameters. Then the values of the parameters k, K_R, K_c, and q were obtained from "#A" parameters. These data are shown in Table XXI.

All of the best fit curves of two HPC with organic substrates are shown as follows. Figures 36, 37, and 38 are for $K_6[SiW_{11}CoO_{40}H_2]\bullet15H_2O$ at 9.326 x 10^{-4} M with IPA, acetone, and ACN in order. Figure 39 is for $K_6[SiW_{11}CoO_{40}H_2]\bullet15H_2O$ at 5.227 x 10^{-4} M with IPA. Figures 40, 41, and 42 are for $H_3[PW_{12}O_{40}]\bullet29\ H_2O$ at 9.17 x 10^{-4} M with IPA, acetone, and ACN in order. The curve fit coefficients for these curves range from 4.303 x 10^{-8} to 2.528 x 10^{-5}. The r^2 values range from 0.8923 to 0.9995. The values are given in the figures.

Trial values for these parameters are supplied to the Peakfit program and adjusted to approximate the data. Then the program automatically finds a best fit. Different starting parameters resulted in essentially the same values for these parameters.

One of the advantages of the Peakfit program relative to Quattro Pro is that the entire data set is used to fit all the parameters. Another advantage is the parameters are automatically obtained. Confidence in the results is much greater than with the Quattro Pro technique.

3. Analysis of the Association Complex Parameters

For the Quattro Pro results, K_R was presumed to be zero in Equation 6. The value of k obtained from this equation is about 30 in each case (see Table XX). From the Peakfit program, an average of 1.16 was obtained for K_R. If in the Quattro Pro results the value of K_R is assumed to be 1.0 and not zero, then the value of k is calculated to be 64. This value is approximately the same as the value obtained using the Peakfit program. Hence, the results of the two calculations can be considered to agree. This means that k remains constant and is similar in size for each case.

The results from both programs (see Table XXII) yield similar trends for the values of the K_C and q parameters. For most cases the same order of magnitude was obtained using both programs. For example, K_C for IPA with $K_6[SiW_{11}CoO_{40}H_2]\bullet 15H_2O$ at 9.326×10^{-4} M was 4.4×10^3 with Peakfit and 8.4×10^3 with Quattro Pro. The values of q show less regularity, but all values are less than 5. This appears to indicate that the substrate binds at a few specific sites.

The formation constant (K_C) of the association complex with IPA is much greater than with acetone or ACN. The most likely reason for this is hydrogen bonding between HPC and IPA which is not possible with acetone and ACN. For acetone and ACN, the formation of association complexes can only result from weaker dipole attractions. Therefore, the formation constants (K_C) of the association complexes with acetone and ACN are much lower. Since the dipole moment of acetone (2.69 Debyes) and ACN (3.44 Debyes) are similar [100], the size of the formation constant (K_C) of association complexes should be similar in size. This is the case. For $K_6[SiW_{11}CoO_{40}H_2]\bullet 15H_2O$, the value of K_C is about 10^{-1} for ACN and about 10^{+1} for acetone.

IV-5. Overall Conclusion and Summary

Clearly many more experiments need to be done. These might include measurements of cyclic voltammetry(CV) using a graphite electrode instead of a dropping mercury electrode; investigations with more solutions of HPC with concentrations greater than the threshold values; or the use of other 1:12 and 1:1:11 HPC anions. The CV measurements will give data about the reversibility of the reductions. Use of a graphite electrode will eliminate the possibility of mercury adsorption. Addition concentrations of HPC will decrease the error of the parameters. The generality of the conclusions in this study can be determined if addition HPC anions exhibit similar behavior.

CHAPTER V. CONCLUSIONS

From the results of this research, several conclusions about the reduction of two typical HPC upon addition of IPA, acetone, and ACN can be deduced. These conclusions are briefly stated in the following sentences.

1. Sweep rate does not affect the peak height.

2. Half-wave potential does not change upon changing the concentration of IPA, acetone, or ACN.

3. At low concentration, the first-peak heights are essentially independent of concentrations of IPA, acetone, or ACN.

4. Above threshold values, the first-peak height decreases rapidly as the concentration of IPA, acetone, and ACN increases.

5. Threshold values increase when the substrate is changed from IPA to acetone to ACN for the heteropoly anions studied.

6. The equilibrium constant(Kc) for the formation of association complexes decreases when the substrate is changed from IPA, to acetone, to ACN.

7. A small number of organic substrate molecules associate at specific sites on the HPC.

BIBLIOGRAPHY

1. Moeller, T. Inorganic Chemistry; John Wiley and Sons: New York, 1982; Chapter 8.

2. Misono, M. Catal. Rev. Sci. Eng., **1987**, 29, 269.

3. Pope, M. T.; Muller, A. Angew. Chem. Int. Ed. Engl., **1991**, 30, 30.

4. Pope, M. T. Heteropoly and Isopoly Oxometalates; Christian, K., Ed.; Inorganic Chemistry Concepts; Springer-Verlag: New York, 1983; Vol. 8.

5. Cotton, F. A.; Wilkinson, G. Advanced Inorganic Chemistry; John Wiley and Sons: New York, 1988; Chapter 19.

6. Tsigdinos, G. A. In Heteropoly Compounds of Molybdenum and Tungsten; Dewer, M. J. S., Ed.; Topic in Current Chemistry; Spring-Verlag: New York, 1978; Vol. 76, pp1-64.

7. Papaconstantinou, E. Photochemistry of Polyoxometallates of Molybdenum and Tungsten and/or Vanadium; Bagnall, K. W., Ed.; Chemical Society 18, pp1-31.

8. Moffat, J. B. Chem. Eng. Comm., **1989**, 83, 9.

9. Berzelius, J. J. P. Ann. Phys. Chem., **1826**, 6, 369, 380.

10. Pauling, L. C. J. Am. Chem. Soc., **1929**, 51, 2868.

11. Keggin, J. F. Nature, **1933**, 131, 908.

12. Evans, H. T. Jr. J. Am. Chem. Soc., **1948**, 70, 1291.

13. Anderson, J. S. Nature, **1937**, 140, 850.

14. Evans, H. T. Jr. Perspect. Struct. Chem. **1971**, 4, 1.

15. Rong, C.; Anson, F. C. Inorg. Chem. **1994**, 33, 1064, and references cited therein.

16. Yu, W.; Freiser, H. Anal. Sci., **1987**, 3, 401.

17. Koryta, J.; Skalicky, M.; J. Electroanal. Chem. Interfacial Electrochem., **1987**, 229, 265.

18. Osakai, T.; Katano, H.; Maeda, K.; Himeno, S.; Saito, A. Bull. Chem. Soc. Jpn., **1993**, 66, 1111, and references cited therein.

19. Wang, H.; Yu, Z.; Wang, En.; Wang, Er. J. Electroanal. Chem. **1995**, 380, 69, and references cited therein.

20. Rong, C.; Anson, F. C. Anal. Chem., **1994**, 66, 3124.

21. Kozik, M.; Baker, L. C. W. In Blue Electron Distributions Reduced Heteropoly Tungstates. Insights Concerning Conduction Pathways and Spin Coupling Patterns. ^{183}W NMR Chemical Shift Calculations; Pope, M. T. and Muller, A., Ed.; Polyoxometalates: From Platonic Solids to Anti-retroviral Activity; Kluwer Academic: Boston, 1994; pp191-202, and references cited therein.

22. Delgado, O. and Dress, A. In Polyoxometalates: A Class of Compounds with Remarkable Topology; Pope, M. T. and Muller, A., Ed.; Polyoxometalates: From Platonic Solids to Anti-retroviral Activity; Kluwer Academic: Boston, 1994; pp7-26.

23. Kerpert, D. L. In Isopolyanions and Heteropolyanions; Trotman-Dickenson, A. F., Ed.; Comprehensive Inorganic Chemistry; Pergamon Press: New York, 1973; Vol. 4, pp 607-671.

24. Yannoni, N. F. Ph. D Thesis, Boston University, 1961.

25. Kepert, D. L. Inorg. Chem., **1969**, **8**, 1556.

26. Kepert, D. L. In Isopolytungstates; Cotton, F. A., Ed.; Progress in Inorganic Chemistry; Interscience Publishers: New York, 1962; Vol. 4, pp 199-274.

27. Altenau, J. J.; Pope, M. T.; Prados, R. A.; So, H. Inorg. Chem., **1975**, 14, 417.

28. Simmons, V. E.; Baker, L. C. W. Proc. Int. Conf. Cood. Chem., 7th, 1963., **1962**, 195.

29. Baker, L. C. W.; Simmons, V. E.; Wasfi, S. H.; Candela, G. A.; Kahn, A. H. J. Chem. Phys., **1972**, 56, 4917.

30. Figgis, J. S.; Baker, L. C. W. J. Am. Chem. Soc., **1970**, 92, 3794.

31. Landis, A. M. Ph. D. Thesis, Georgetown University, 1977.

32. Kazanskii, L. P.; Feist, M.; Torchenkova, E. A.; Spitsyn, V. I. Z. Inorg. Chem., **1980**, 476, 201.

33. Kozik, M.; Hammer, C. F.; Baker, L. C. W. J. Am. Chem. Soc., **1986**, 108, 7627.

34. Pope, M. T. NATO Adv. Study Inst. Ser., Ser. C, **1980**, 58, 365.

35. Vogel, A. I. A Text Book of Quantitative Inorganic Analysis, 3rd Ed., Wiley and Sons Inc., N.Y., 1966.

36. Wu, H. J. Biol. Chem., **1920**, 43, 189.

37. Cotton, R. J.; Guzman, A. M.; Rabalais, J. W. Acc. Chem. Res., **1978**, 11, 170.

38. Lipscomb, W. N. Inorg. Chem., **1965**, 4, 132.

39. Pope, M. T. Inorg. Chem., **1972**, 11, 1973.

40. Souchay, P. Ann. Chim., **1943**,[11], 19, 102.

41. Souchay, P.; Herve, G. Compt. Rend., **1965**, 261, 2486.

42. Matsumoto, K. Y.; Kobayaski, A.; Sasaki, Y. Bull. Chem. Soc. Japan, **1975**, 48, 3146.

43. Souchay, P.; Contant, R. C. R. Acad. Sci., Ser. C, **1967**, 265, 723.

44. Massart, R. Ann. Chim., **1968**, 3, 507.

45. Massart, R. Ann. Chim., **1969**, 4, 285.

46. Massart, R. Ann. Chim., **1969**, 4, 365.

47. Massart, R. Ann. Chim., **1969**, 4, 441.

48. Launay, J. P. Doctoral Thesis, Universite Pierre et Marie Curie, Paris, 1974.

49. Launay, J. P. J. Inorg. Nucl. Chem., **1976**, 38, 807.

50. Launay, J. P. J. Inorg. Nucl. Chem., **1976**, 38, 243.

51. Cotton, F. A. Inorg. Chem. **1964**, 3, 1217.

52. Jeannin, Y.; Fournier, M. Pure Appl. Chem. **1987**, 59, 1529.

53. Barcza, L.; Pope, M. T. J. Phys. Chem., **1975**, 79, 92.

54. Izumi, Y.; Matsuo, K.; Urabe, K. J. Mol. Catal., **1983**, 18, 299.

55. Kozhevnikov, I. V.; Matveev, K. I. Appl. Catal., **1983**, 5, 135.

56. Ono, Y. Perspectives in Catalysis, Thomas, J. M. and Zamaraev, K. I., Eds; Blackwell; London, 1992, p. 431.

57. Pope, M. T.; Varga, Jr. G. M. Inorg. Chem., **1966**, 5, 1249.

58. Pope, M. T.; Papaconstantinou, E. Inorg. Chem., **1967**, 6, 1147.

59. Papaconstantinou, E.; Pope, M. T. Inorg. Chem., **1967**, 6, 1152.

60. Polotebnova, N. A.; Furtune, L. A. Russ. J. Inorg. Chem., **1969**, 14, 1615.

61. Odyakov, V. F.; Kuzuetsova, L. I.; Matveev, K. I. Russ. J. Inorg. Chem., **1978**, 23, 254.

62. Lanuay, J. P. J. Inorg. Nucl. Chem., **1976**, 38, 807.

63. Kazanskii, L. P.; Lanuay, J. P. Chem. Phys. Lett., **1977**, 51, 242.

64. Mossoba, M. M.; O'Conner, C. J.; Pope, M. T.; Sinn, E.; Herve, G.; Teze, A. J. Am. Chem. Soc., **1980**, 102, 6864.

65. Harmalker, S. P. ; Pope ,M. T. J. Am. Chem. Soc., **1981**, 103, 7381.

66. Clabaugh, W. S.; Jackson, A. J. Res. Nat. Bur. Stand., **1959**, 62, 201.

67. Simon, S. J.; Boltz, D. F. Anal. Chem., **1975**, 47, 1758.

68. Going, J. E.; Thompson, J. Microchem. J., **1976**, 21, 98.

69. Golubev, A. M.; Kazanskii, L. P.; Torchenkova, E. A.; Simonov, V. I.; Spitsyn, V. I. Dokl. Chem., **1975**, 221, 198.

70. Johnson, H. N.; Kirkbright, G. F.; Whitehouse, R. J. Anal. Chem., **1973**, 45, 1603.

71. Fogg, A. G.; Bsebsu, N. K.; Birch, B. J. Talanta, **1981**, 28, 473.

72. Braungart, M.; Russell, H. Chromatographia, **1984**, 19, 185.

73. Brzezinski, M. A.; Nelson, D. M. Mar. Chem., **1986**, 19, 139.

74. Semenovskaya, E. N. Zh. Anal. Khim. **1986**, 41, 1925; J. Anal. Chem. USSR (Engl. Transl.) **1986**, 41, 1339.

75. Matheke, M. L; Kessel, G. ; Chan, K. M. Clin. Chem. (Winston-Salem, NC), **1987**, 33, 2109.

76. Legler, G.; Muller-Platz, C. M.; Mentges-Hettkamp, M.; Pflieger, G.; Julich, E. Anal. Biochem., **1985**, 150, 278.

77. Warnick, G. R.; Mayfield, C.; Benderson, J.; Chen, S.; Albers, J. J. Am. J. Clin. Pathol., **1982**, 78, 718.

78. Keana, J. F. W.; Ogan, M. D.; Lu, Y.; Beer, M.; Varkey, J. J. Am. Chem. Soc., **1985**, 107, 6714.

79. Keana, J. F. W.; Wu, Y.; Wu, G. J. Org. Chem. **1987**, 52, 2571.

80. Misono, M. Catal. Rev. Sci. Eng., **1988**, 30, 339.

81. Misono, M. In Catalic Chemistry of Solid Polyoxometalates and Their Industrial Applications; Pope, M. T. and Muller, A., Ed.; Polyoxometalates: From Platonic Solids to Anti-retroviral Activity; Kluwer Academic: Boston, 1994, P.255-265.

82. Serwicka, E. M.; Black, J. B.; Goodenough, J. B. J. Catal., **1987**, 106, 23.

83. Ahmed, S.; Moffat, J. B. Appl. Catal. **1988**, 40, 101.

84. Siedle, A. R.; Newmark, R. A.; Gleason, W. B.; Skarjune, R. P.; Hodgson, K. O.; Roe, A. L.; Day, V. W. Solid State Ionics, **1988**, 26, 109.

85. Siedle, A. R.; Newmark, R. A.; Brown-Wensley, K. A.; Skarjune, R. P.; Haddad, L. C.; Hodgson, K.O.; Roe, A. L. Organometalics, **1988**, 7, 2078.

86. Kozhevnikov, I. V. Usp. Khim., **1987**, 56, 1417; Russ. Chem. Rev. (Engl. Transl.), **1987**, 56, 811.

87. Neumann, R.; Lissel, M. J. Org. Chem., **1989**, 54, 4607.

88. Hill, C. L.; Bouchard, D. A. J. Am. Chem. Soc., **1985**, 107, 148.

89. Yamase, T. Polyhedron, **1986**, 5, 79.

90. Faraj, M.; Hill, C. L. J. Chem. Soc. Chem. Commun., **1987**, 1487.

91. Kiwi, J.; Gratzel, M. J. Phys. Chem., **1987**, 91, 6673.

92. Keita, B.; Nadjo, L. J. Electroanal. Chem. Interfacial Electrochem., **1988**, 243, 87.

93. Willard, H. H; Merritt, Jr. L. L.; Dean, J. A., "Instrumental Methods of Analysis", 3rd Ed., D. van Nostrand Co., Inc., Princeton, 1963.

94. Varga, G. M. Jr. Doctoral Disseration, Georgetown University, 1968.

95. Papaconstantinou, E. Doctoral Disseration, Georgetown University, 1968.

96. Souchay, P. Talanta, **1965**, 12, 1187.

97. Pope, M. T., "Progress in Coordination Chemistry", Cais, M. Ed., (Proceedings of the Tenth International Conference on Coordination Chemistry, Haifa, Israel, 1967), Elsevier, 1968.

98. Ripan, R.; Duca, A.; Puscasiu, M.; Stanescu, D. Bull. Soc. Chim., **1961**, 765.

99. Harris, D. C. Quantitative Chemical Analysis; W. H. Freeman and Company: New York, 1982; Chapter 18.

100. Przybytek, J. T. High Purity Solvent Guide; Burdick & Jackson Laboratories: Michigan, 1980; p 125.

Appendix A

Figures

Figure 1

Keggin Structure (T_d)
1:12 Heteropoly Anion

Based upon Basic (parent) Clusters with High Symmetry Built up from MO_6 Octahedra with a Central Tetrahedron (O_4),
e.g. $[W_{12}O_{36}(PO_4)]^{3-}$

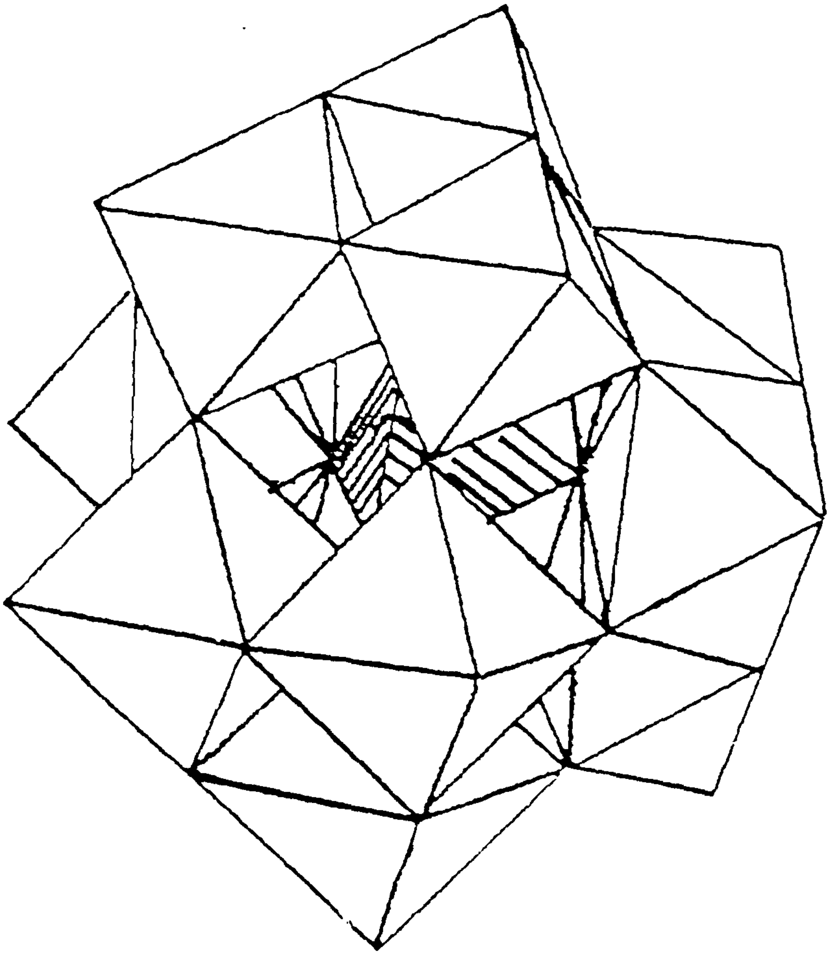

Figure 2

Parent Cluster with a Central Octahedron

Based upon Basic (parent) Clusters with High Symmetry Built up from MO_6 Octahedra with a Central Octahedron (O_6), e.g. $[(OV)_2V_{12}O_{32}(AsO_6)]^{7-}$

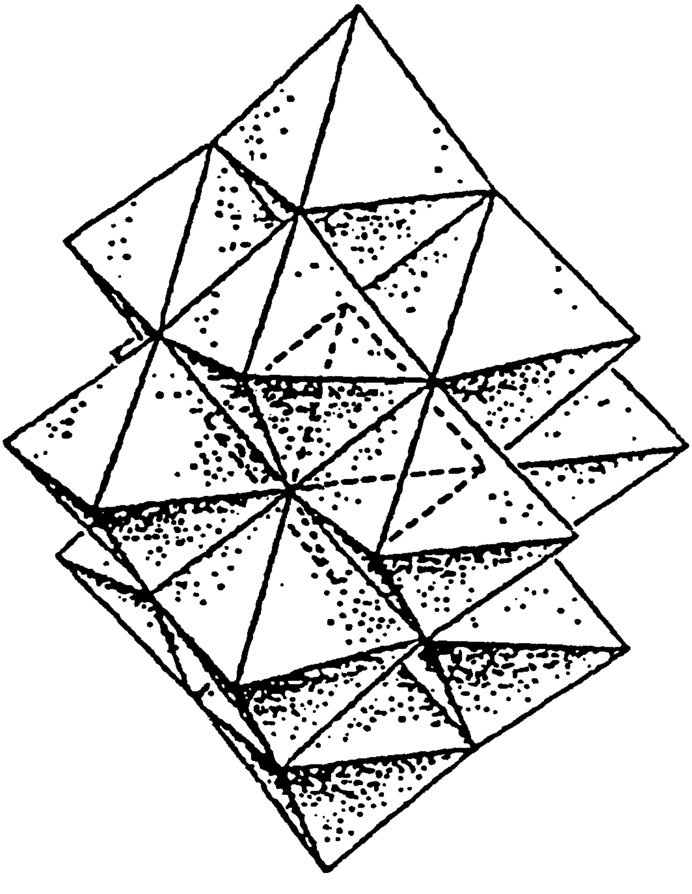

Figure 3

Silverton Structure

Based upon Basic (parent) Clusters with High Symmetry Built up from MO_6 Octahedra with a Central Icosahedron (O_{12}),
e.g. $[Mo_{12}O_{30}(CeO_{12})]^{8-}$

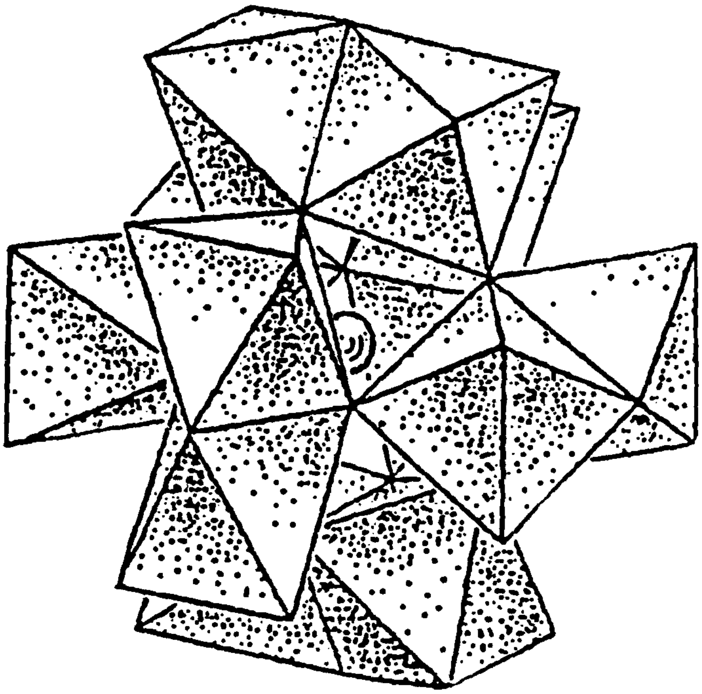

Figure 4

Another Parent Cluster with a Central Tetrahedron

Based upon Basic (parent) Clusters with High Symmetry Built up from MO_6 Octahedra with a Central Tetrahedron(O_4),
e.g. $[H_6V_{18}O_{42}(VO_4)]^{6-}$

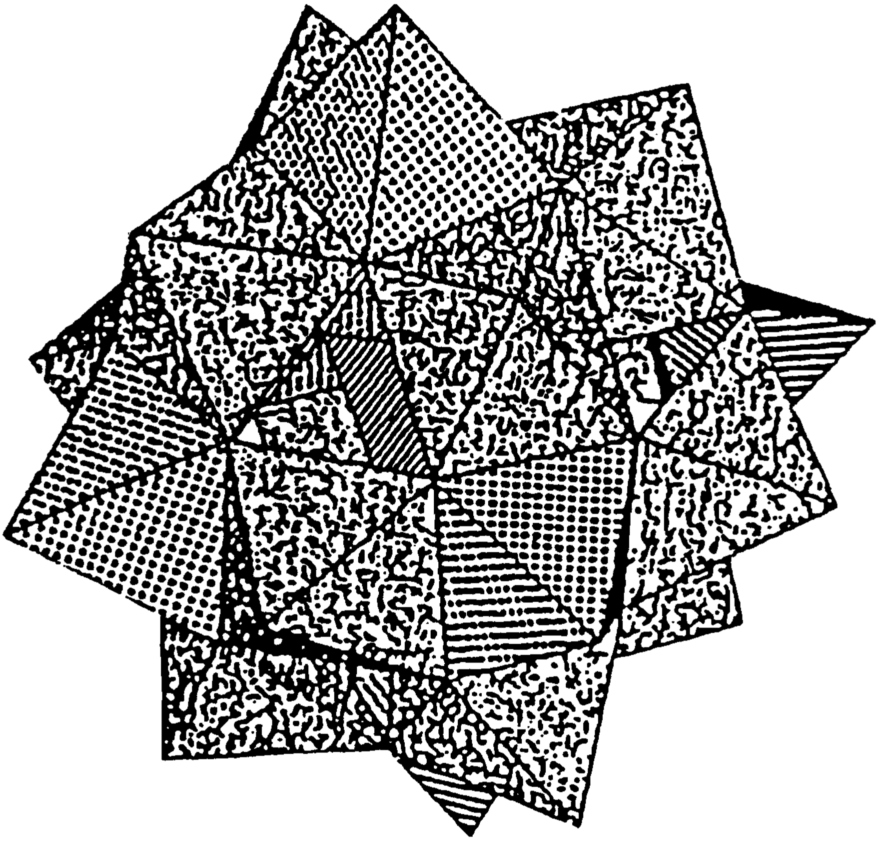

Figure 5

Modification of Keggin Structure(T_d)
1:1:11 Heteropoly Anion

Based upon Basic (parent) Clusters with High Symmetry Built up from MO_6 Octahedra with a Central Tetrahedron (O_4), e.g. $[SiO_4W_{11}O_{30}CoO_6H_2]$

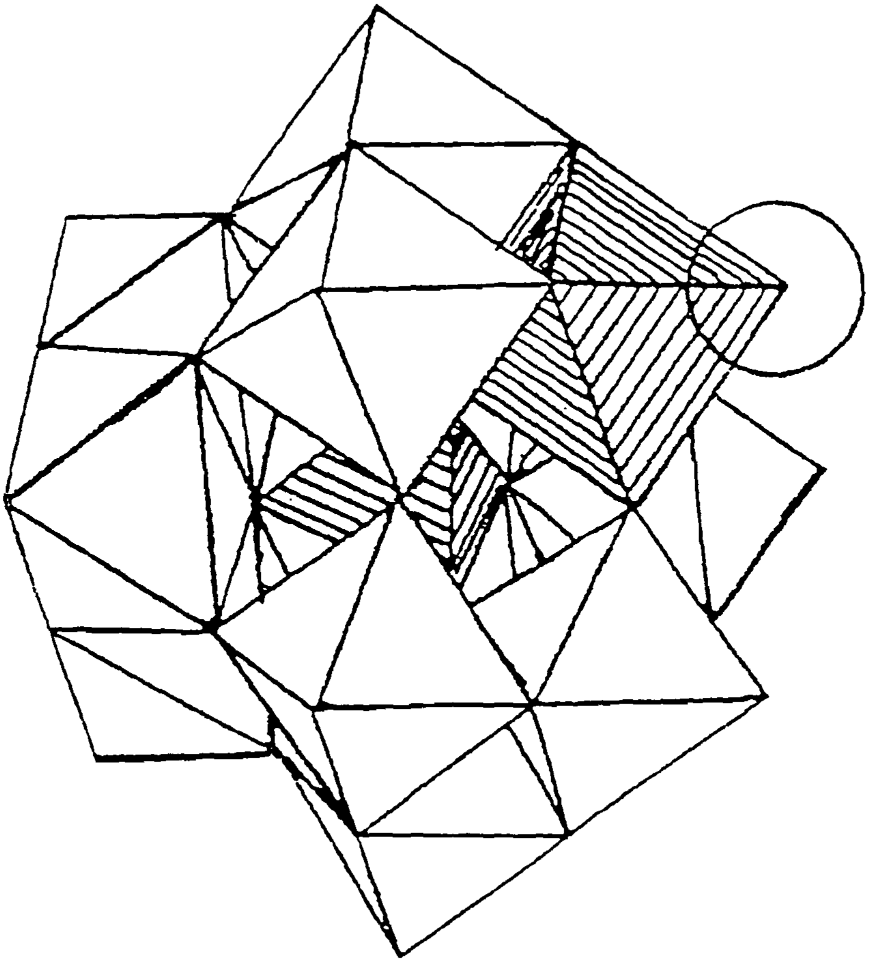

Figure 6

Molecular Orbital Scheme for MOL_5 Complexes of C_{4v} Symmetry

Assuming No Inplane (xy) Pi-bonding

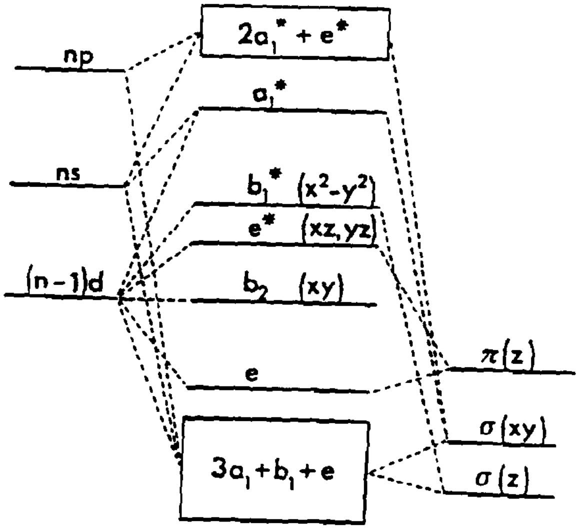
$2a_1^* + e^*$
np
a_1^*
ns
b_1^* (x^2-y^2)
e^* (xz,yz)
$(n-1)d$
b_2 (xy)
$\pi(z)$
e
$\sigma(xy)$
$3a_1+b_1+e$
$\sigma(z)$

Figure 7

Comparison of the Reduction Potentials for Primes and Unprimed Series of Reduced 1-molybdosilicates

(From Ref. Launay, J. P., Doctoral Thesis, Universite Pierre et Marie Curie, Paris, 1974)

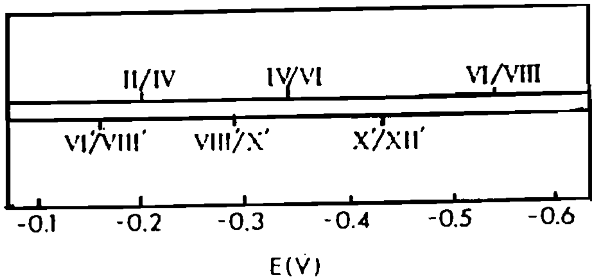
II/IV
IV/VI
VI/VIII
VI'/VIII'
VIII'/X'
X'/XII'
-0.1
-0.2
-0.3
-0.4
-0.5
-0.6
E(V)

Figure 8

Variation of Half-wave Potentials of $XW_{12}O_{40}{}^{n-}$ with Ionic Charge

X=P(V), Si(IV), Fe(III), Co(II) and H_2: ○ and ●, First and Second One-electron Reductions Respectively [57]

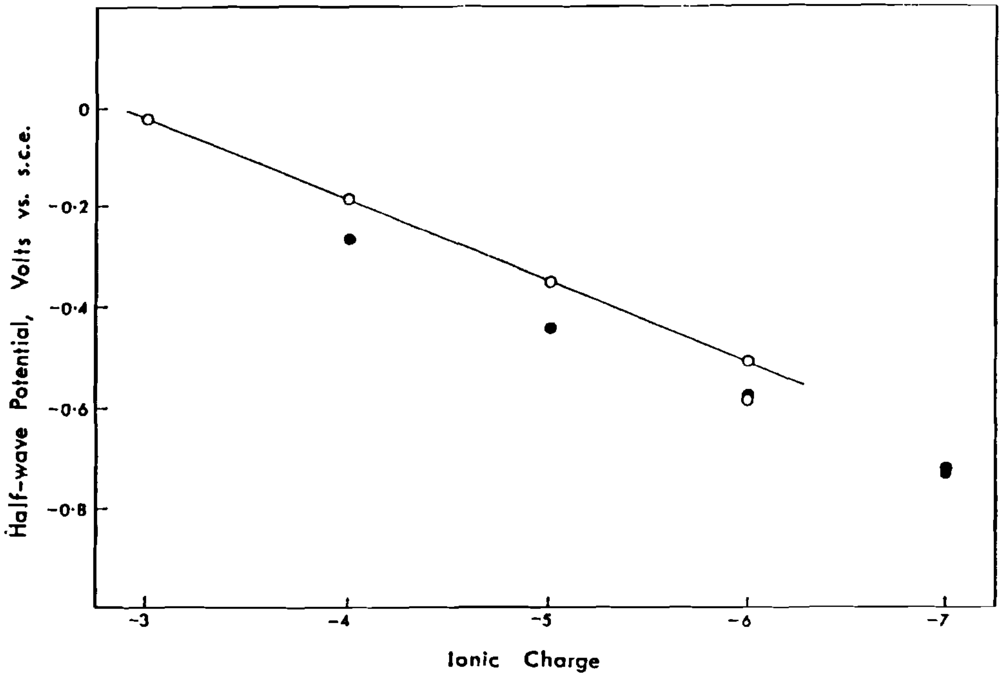
Half-wave Potential, Volts vs. s.c.e.
0
-0·2
-0·4
-0·6
-0·8
-3
-4
-5
-6
-7
Ionic Charge

Figure 9

A Sketch of the Scrubbing Tower

(Nitrogen De-oxygenation Device)

1. Empty
2. 0.1 M vanadium(II) in 0.5 M sulfuric acid and amalgamated zinc
3. Empty
4. Water
5. Empty

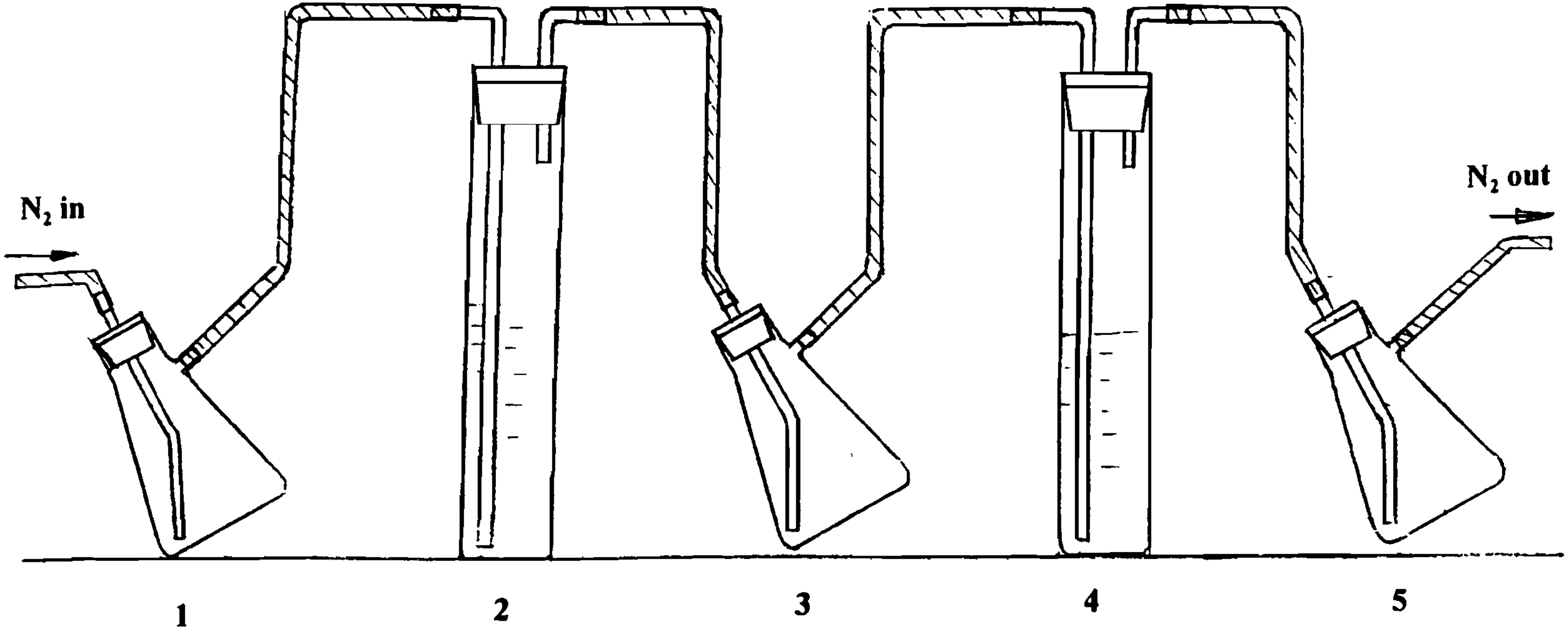

Figure 10

A Graphical Method of the Wave Heights and Half-wave Potentials

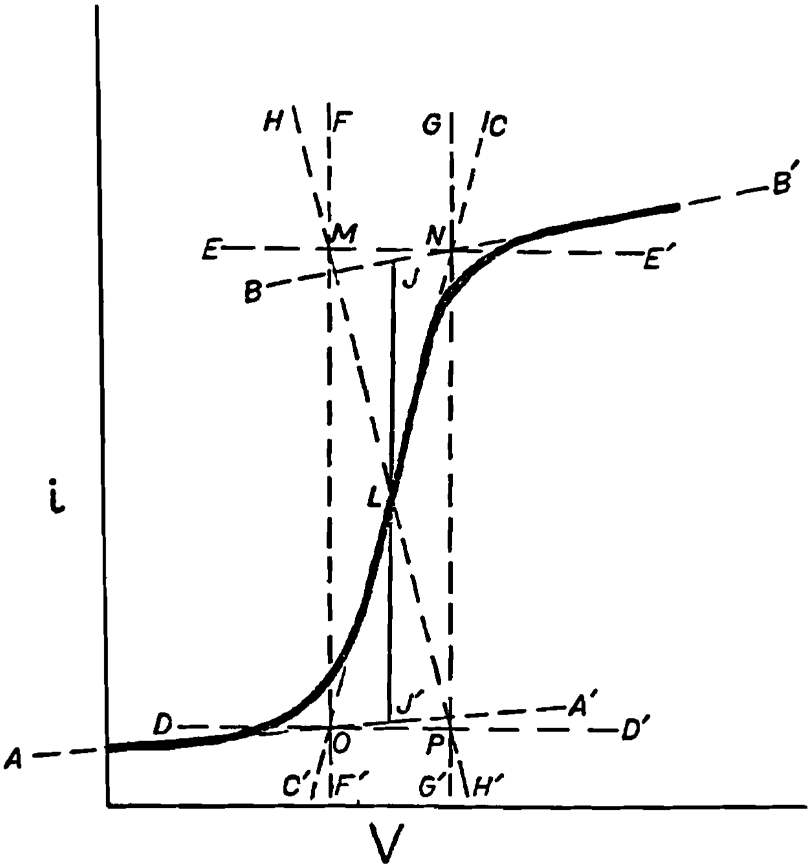

H
F
G
C
B'
E
M
N
E'
B
J
i
L
J'
A'
D
D'
A
O
P
C'
F'
G'
H'
V

Figure 11

DME Polarogram of pH 4.99 Buffer

0.1 M Sodium Acetate/acetic Acid Buffer in 1.0 M Sodium Sulfate after Oxygen-free Nitrogen Bubbled for Fifteen Minutes.

Current range: 0.5 μA
Sweep rate : 10 mV/sec
Scan range : from +0.214 to -1.800 V
Record : 2.5 cm/min
Knock timer : 0
Temperature : 23.0 °C

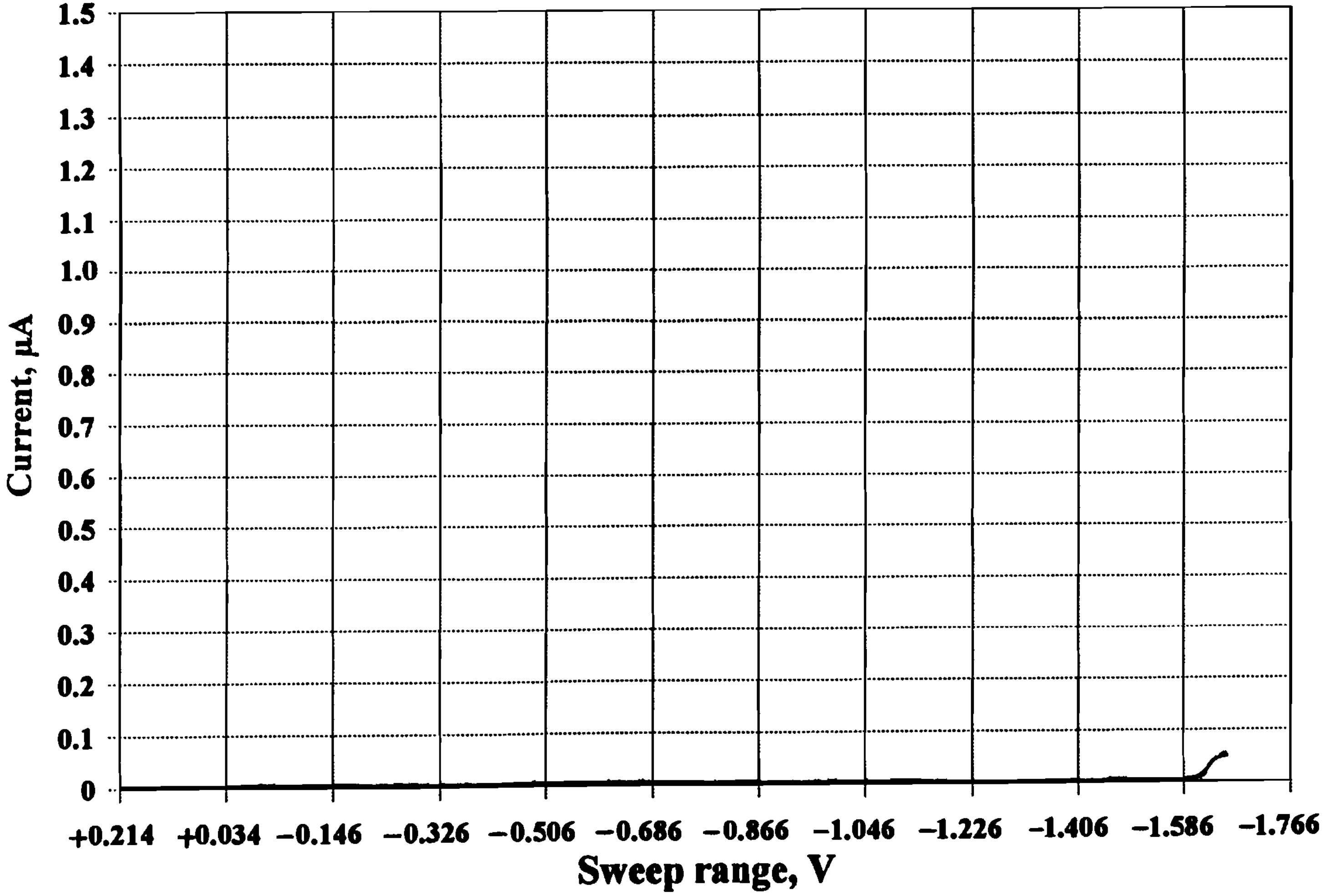
1.5
1.4
1.3
1.2
1.1
1.0
0.9
0.8
0.7
0.6
0.5
0.4
0.3
0.2
0.1
0
Current, μA
+0.214
+0.034
−0.146
−0.326
−0.506
−0.686
−0.866
−1.046
−1.226
−1.406
−1.586
−1.766
Sweep range, V

Figure 12

DME Polarogram of $K_6[SiO_4W_{11}O_{30}CoO_6H_2]\cdot15H_2O$ at pH 5.07 with 0.050 mL IPA.

Current range : 2 µA
Sweep rate : 10 mV/sec
Scan range : from -0.600 to -1.750 V
Record : 2.5 cm/min
Knock timer : 1.0
Temperature : 23.2 °C
Conc. of HPC : 9.3×10^{-4} M

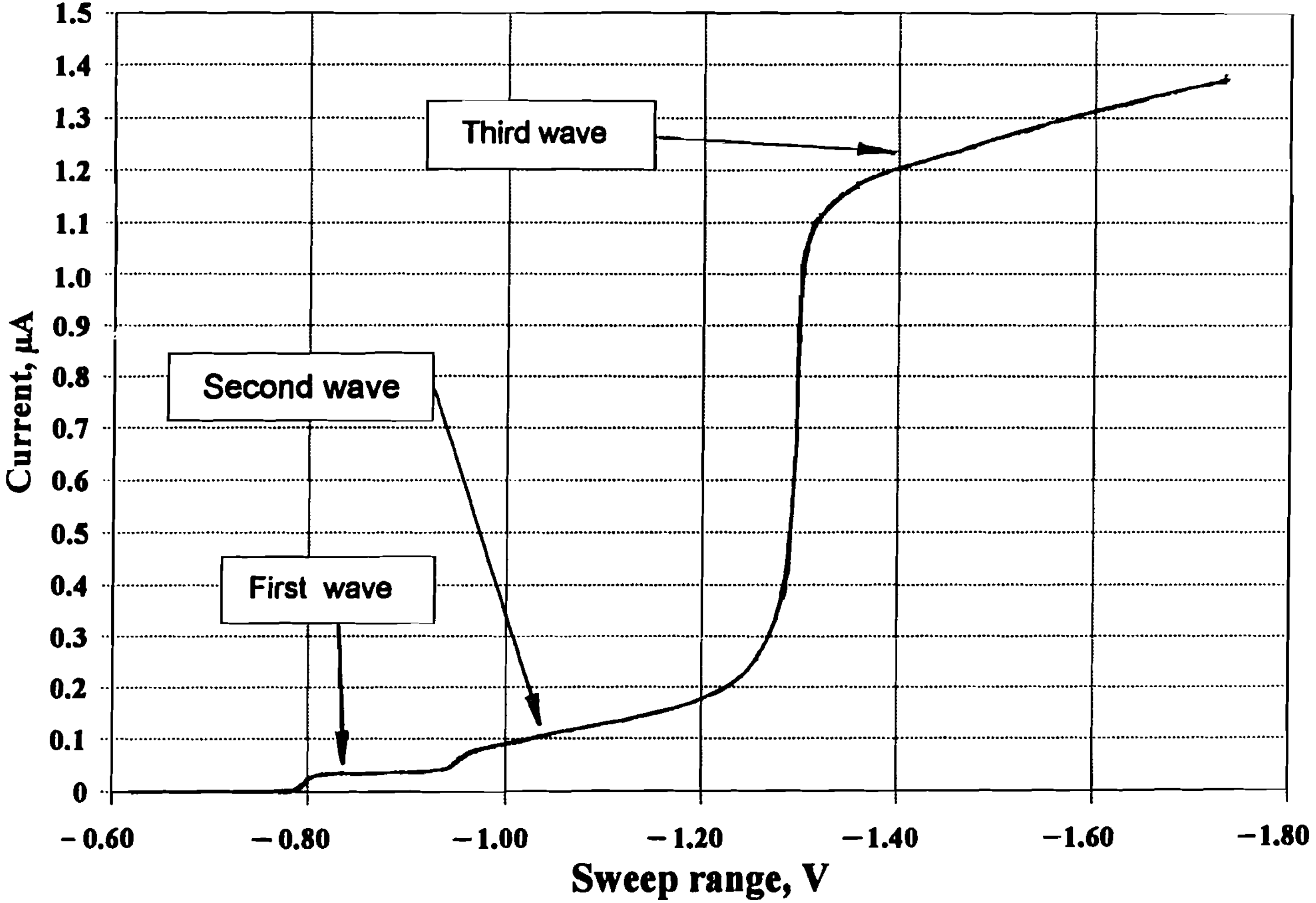
1.5
1.4
1.3
1.2
1.1
1.0
0.9
0.8
0.7
0.6
0.5
0.4
0.3
0.2
0.1
0
Current, µA
Third wave
Second wave
First wave
− 0.60
− 0.80
−1.00
−1.20
−1.40
−1.60
−1.80
Sweep range, V

Figure 13

DME Polarogram of $K_6[SiO_4W_{11}O_{30}CoO_6H_2]\cdot 15\ H_2O$ at pH 4.99 with 0.050 mL Acetone

Current range: 2 μA
Sweep rate : 15 mV/sec
Scan range : from -0.600 to -1.750 V
Record : 2.5 cm/min
Knock timer : 1.0
Temperature : 25.0 °C
Conc. of HPC : 9.3×10^{-4} M

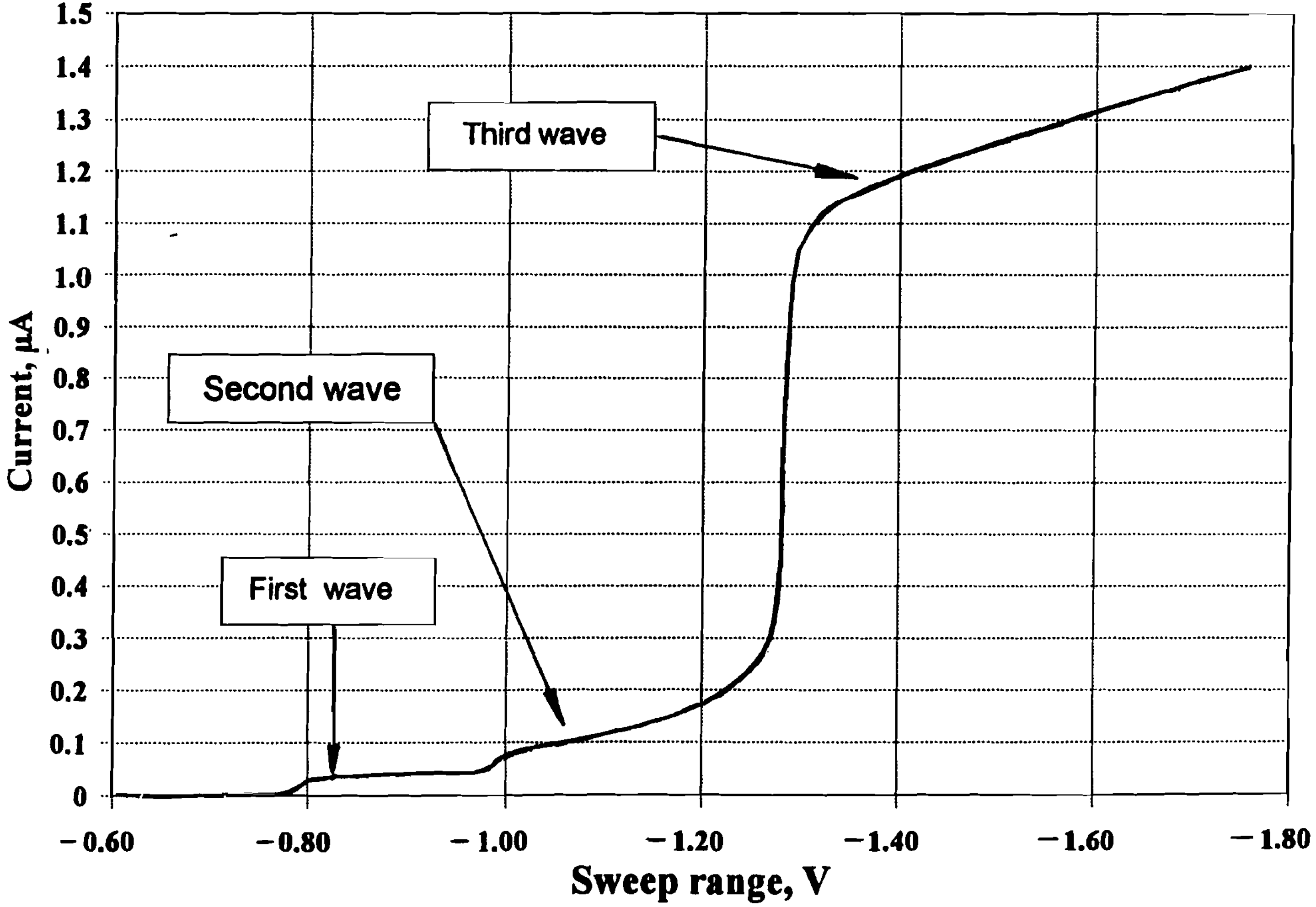
1.5
1.4
1.3
1.2
1.1
1.0
0.9
0.8
0.7
0.6
0.5
0.4
0.3
0.2
0.1
0
Current, μA
Third wave
Second wave
First wave
− 0.60
− 0.80
− 1.00
− 1.20
−1.40
−1.60
− 1.80
Sweep range, V

Figure 14

DME Polarogram of $K_6[SiO_4W_{11}O_{30}CoO_6H_2]\cdot 15H_2O$ at pH 4.97 with 0.20 mL ACN

Current range : 2 μA
Sweep rate : 15 mV/sec
Scan range : from -0.600 to -1.730 V
Record : 2.5 cm/min
Knock timer : 1.0
Temperature : 26.0 °C
Conc. of HPC : 9.3×10^{-4} M

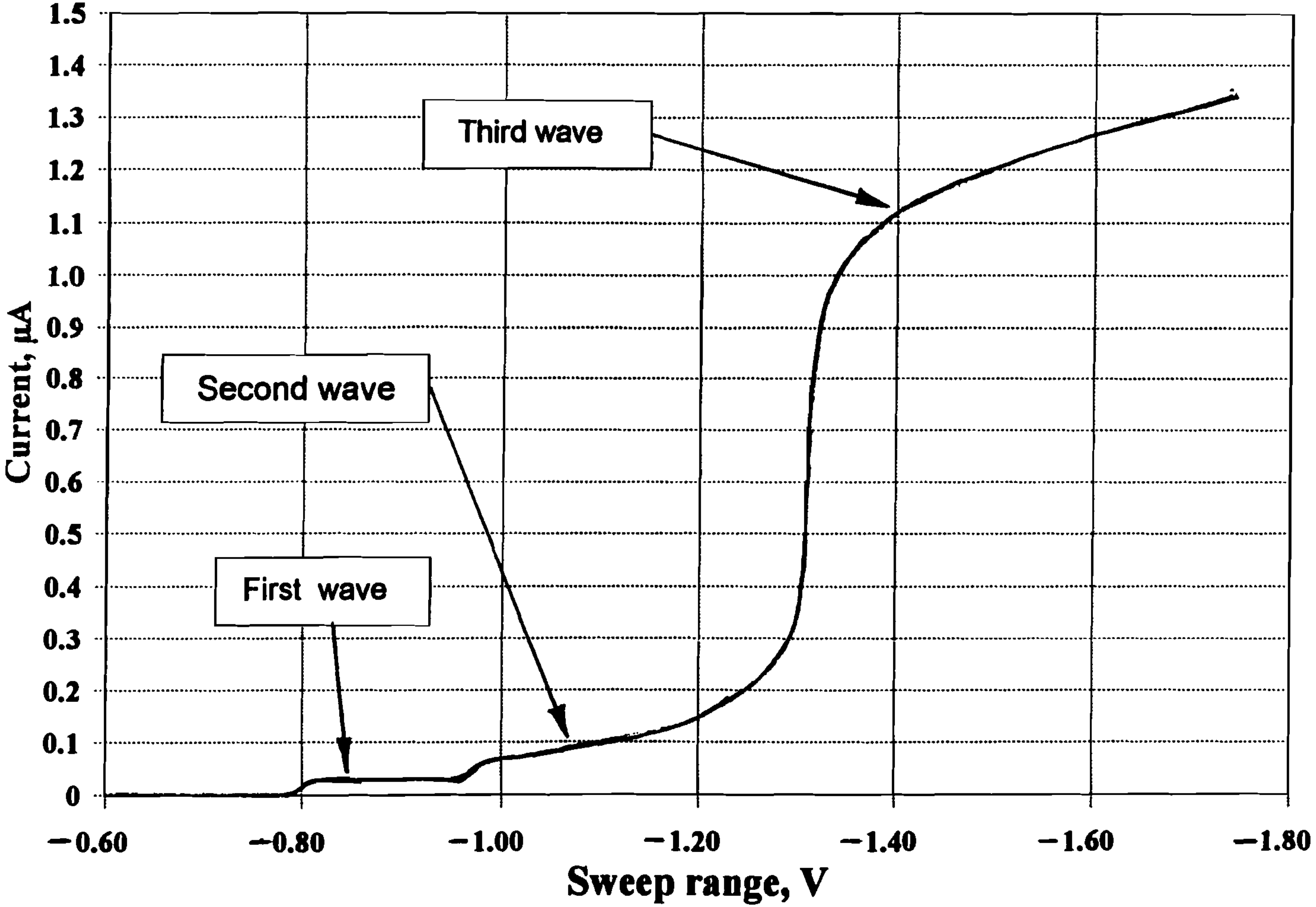
Third wave
Second wave
First wave
Current, µA
1.5
1.4
1.3
1.2
1.1
1.0
0.9
0.8
0.7
0.6
0.5
0.4
0.3
0.2
0.1
0
−0.60
−0.80
−1.00
−1.20
−1.40
−1.60
−1.80
Sweep range, V

Figure 15

DME Polarogram of $K_6[SiO_4W_{11}O_{30}CoO_6H_2]\cdot 15H_2O$ at pH 4.87 without any Organic Substrate

Current range: 2 μA
Sweep rate : 15 mV/sec
Scan range : from -0.600 to -1.750 V
Record : 2.5 cm/min
Knock timer : 1.0
Temperature : 24.5 °C
Conc. of HPC : 5.2×10^{-4} M

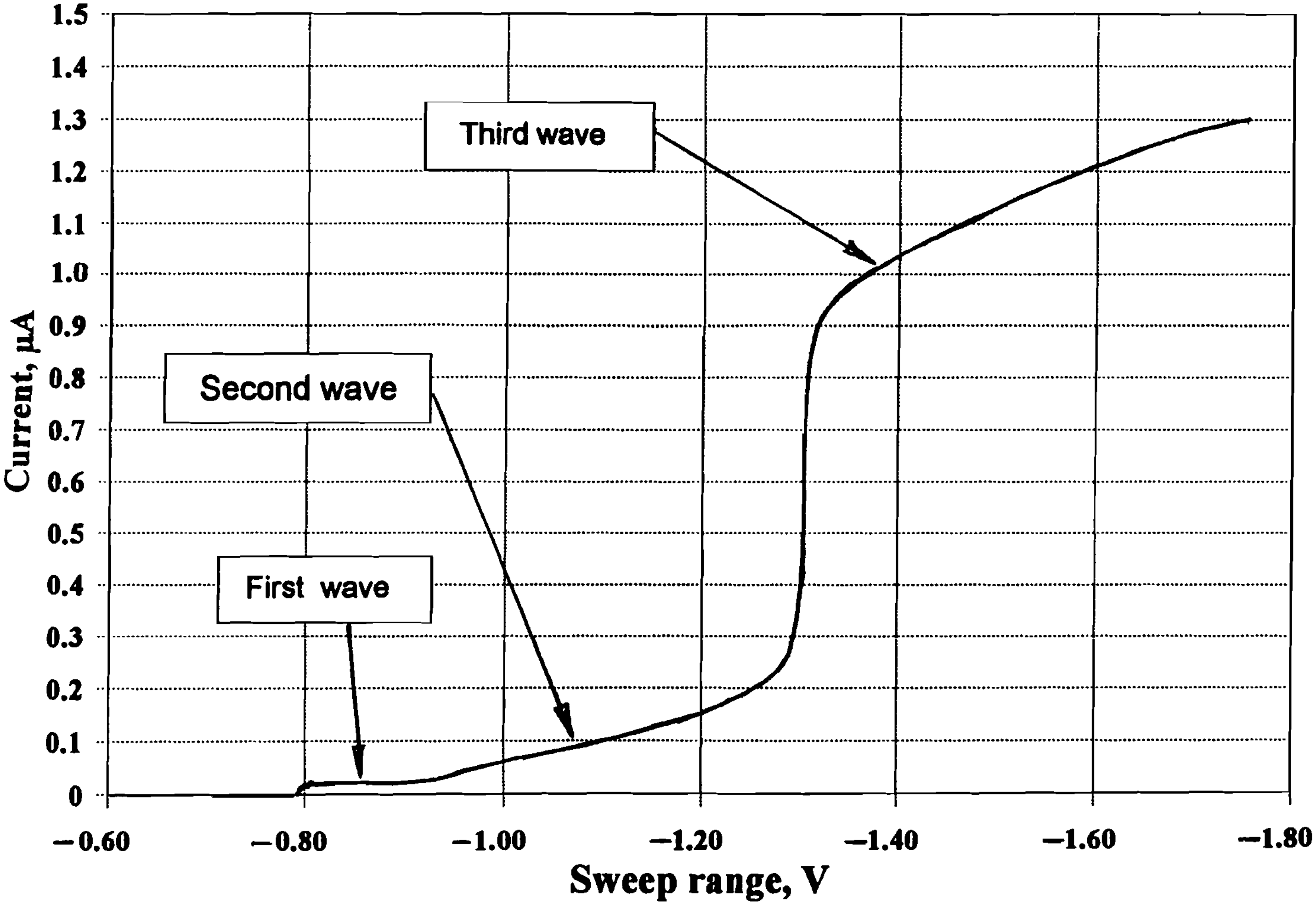
Current, µA
1.5
1.4
1.3
1.2
1.1
1.0
0.9
0.8
0.7
0.6
0.5
0.4
0.3
0.2
0.1
0
−0.60
−0.80
−1.00
−1.20
−1.40
−1.60
−1.80
Sweep range, V
Third wave
Second wave
First wave

Figure 16

DME Polarogram of $K_6[SiO_4W_{11}O_{30}CoO_6H_2]\cdot15H_2O$ at pH 4.87 with 0.050 mL IPA

Current range: 2 μA
Sweep rate : 15 mV/sec
Scan range : from -0.600 to -1.20 V
Record : 2.5 cm/min
Knock timer : 1.0
Temperature : 24.5 °C
Conc. of HPC : 5.2 x 10^{-4} M

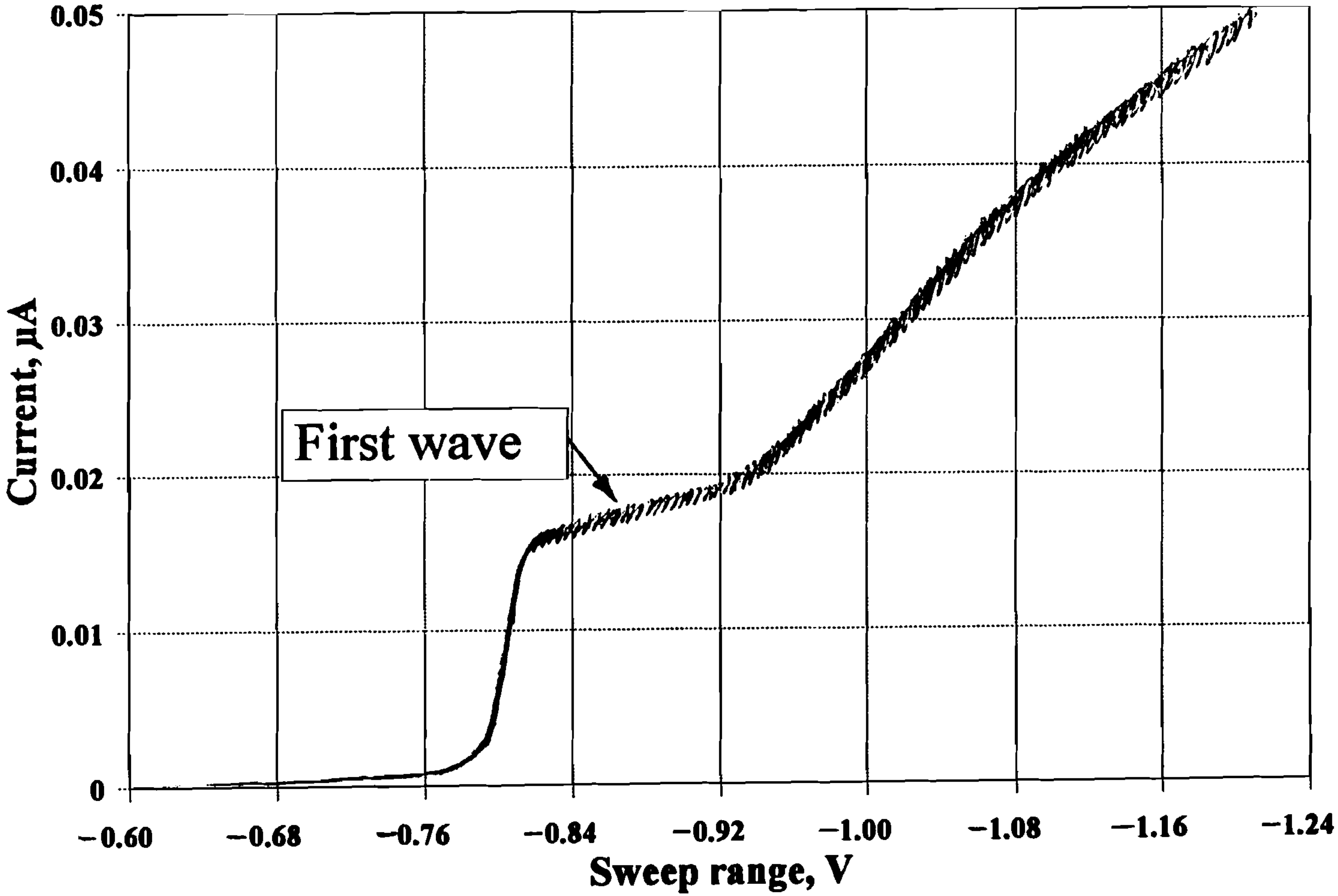
0.05
0.04
0.03
0.02
0.01
0
Current, µA
First wave
−0.60
−0.68
−0.76
−0.84
−0.92
−1.00
−1.08
−1.16
−1.24
Sweep range, V

Figure 17

DME Polarogram of $H_3[PW_{12}O_{40}]\cdot 29\ H_2O$ at pH 4.84 with 0.075 mL IPA

Current range: 2 µA
Sweep rate : 10 mV/sec
Scan range : from -0.600 to -1.730 V
Record : 2.5 cm/min
Knock timer : 1.0
Temperature : 25.0 °C
Conc. of HPC : 9.2×10^{-4} M

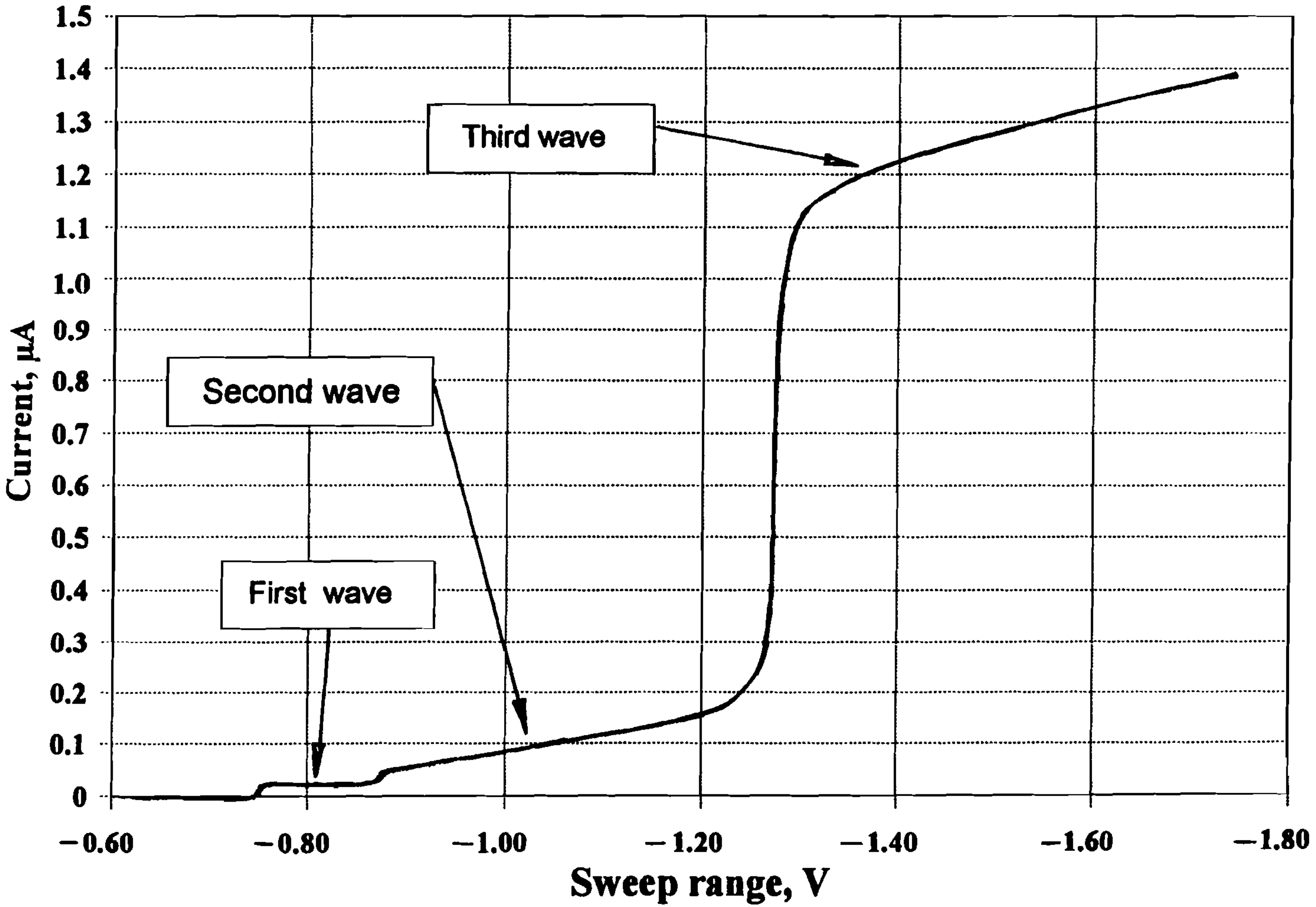
Third wave
Second wave
First wave
Current, μA
1.5
1.4
1.3
1.2
1.1
1.0
0.9
0.8
0.7
0.6
0.5
0.4
0.3
0.2
0.1
0
−0.60
−0.80
−1.00
−1.20
−1.40
−1.60
−1.80
Sweep range, V

Figure 18

DME Polarogram of $H_3[PW_{12}O_{40}]\cdot 29\ H_2O$ at pH 4.84 with 0.075 mL Acetone

Current range: 2 μA
Sweep rate : 10 mV/sec
Scan range : from -0.600 to -1.730 V
Record : 2.5 cm/min
Knock timer : 1.0
Temperature : 25.2 °C
Conc. of HPC : 9.2 x 10^{-4} M

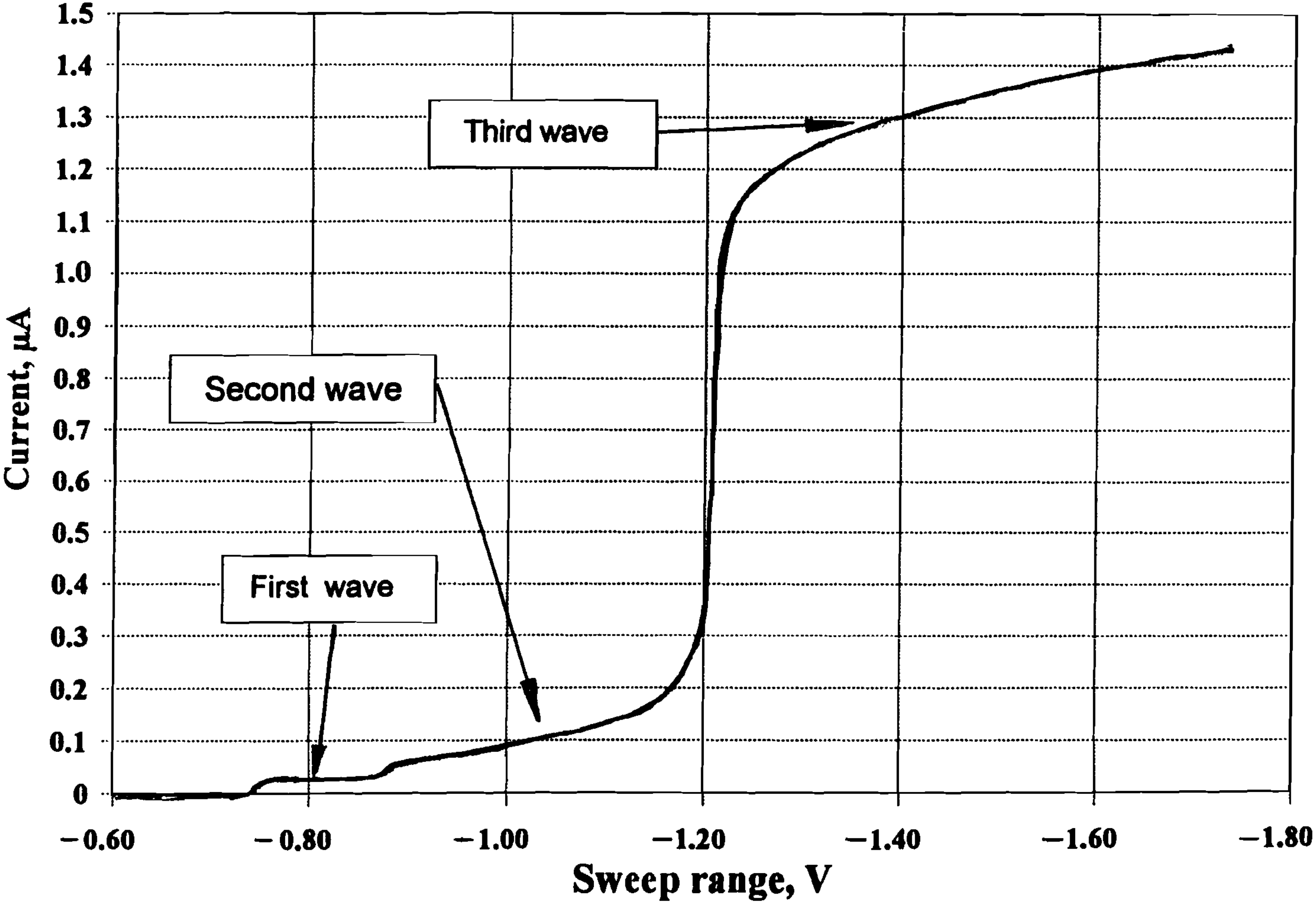

1.5
1.4
1.3
1.2
1.1
1.0
0.9
0.8
0.7
0.6
0.5
0.4
0.3
0.2
0.1
0
Current, μA
Third wave
Second wave
First wave
−0.60
−0.80
−1.00
−1.20
−1.40
−1.60
−1.80
Sweep range, V

Figure 19

DME Polarogram of $H_3[PW_{12}O_{40}]\cdot 29H_2O$ at pH 4.86 with 0.075 mL ACN

Current range: 2 μA
Sweep rate : 10 mV/sec
Scan range : from -0.600 to -1.730 V
Record : 2.5 cm/min
Knock timer : 1.0
Temperature : 26.0 °C
Conc. of HPC : 9.2×10^{-4} M

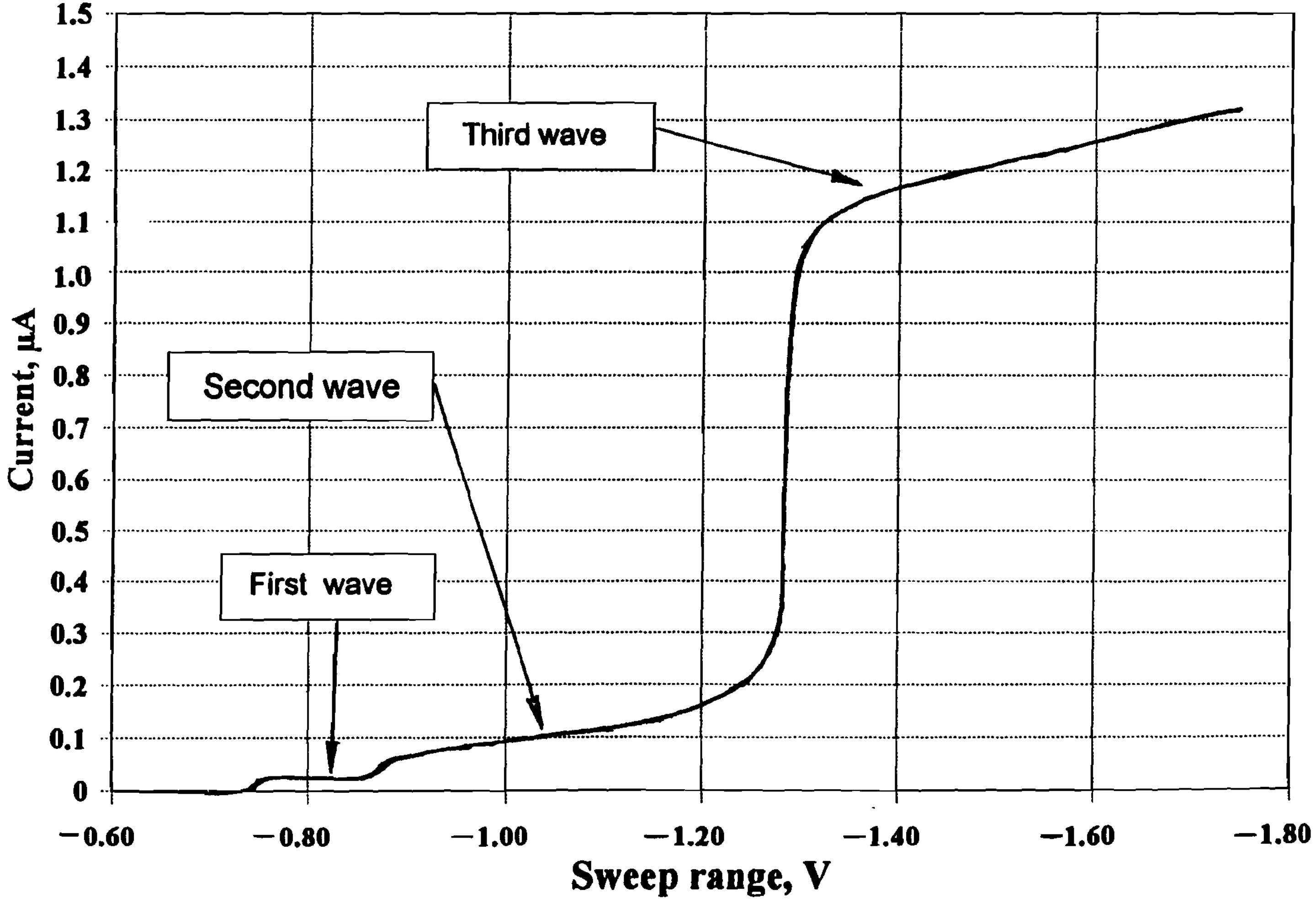
Third wave
Second wave
First wave
1.5
1.4
1.3
1.2
1.1
1.0
0.9
0.8
0.7
0.6
0.5
0.4
0.3
0.2
0.1
0
Current, µA
−0.60
−0.80
−1.00
−1.20
−1.40
−1.60
−1.80
Sweep range, V

Figure 20

The Peak Heights of First-wave(μA) Versus Concentration of IPA(M) with Constant Concentration of 9.326 x 10^{-4} M $K_6[SiO_4W_{11}O_{30}CoO_6H_2]\cdot15H_2O$

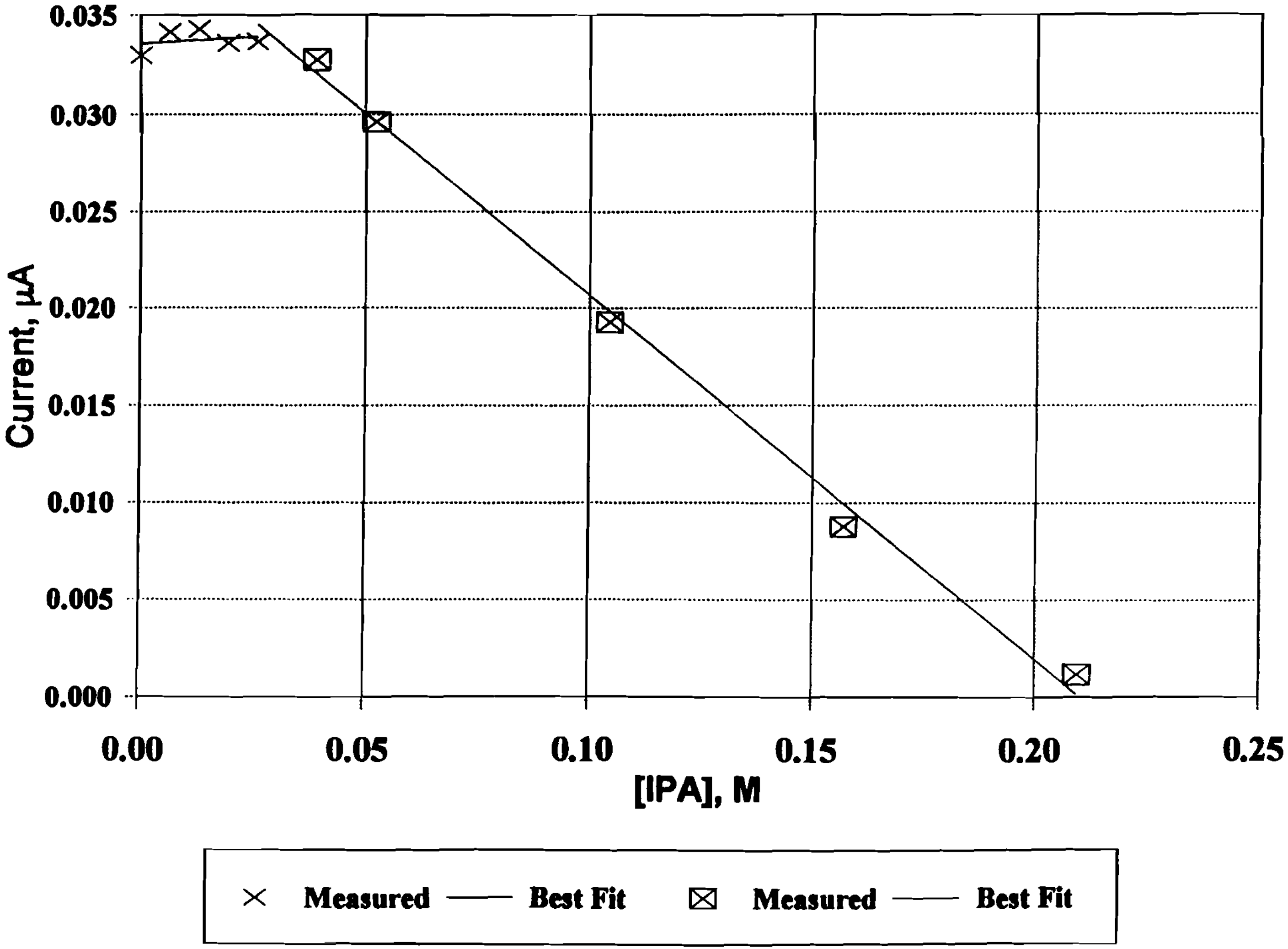
0.035
0.030
0.025
0.020
0.015
0.010
0.005
0.000
Current, µA
0.00
0.05
0.10
0.15
0.20
0.25
[IPA], M
Measured
Best Fit
Measured
Best Fit

Figure 21

The Peak Heights of First-wave(μA) Versus Concentration of Acetone(M) with Constant Concentration of 9.326 x 10^{-4} M $K_6[SiO_4W_{11}O_{30}CoO_6H_2]\cdot 15H_2O$

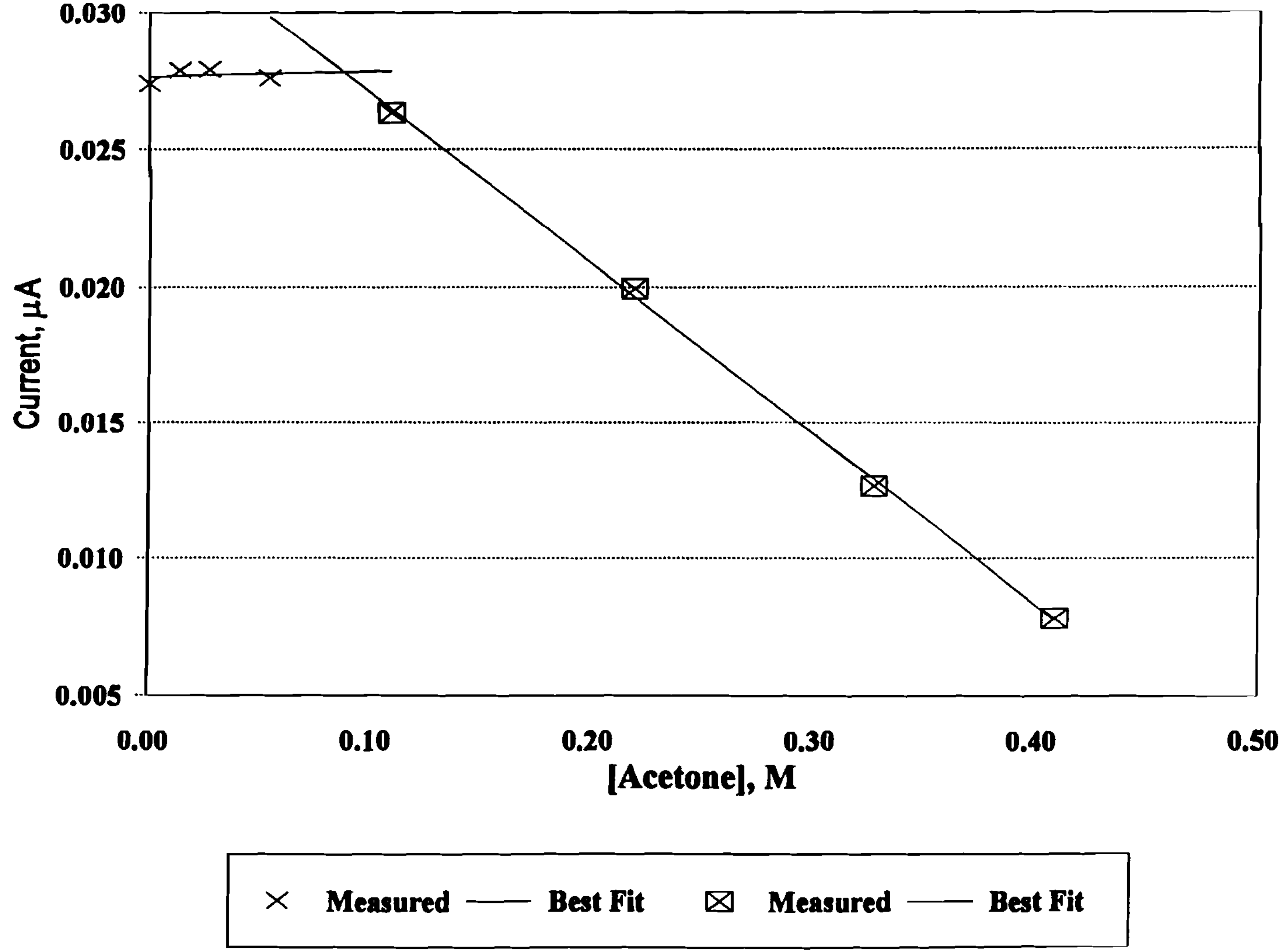
0.030
0.025
0.020
0.015
0.010
0.005
Current, µA
0.00
0.10
0.20
0.30
0.40
0.50
[Acetone], M
× Measured
—— Best Fit
⊠ Measured
—— Best Fit

Figure 22

The Peak Heights of First-wave(μA) Versus Concentration of ACN(M) with Constant Concentration of 9.326 x 10^{-4} M $K_6[SiO_4W_{11}O_{30}CoO_6H_2]\cdot 15H_2O$

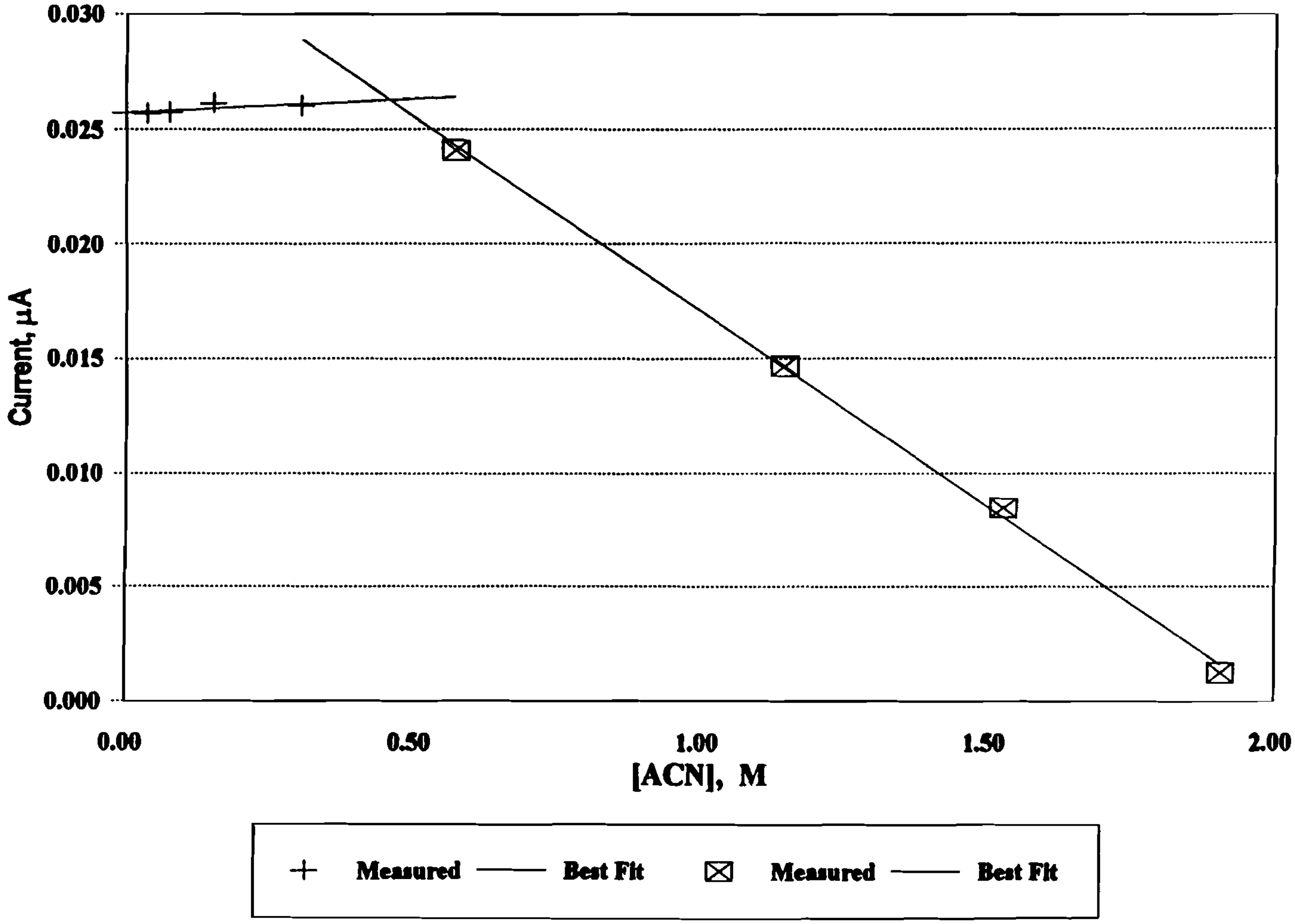
0.030
0.025
0.020
0.015
0.010
0.005
0.000
Current, μA
0.00
0.50
1.00
1.50
2.00
[ACN], M
Measured
Best Fit
Measured
Best Fit

Figure 23

The Peak Heights of First-wave(μA) Versus Concentration of IPA(M) with Constant Concentration of 5.227 x 10^{-4} M $K_6[SiO_4W_{11}O_{30}CoO_6H_2]\cdot15H_2O$

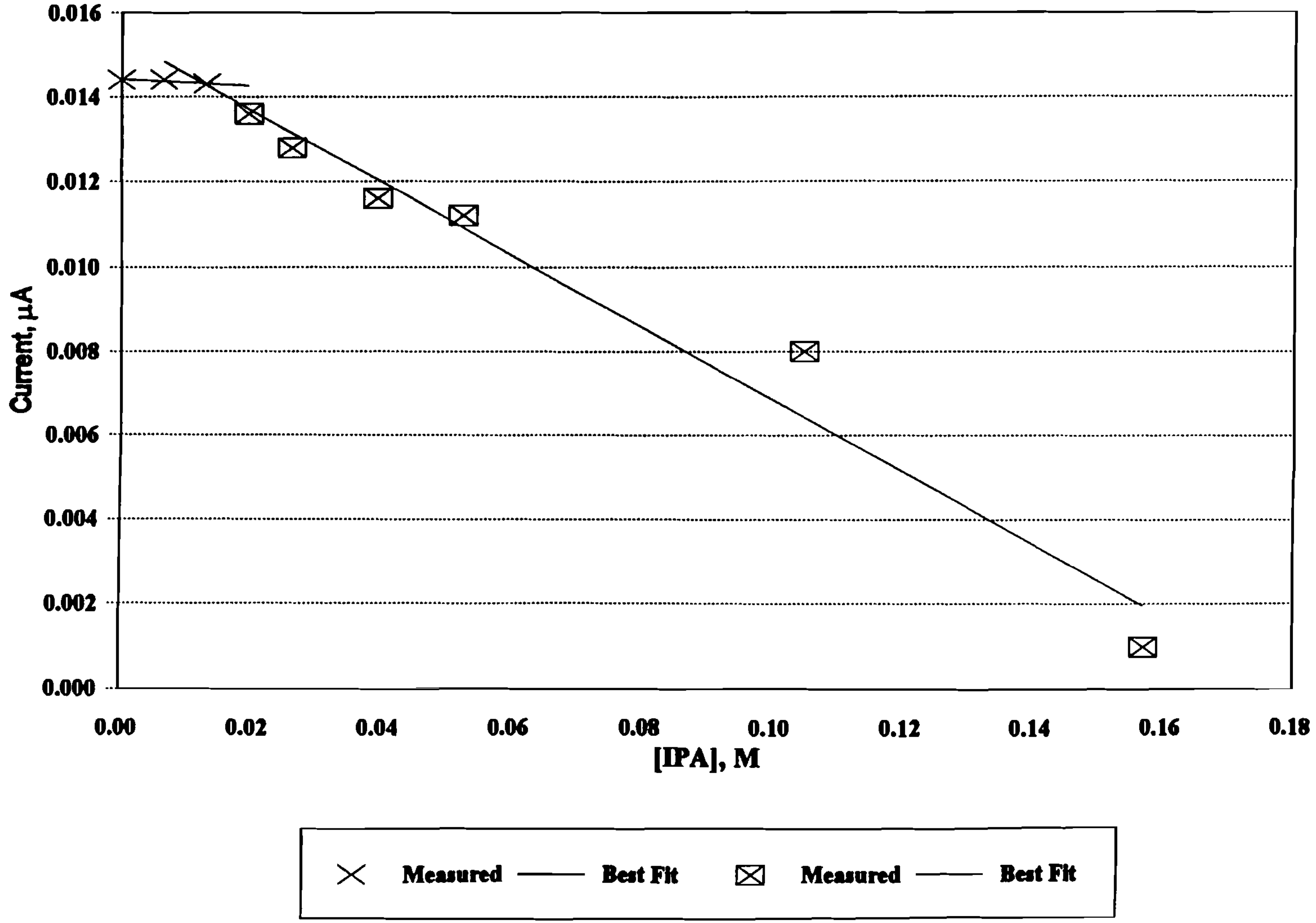
0.016
0.014
0.012
0.010
0.008
0.006
0.004
0.002
0.000
Current, µA
0.00
0.02
0.04
0.06
0.08
0.10
0.12
0.14
0.16
0.18
[IPA], M
Measured
Best Fit
Measured
Best Fit

Figure 24

The Peak Heights of First-wave(μA) Versus Concentration of IPA(M) with Constant Concentration of 9.17 x 10^{-4} M $H_3[PW_{12}O_{40}]\cdot 29H_2O$

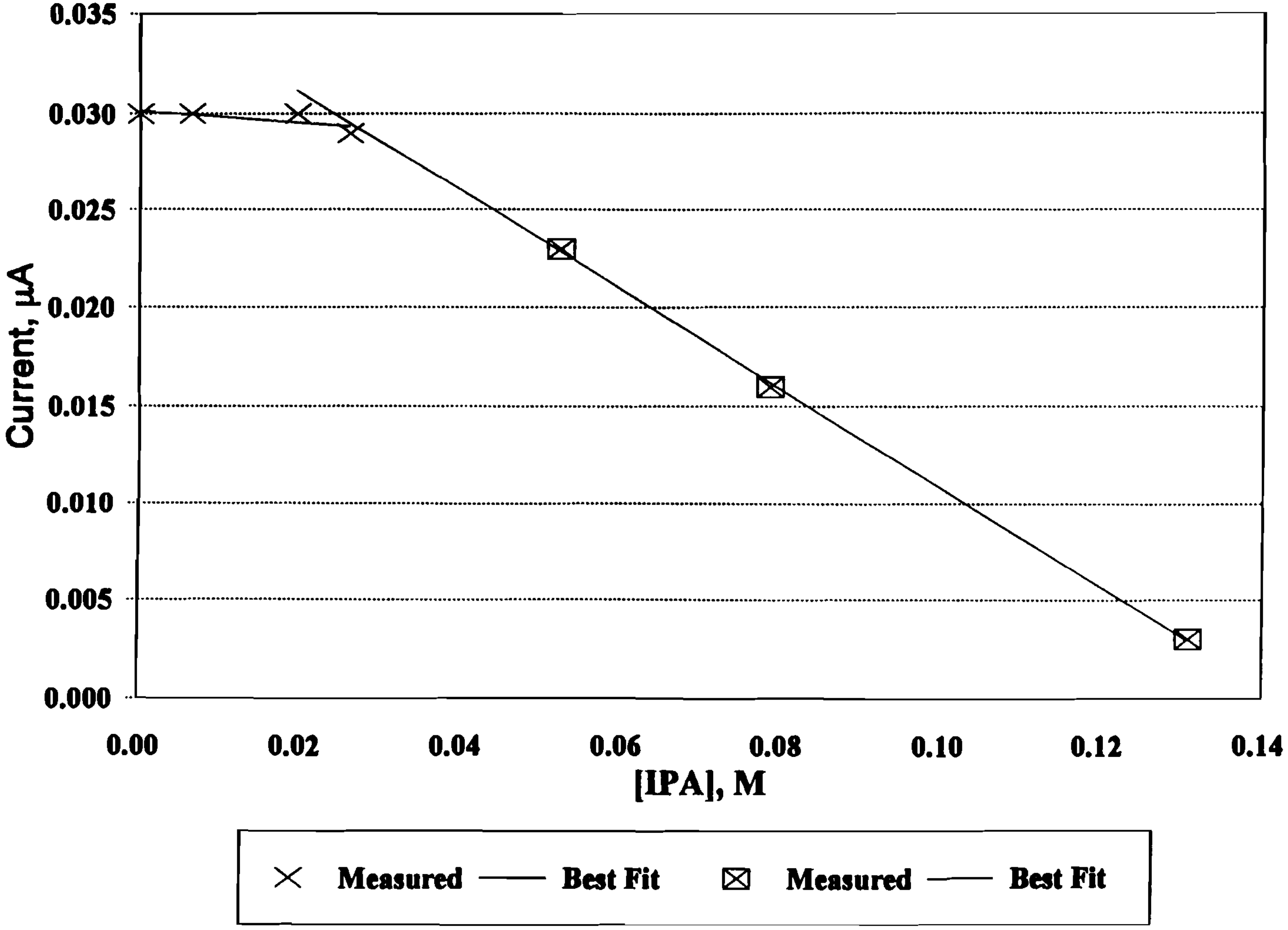
0.035
0.030
0.025
0.020
0.015
0.010
0.005
0.000
Current, µA
0.00
0.02
0.04
0.06
0.08
0.10
0.12
0.14
[IPA], M
Measured
Best Fit
Measured
Best Fit

Figure 25

The Peak Heights of First-wave(μA) Versus Concentration of Acetone(M) with Constant Concentration of 9.17×10^{-4} M $H_3[PW_{12}O_{40}]\cdot 29H_2O$

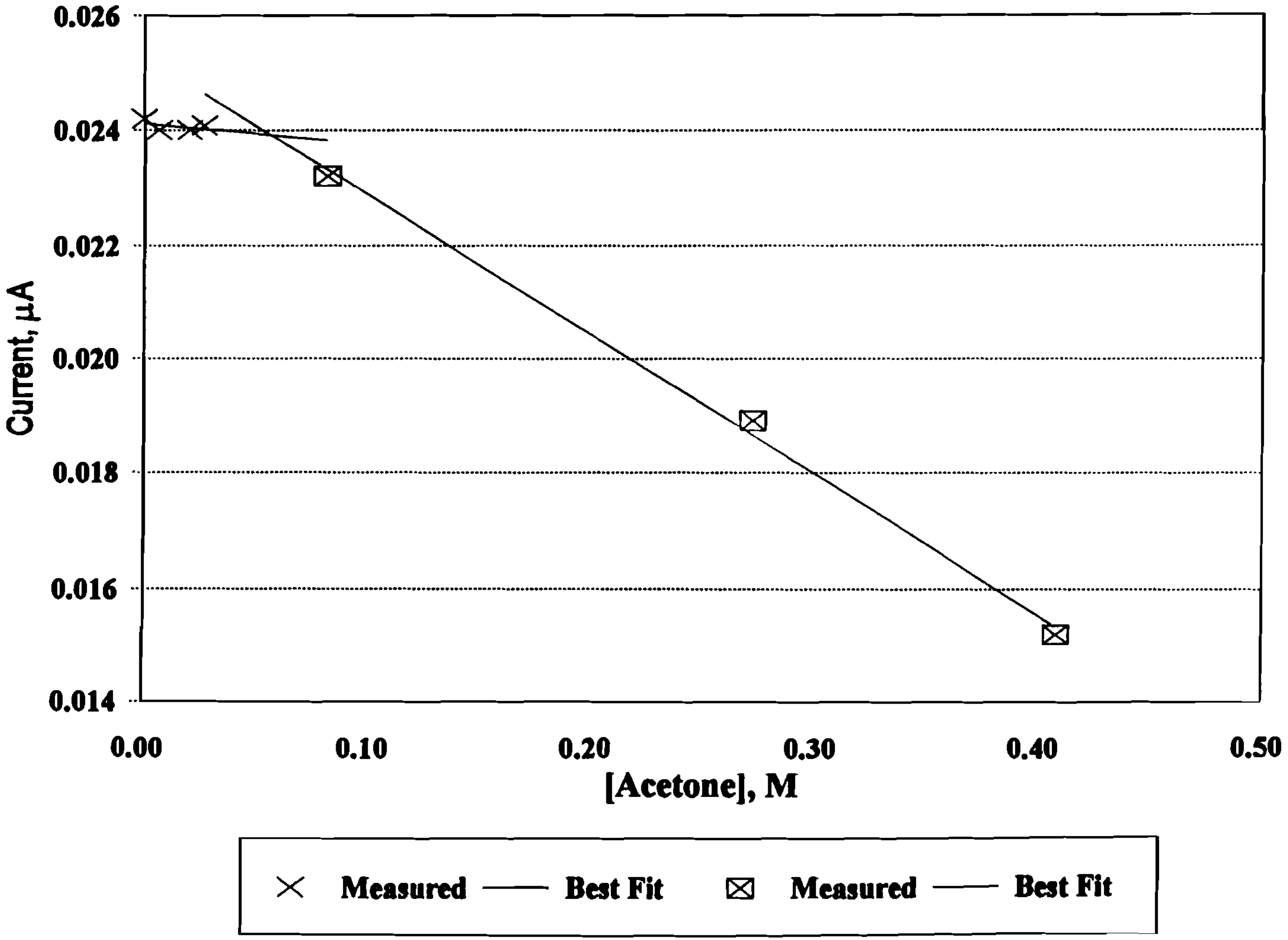
0.026
0.024
0.022
0.020
0.018
0.016
0.014
Current, μA
0.00
0.10
0.20
0.30
0.40
0.50
[Acetone], M
Measured
Best Fit
Measured
Best Fit

Figure 26

The Peak Heights of First-wave(μA) Versus Concentration of ACN(M) with Constant Concentration of 9.17 x 10^{-4} M $H_3[PW_{12}O_{40}]\cdot 29H_2O$

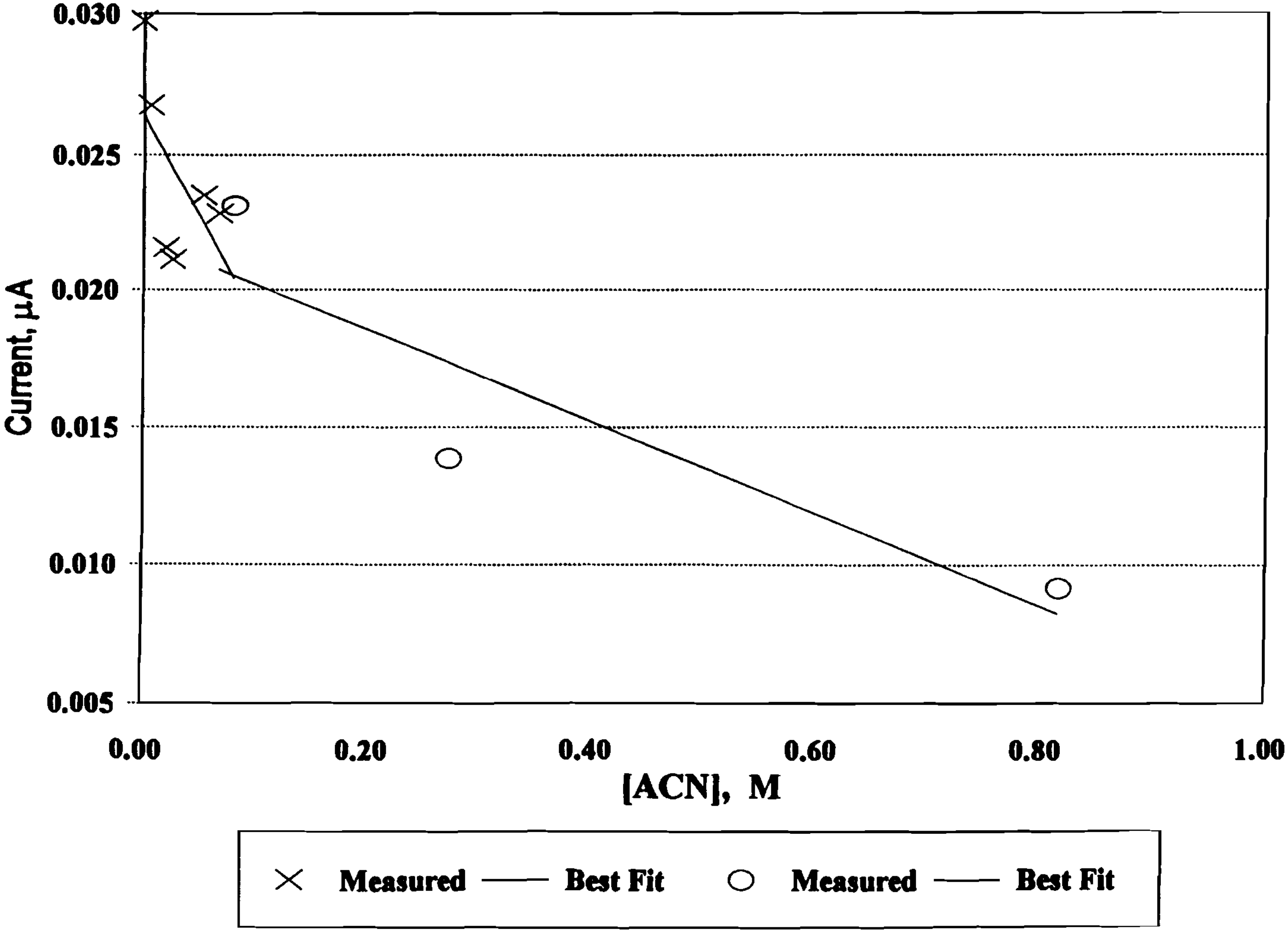
0.030
0.025
0.020
0.015
0.010
0.005
Current, µA
0.00
0.20
0.40
0.60
0.80
1.00
[ACN], M
× Measured
—— Best Fit
○ Measured
—— Best Fit

Figure 27

DME Polarogram of $Cd(NO_3)_2{\bullet}4H_2O$ at pH 5.00 without Organic Substrates

Current range	**: 0.5 μA**
Sweep rate	**: 10 mV/sec**
Scan range	**: from -0.200 to -1.200 V**
Record	**: 2.5 cm/min**
Knock timer	**: 1.0**
Temperature	**: 24.2 °C**
Conc. of $Cd(NO_3)_2{\bullet}4H_2O$	**: 1.1×10^{-3} M**

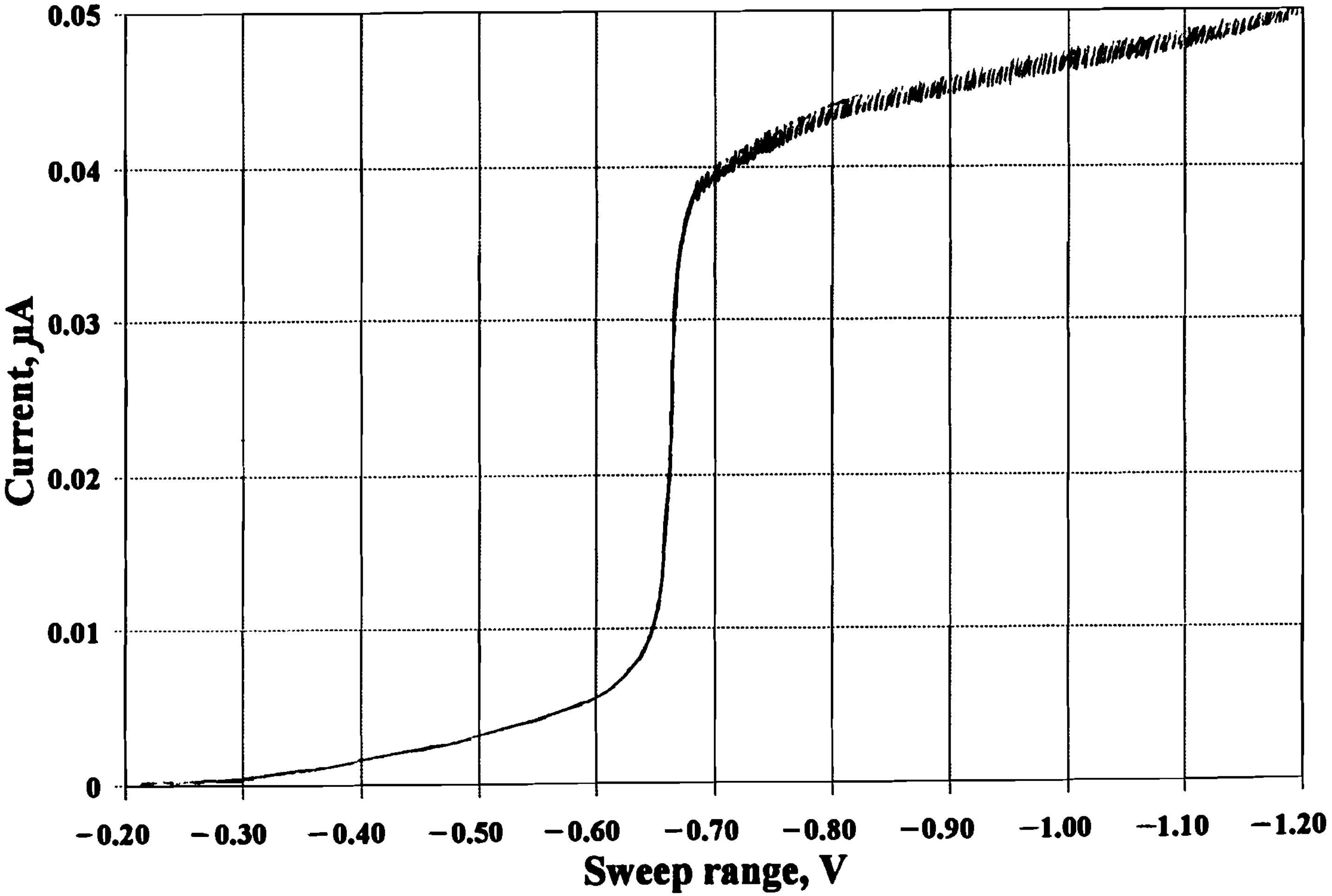
Current, µA
0.05
0.04
0.03
0.02
0.01
0
−0.20
−0.30
−0.40
−0.50
−0.60
−0.70
−0.80
−0.90
−1.00
−1.10
−1.20
Sweep range, V

Figure 28

The Peak Heights of $Cd(NO_3)\cdot 4H_2O$ at Constant Concentration 1.1×10^{-3} M Versus Various Concentrations of IPA

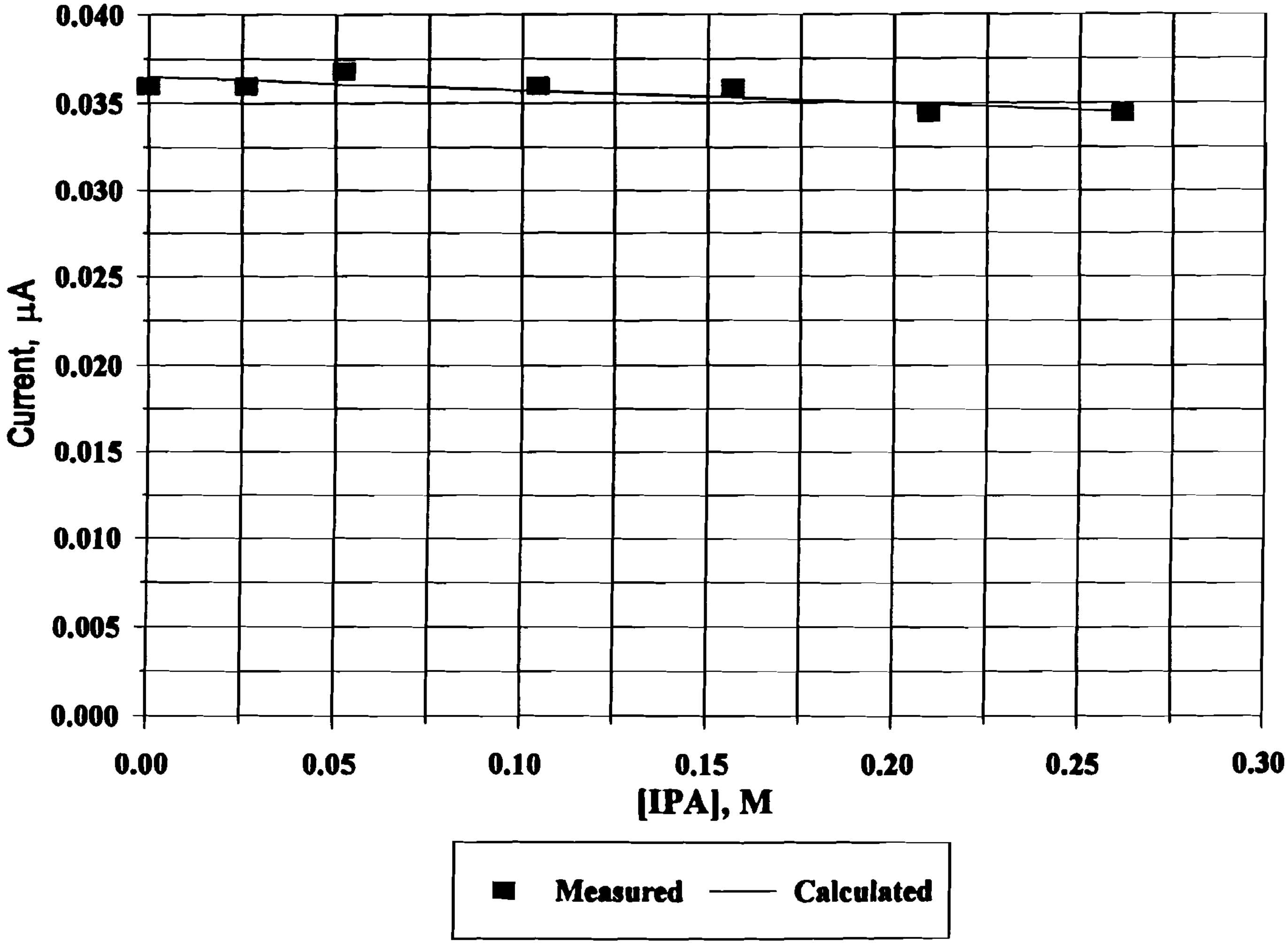
0.040
0.035
0.030
0.025
0.020
0.015
0.010
0.005
0.000
Current, µA
0.00
0.05
0.10
0.15
0.20
0.25
0.30
[IPA], M
Measured
Calculated

Figure 29

The Logarithm of First-peak Heights Versus the Logarithm of Concentrations of IPA

at Second Region with High Concentration of IPA and with Constant Concentration of 9.326 x 10^{-4} M $K_6[SiO_4W_{11}O_{30}CoO_6H_2]\cdot 15H_2O$

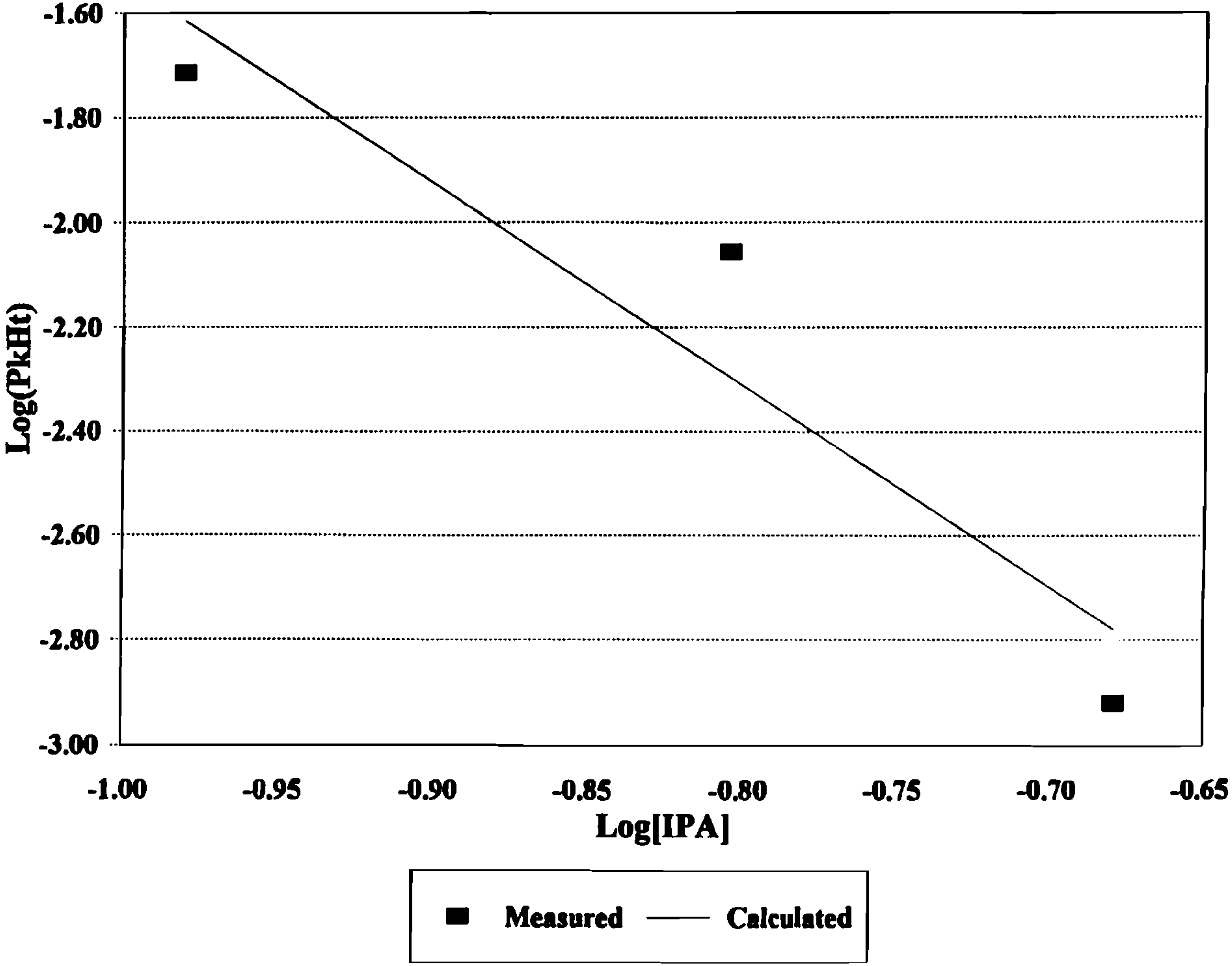
-1.60
-1.80
-2.00
-2.20
-2.40
-2.60
-2.80
-3.00
Log(PkHt)
-1.00
-0.95
-0.90
-0.85
-0.80
-0.75
-0.70
-0.65
Log[IPA]
■ Measured
—— Calculated

Figure 30

The Logarithm of First-peak Heights Versus the Logarithm of Concentrations of Acetone

at Second Region with High Concentration of Acetone and with Constant Concentration of 9.326 x 10^{-4} M $K_6[SiO_4W_{11}O_{30}CoO_6H_2]\cdot15H_2O$

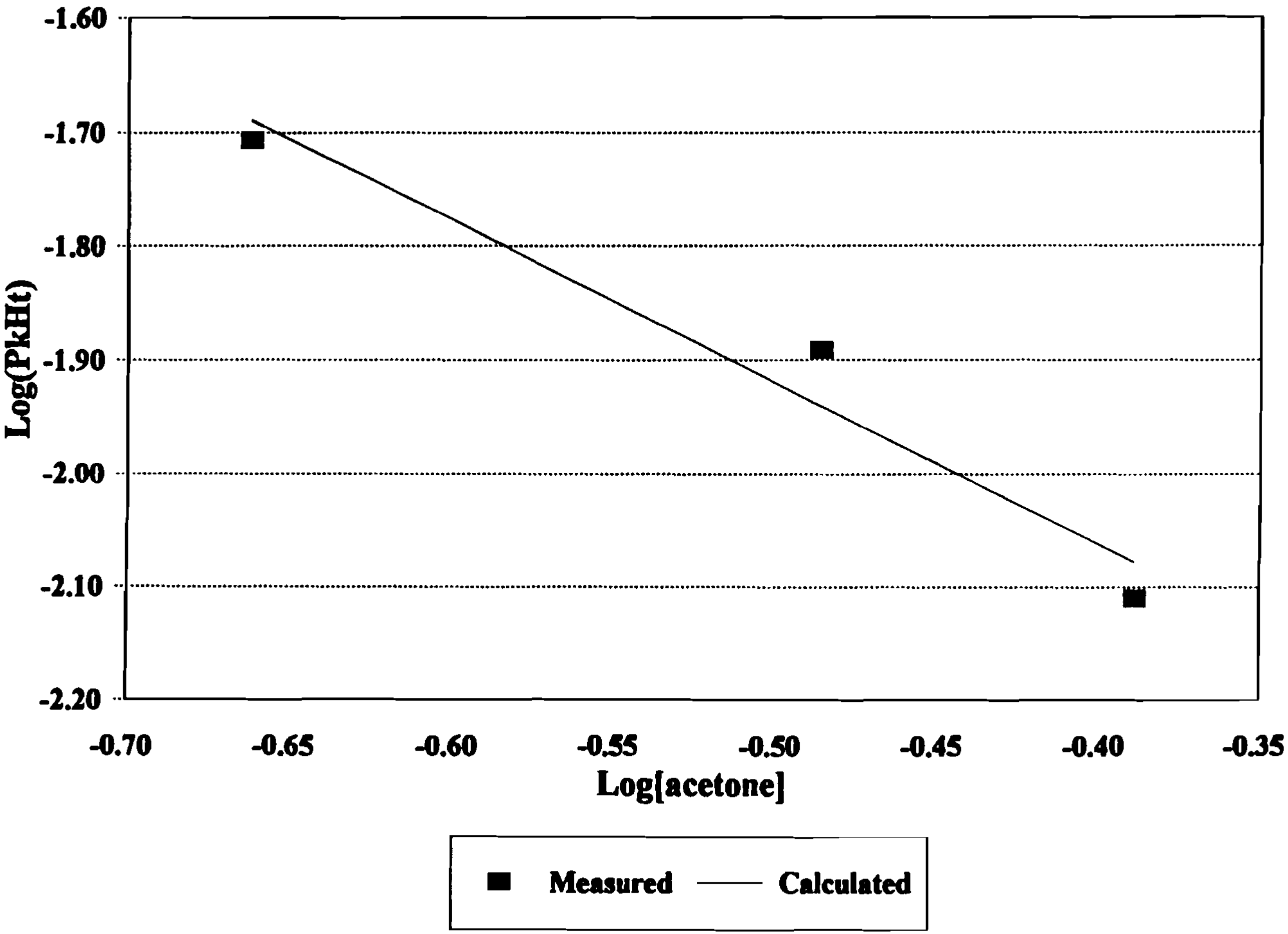
-1.60
-1.70
-1.80
-1.90
-2.00
-2.10
-2.20
Log(PkHt)
-0.70
-0.65
-0.60
-0.55
-0.50
-0.45
-0.40
-0.35
Log[acetone]
■ Measured
—— Calculated

Figure 31

The Logarithm of First-peak Heights Versus the Logarithm of Concentrations of ACN

at Second Region with High Concentration of ACN and with Constant Concentration of 9.326 x 10^{-4} M $K_6[SiO_4W_{11}O_{30}CoO_6H_2]\cdot15H_2O$

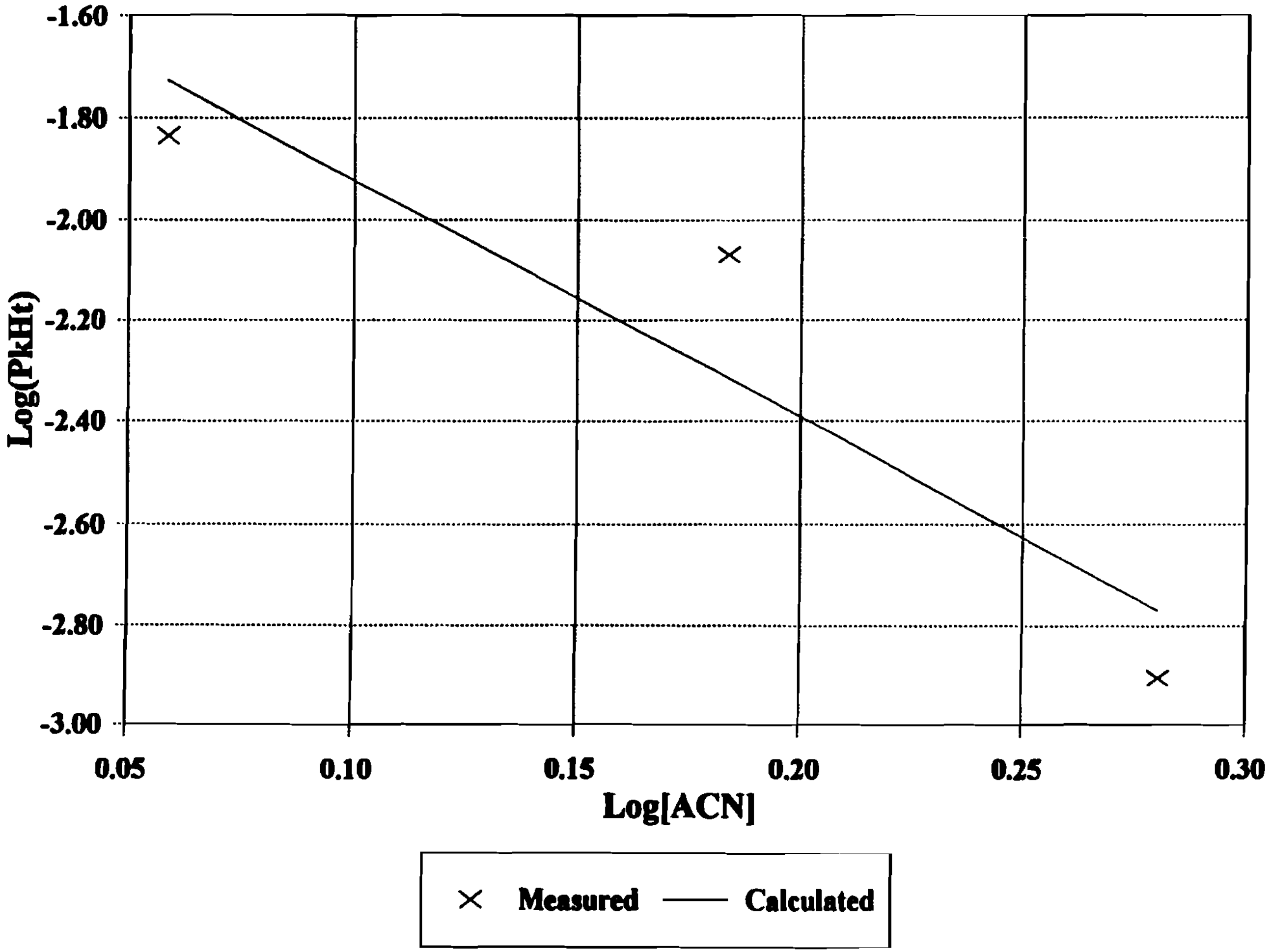
-1.60
-1.80
-2.00
-2.20
-2.40
-2.60
-2.80
-3.00
Log(PkHt)
0.05
0.10
0.15
0.20
0.25
0.30
Log[ACN]
Measured
Calculated

Figure 32

The Logarithm of First-peak Heights Versus the Logarithm of Concentrations of IPA

at Second Region with High Concentration of IPA and with Constant Concentration of 5.227 x 10^{-4} M $K_6[SiO_4W_{11}O_{30}CoO_6H_2]\cdot 15H_2O$

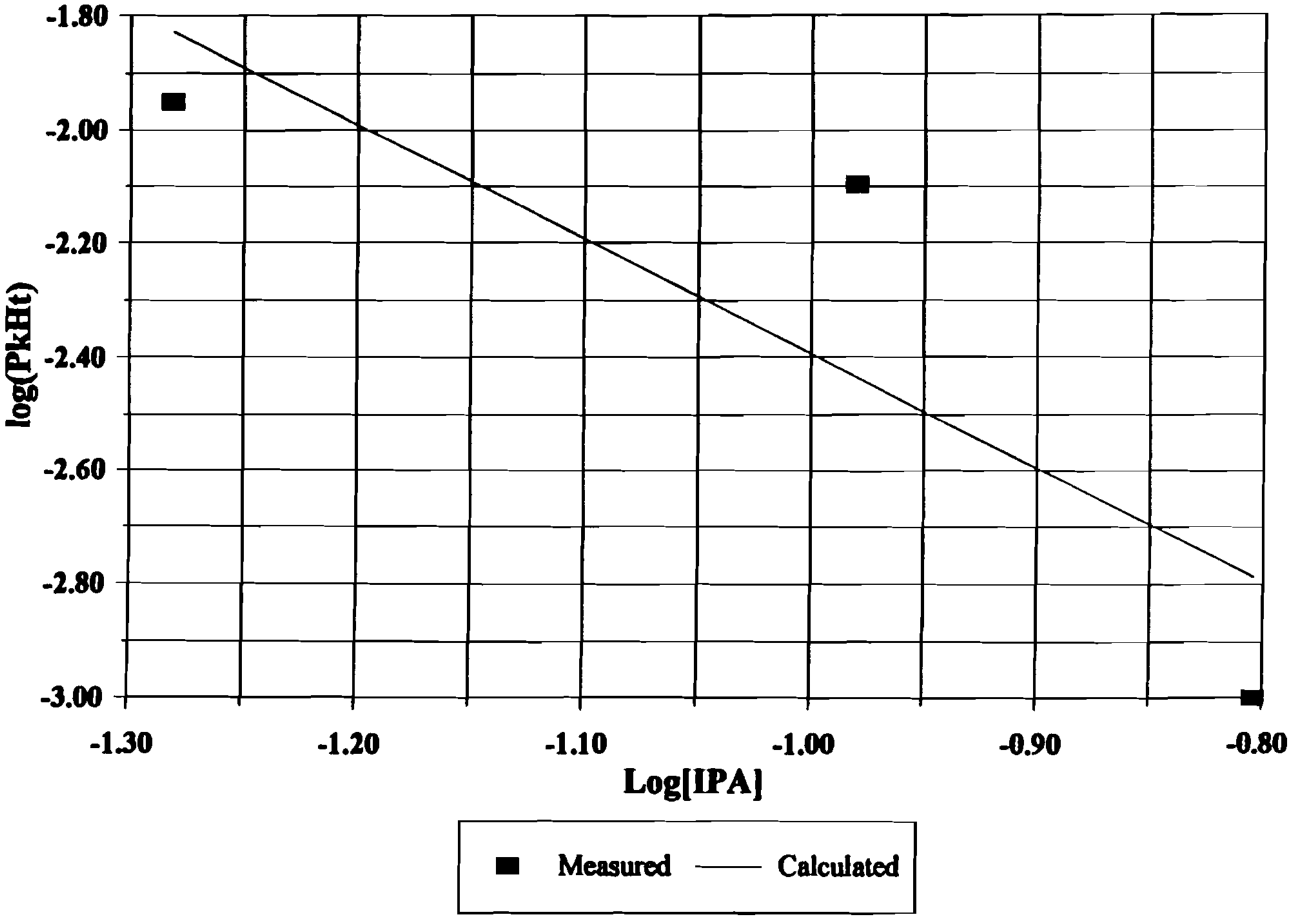
-1.80
-2.00
-2.20
-2.40
-2.60
-2.80
-3.00
log(PkHt)
-1.30
-1.20
-1.10
-1.00
-0.90
-0.80
Log[IPA]
Measured
Calculated

Figure 33

The Logarithm of First-peak Heights Versus the Logarithm of Concentrations of IPA

at Second Region with High Concentration of IPA and with Constant Concentration of 9.17 x 10^{-4} M $H_3[PW_{12}O_{40}]\cdot29H_2O$

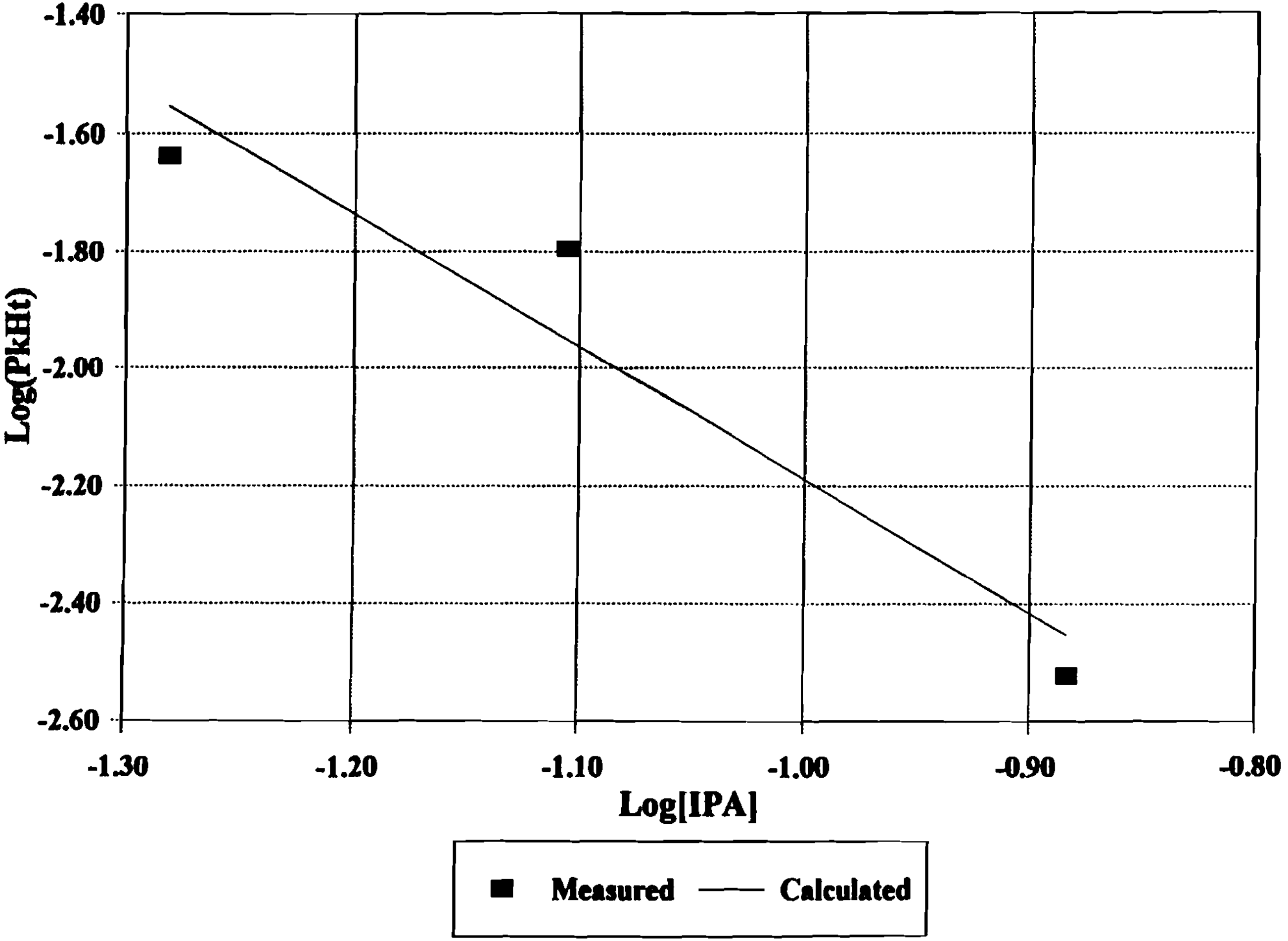
-1.40
-1.60
-1.80
-2.00
-2.20
-2.40
-2.60
Log(PkHt)
-1.30
-1.20
-1.10
-1.00
-0.90
-0.80
Log[IPA]
■ Measured
—— Calculated

Figure 34

The Logarithm of First-peak Heights Versus the Logarithm of Concentrations of Acetone

at Second Region with High Concentration of Acetone and with Constant Concentration of 9.17 x 10^{-4} M $H_3[PW_{12}O_{40}]\cdot 29H_2O$

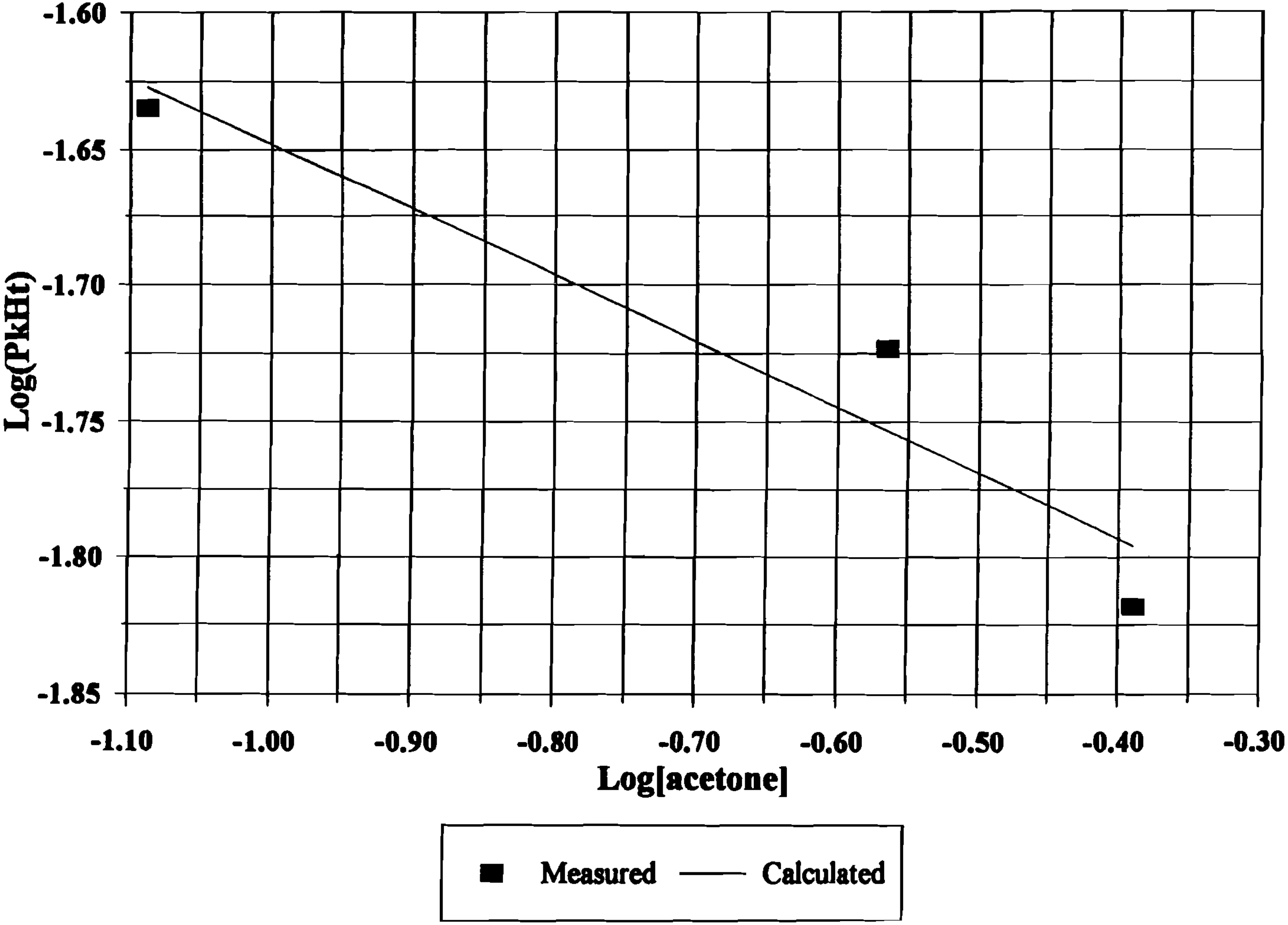
-1.60
-1.65
-1.70
-1.75
-1.80
-1.85
Log(PkHt)
-1.10
-1.00
-0.90
-0.80
-0.70
-0.60
-0.50
-0.40
-0.30
Log[acetone]
■ Measured
Calculated

Figure 35

The Logarithm of First-peak Heights Versus the Logarithm of Concentrations of ACN

at Second Region with High Concentration of ACN and with Constant Concentration of 9.17 x 10^{-4} M $H_3[PW_{12}O_{40}]\cdot 29H_2O$

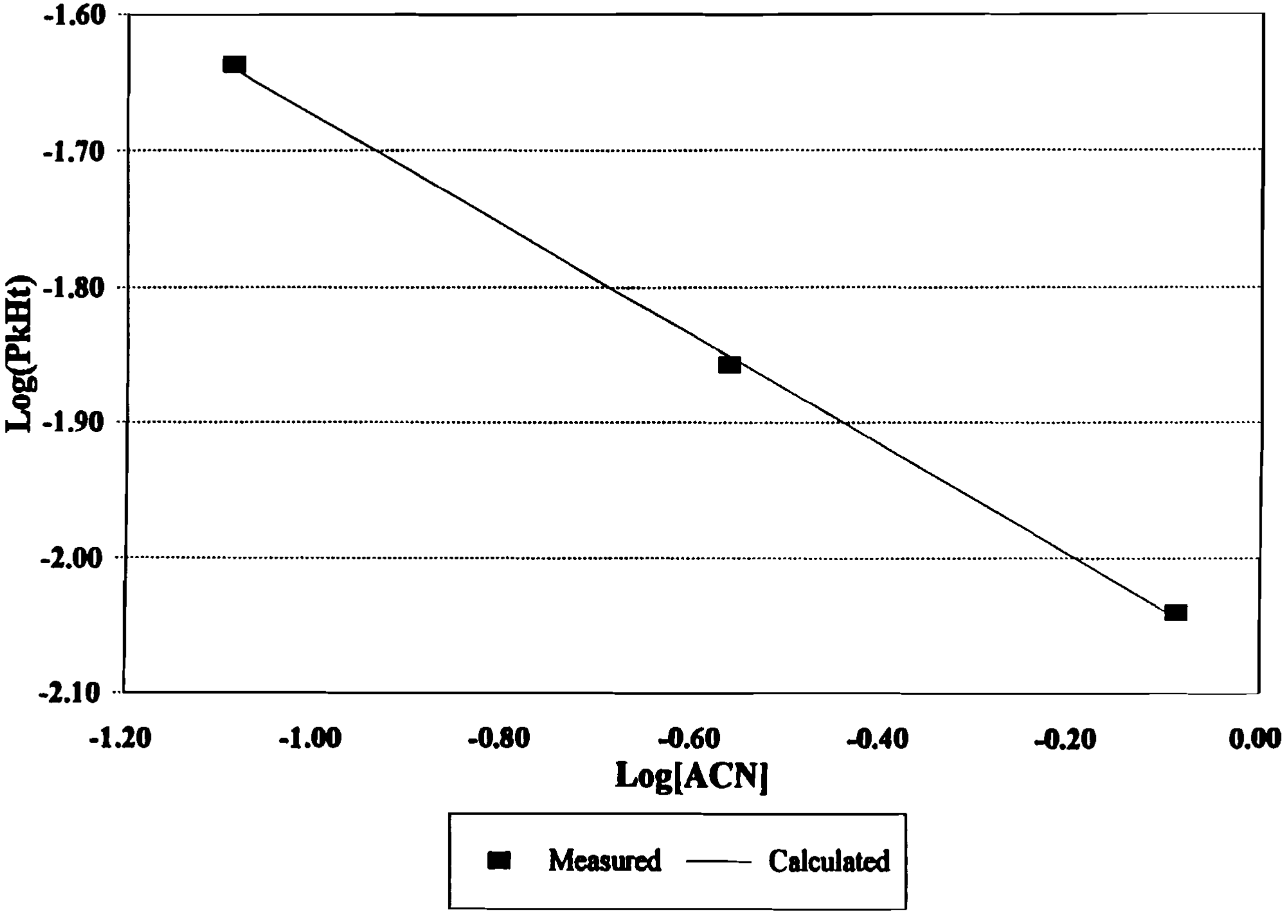
-1.60
-1.70
-1.80
-1.90
-2.00
-2.10
Log(PkHt)
-1.20
-1.00
-0.80
-0.60
-0.40
-0.20
0.00
Log[ACN]
■ Measured
—— Calculated

Figure 36

Best Fit in Peakfit Program

The Peak Heights of First-wave(μA) Versus Concentration of IPA (M) with Constant Concentration of 9.326 x 10^{-4} M $K_6[SiO_4W_{11}O_{30}CoO_6H_2]\cdot 15H_2O$

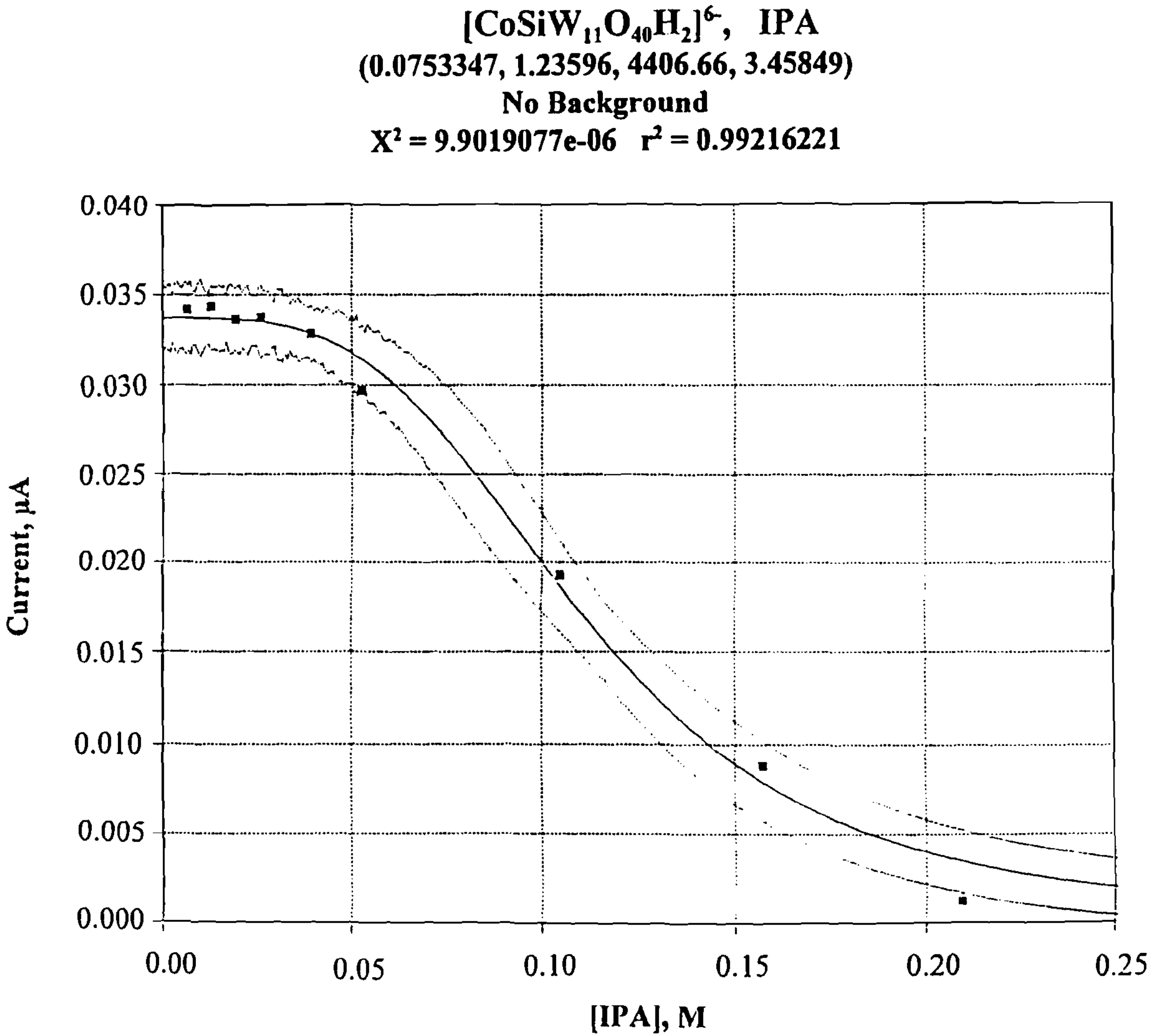
$[CoSiW_{11}O_{40}H_2]^{6-}$, IPA
(0.0753347, 1.23596, 4406.66, 3.45849)
No Background
$X^2 = 9.9019077e-06$ $r^2 = 0.99216221$
Current, µA
0.040
0.035
0.030
0.025
0.020
0.015
0.010
0.005
0.000
0.00
0.05
0.10
0.15
0.20
0.25
[IPA], M

Figure 37

Best Fit in Peakfit Program

The Peak Heights of First-wave(μA) Versus Concentration of Acetone (M) with Constant Concentration. of 9.326 x 10^{-4} M $K_6[SiO_4W_{11}O_{30}CoO_6H_2]\cdot15H_2O$

$[CoSiW_{11}O_{40}H_2]^{6-}$, Acetone

(0.0645916, 1.32387, 76.7126, 2.91813)

No Background

$X^2 = 2.1866075e\text{-}07$ $r^2 = 0.99946537$

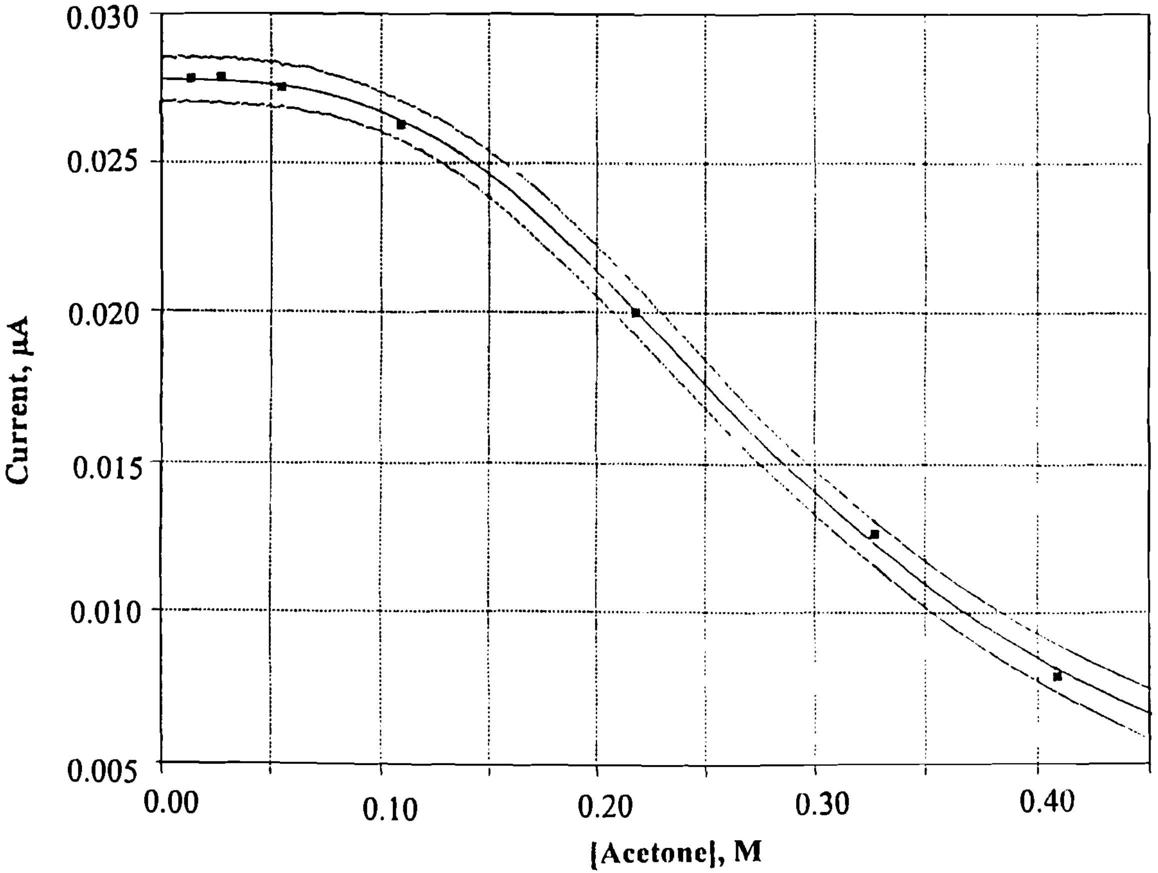

Figure 38

Best Fit in Peakfit Program

The Peak Heights of First-wave(μA) Versus Concentration of ACN (M) with Constant Concentration of 9.326 x 10^{-4} M $K_6[SiO_4W_{11}O_{30}CoO_6H_2]\cdot 15H_2O$

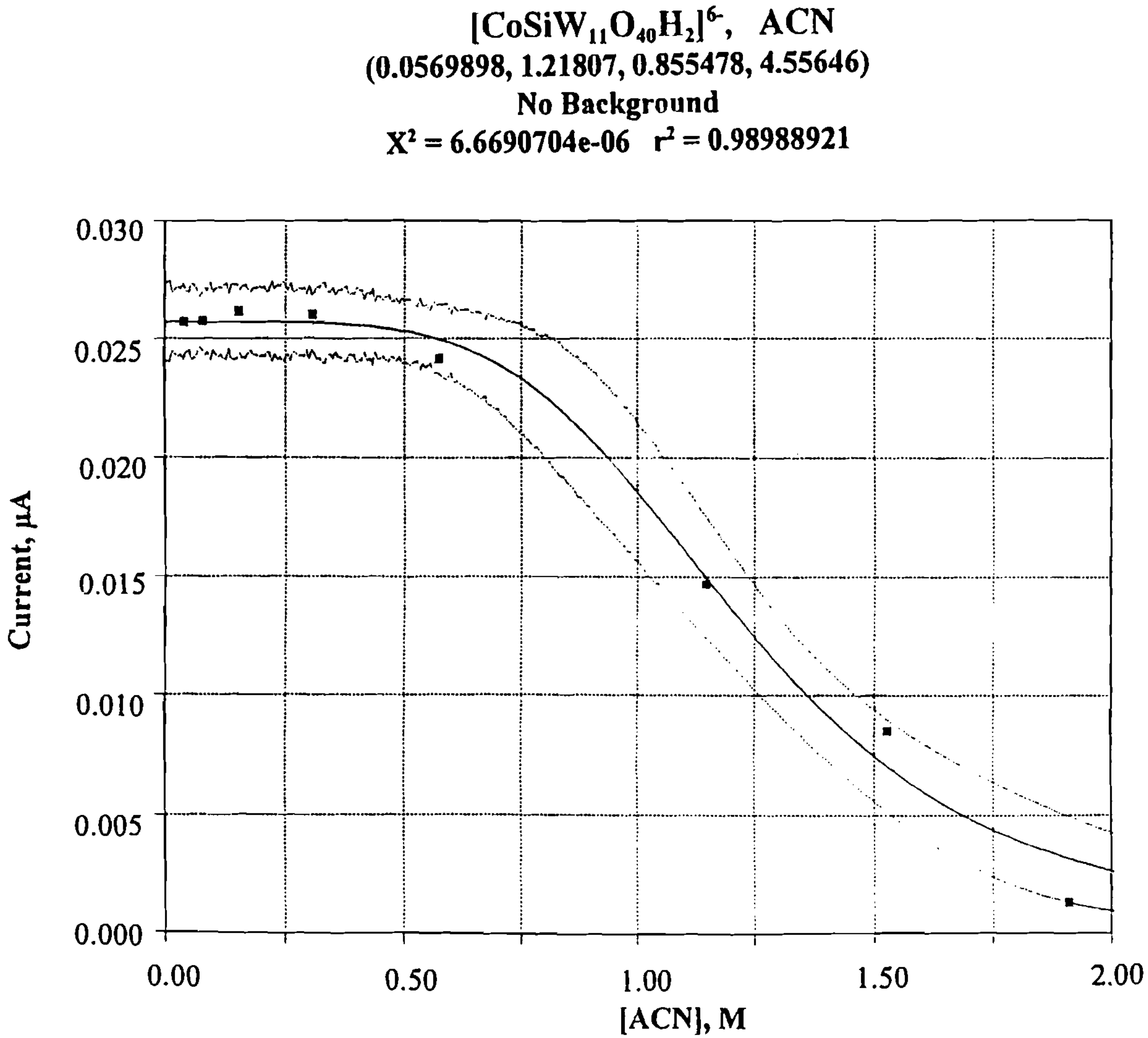
[CoSiW11O40H2]6-, ACN
(0.0569898, 1.21807, 0.855478, 4.55646)
No Background
X2 = 6.6690704e-06 r2 = 0.98988921
0.030
0.025
0.020
0.015
0.010
0.005
0.000
Current, µA
0.00
0.50
1.00
1.50
2.00
[ACN], M

Figure 39

Best Fit in Peakfit Program

The Peak Heights of First-wave(μA) Versus Concentration of IPA (M) with Constant Concentration of 5.227 x 10^{-4} M $K_6[SiO_4W_{11}O_{30}CoO_6H_2]\cdot 15H_2O$

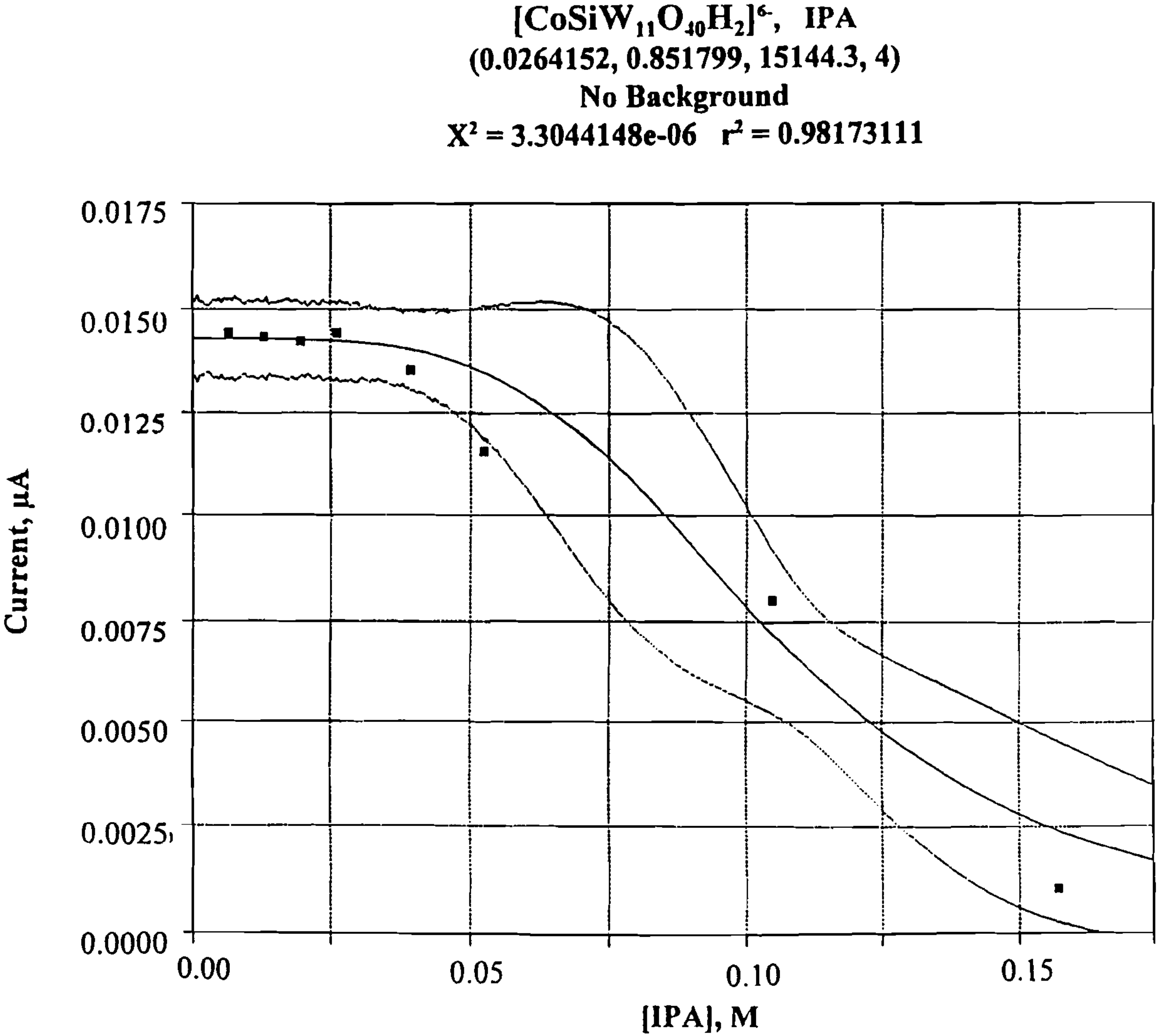
$[CoSiW_{11}O_{40}H_2]^{6-}$, IPA
(0.0264152, 0.851799, 15144.3, 4)
No Background
$X^2 = 3.3044148e-06$ $r^2 = 0.98173111$
Current, µA
0.0175
0.0150
0.0125
0.0100
0.0075
0.0050
0.0025
0.0000
0.00
0.05
0.10
0.15
[IPA], M

Figure 40

Best Fit in Peakfit Program

The Peak Heights of First-wave(μA) Versus Concentration of IPA (M) with Constant Concentration of 9.17 x 10^{-4} M $H_3[PW_{12}O_{40}]\cdot 29H_2O$

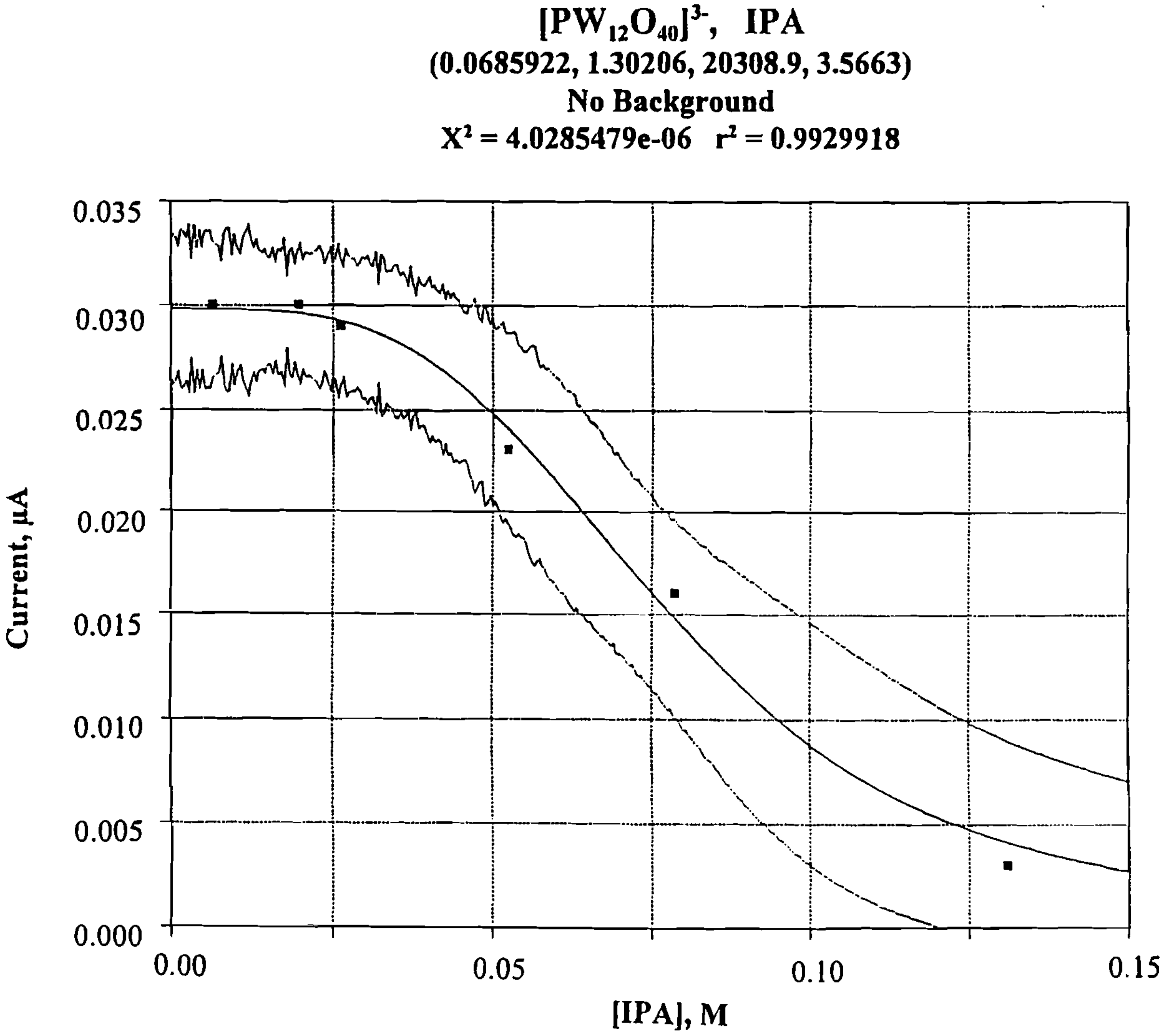

$[PW_{12}O_{40}]^{3-}$, IPA

(0.0685922, 1.30206, 20308.9, 3.5663)

No Background

$X^2 = 4.0285479e\text{-}06 \quad r^2 = 0.9929918$

Figure 41

Best Fit in Peakfit Program

The Peak Heights of First-wave(μA) Versus Concentration of Acetone (M) with Constant Concentration of 9.17 x 10^{-4} M $H_3[PW_{12}O_{40}]\cdot 29H_2O$

$PW_{12}O_{40}]^{3-}$, Acetone
(0.0523285, 1.17598, 6.45395, 1.82668)
No Background
X^2 = 4.3032749e-08 r^2 = 0.99937055

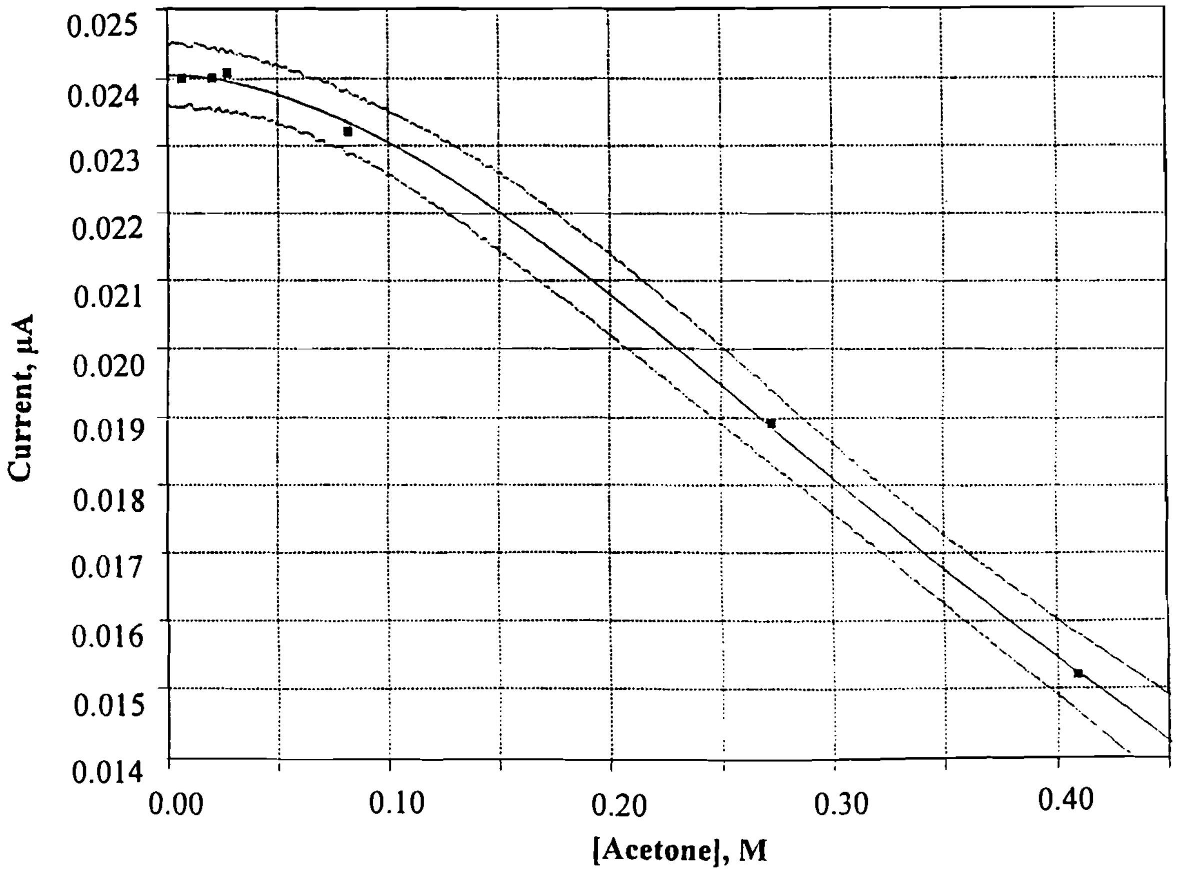

Figure 42

Best Fit in Peakfit Program

The Peak Heights of First-wave(μA) Versus Concentration
of ACN (M) with Constant Concentration
of 9.17 x 10^{-4} M $H_3[PW_{12}O_{40}]\cdot 29H_2O$

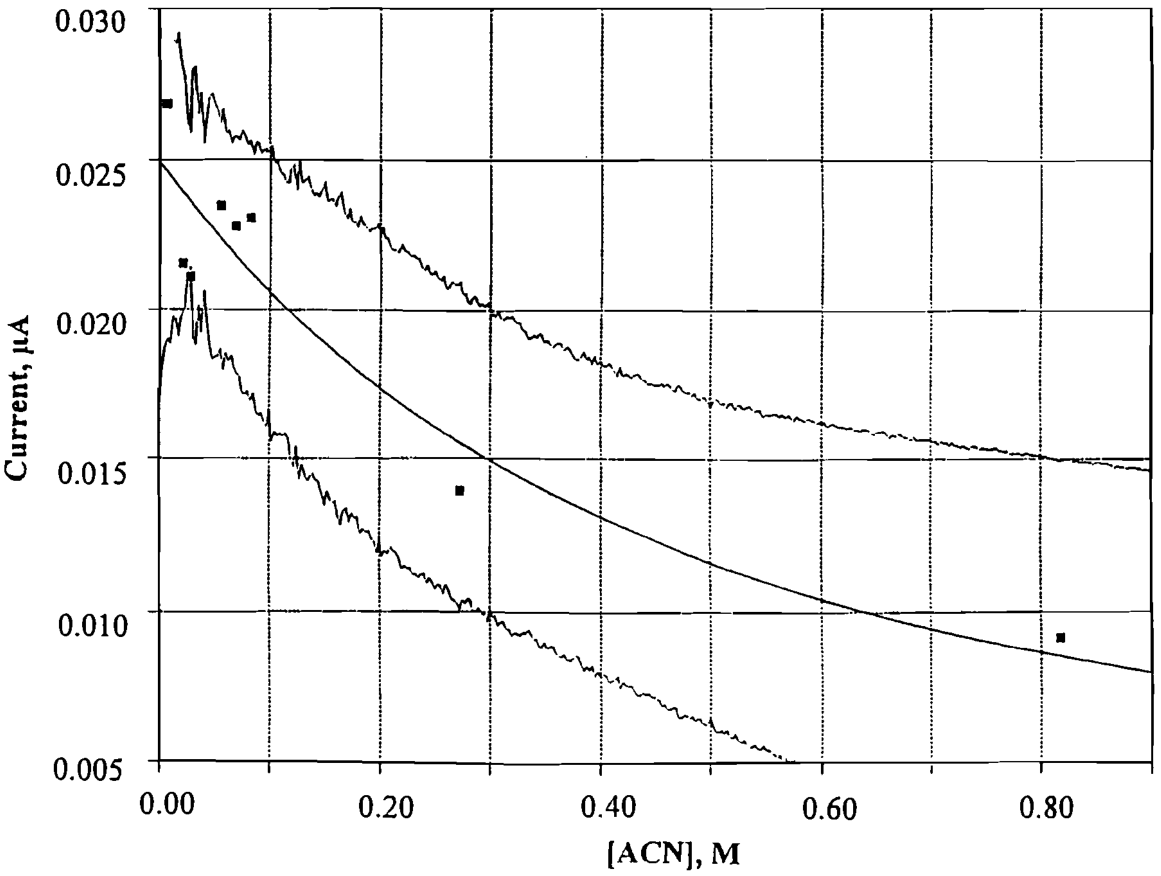

$PW_{12}O_{40}]^{3-}$, ACN

(0.0498839, 1.00323, 4.79732, 1.0566)

No Background

$X^2 = 2.5278714e-05$ $r^2 = 0.8923258$

Appendix B

Tables

Table I

Sixty-nine Elements of Heteroatoms or Central Atoms

1A	2A	3A	4A	5A	6A	7A	8A			1B	2B	3B	4B	5B	6B	7B
H																
Li[a]	Be											B	C			
Na	*Mg*											Al	Si	P	S	
K	*Ca*		Ti	V	Cr	Mn	Fe	Co	Ni	Cu	Zn	Ga	Ge	As	Se	
Rb	*Sr*	Y	Zr	Nb	Mo		*Ru*	Rh		*Ag*		In	Sn	Sb	Te	I
Cs	*Ba*	La	Hf	Ta	W	Re	*Os*		Pt			Tl	*Pb*	*Bi*		

Ce	Pr	Nd		Sm	Eu	Gd	*Tb*		Ho	Er		Yb
Th		U	Np	*Pu*	Am	*Cm*		*Cf*				

[a] Elements shown in italic type have been observed only as secondary heteroatoms.

Table II

Polarographic Half-wave Potentials of Molybdosilicate and -germanate Isomers

Anion	$E_{1/2}$[a] **(number of electron)**		
α - $SiMo_{12}$[b]	+ 0.25 (2)	+ 0.13 (2)	- 0.06 (2)
β - $SiMo_{12}$[b]	+ 0.35 (2)	+ 0.27 (2)	- 0.13 (2)
α - $GeMo_{12}$[c]	+ 0.36 (2)	+ 0.24 (2)	+ 0.06 (2)
β - $GeMo_{12}$[c]	+ 0.50 (2)	+ 0.40 (2)	0.00 (2)

[a] Rotating platinum electrode; vs. SCE.

[b] 0.5 M HCl, 50 % water-ethanol (Ref. Massart, R., Ann. Chim., 1968, 3, 507)

[c] 0.5 M aqueous HCl (Ref. Biquard, M; Souchay, P., Bull. Sco. Chim. France, 1971, 437.)

Table III

Aqueous-mixtures of Various Concentrations of IPA with 9.326 x 10^{-4} M $K_6[SiO_4W_{11}O_{30}CoO_6H_2]\cdot15H_2O$

Samples	0.1 M Buffer	IPA (mL)	HPC (g)	D.D. Water Filled up	pH	Temperature ^0C
1	45.00 mL	0	0.152	to mark	5.00	23.1
2	"	0.025	0.152	to mark	4.98	23.1
3	"	0.050	0.152	to mark	4.95	23.2
4	"	0.075	0.152	to mark	4.93	23.2
5	"	0.100	0.152	to mark	4.90	23.2
6	"	0.150	0.152	to mark	4.85	23.2
7	"	0.200	0.152	to mark	4.80	23.8
8	"	0.400	0.152	to mark	4.60	23.8
9	"	0.600	0.152	to mark	4.40	23.8
10	"	0.800	0.152	to mark	4.20	24.0

Table IV

Aqueous-mixtures of Various Concentrations of Acetone with 9.326 x 10^{-4} M $K_6[SiO_4W_{11}O_{30}CoO_6H_2]\cdot15H_2O$

Samples	0.1 M Buffer	Acetone (mL)	HPC (g)	D.D. Water Filled up	pH	Temperature °C
1	45.00 mL	0	0.152	to mark	5.00	25.0
2	"	0.050	0.152	to mark	4.99	25.0
3	"	0.100	0.152	to mark	4.99	25.0
4	"	0.200	0.152	to mark	4.98	25.0
5	"	0.400	0.152	to mark	4.80	25.0
6	"	0.800	0.152	to mark	4.90	25.0
7	"	1.200	0.152	to mark	4.97	25.0
8	"	1.500	0.152	to mark	5.00	25.0

Table V

Aqueous-mixtures of Various Concentrations of ACN with 9.326 x 10^{-4} M $K_6[SiO_4W_{11}O_{30}CoO_6H_2]\cdot15H_2O$

Samples	0.1 M Buffer	ACN (mL)	HPC (g)	D.D. Water Filled up	pH	Temperature ^0C
1	45.00 mL	0	0.152	to mark	4.92	25.7
2	"	0.100	0.152	to mark	4.95	26.0
3	"	0.200	0.152	to mark	4.97	26.0
4	"	0.400	0.152	to mark	5.01	26.0
5	"	0.800	0.152	to mark	5.02	26.0
6	"	1.500	0.152	to mark	5.04	26.0
7	"	3.00	0.152	to mark	5.08	26.0
8	"	4.00	0.152	to mark	5.11	26.0
9	"	5.00	0.152	to mark	5.15	26.1

Table VI

Aqueous-mixtures of Various Concentrations of IPA with 5.227 x 10^{-4} M $K_6[SiO_4W_{11}O_{30}CoO_6H_2]\cdot15H_2O$

Samples	0.1 M Buffer	IPA (mL)	HPC (g)	D.D. Water Filled up	pH	Temperature °C
1	45.00 mL	0	0.0852	to mark	4.87	24.5
2	"	0.025	0.0852	to mark	4.89	24.5
3	"	0.050	0.0852	to mark	4.87	24.5
4	"	0.075	0.0852	to mark	4.86	24.5
5	"	0.100	0.0852	to mark	4.85	24.7
6	"	0.150	0.0852	to mark	4.86	24.7
7	"	0.200	0.0852	to mark	4.86	24.7
8	"	0.400	0.0853	to mark	4.87	24.7
9	"	0.600	0.0852	to mark	4.87	24.7

Table VII

Aqueous-mixtures of Various Concentrations of IPA with 9.17 x 10^{-4} M $H_3[PW_{12}O_{40}]\cdot 29H_2O$

Samples	0.1 M Buffer	IPA (mL)	HPC (g)	D.D. Water Filled up	pH	Temperature ^{0}C
1	45.00 mL	0	0.156	to mark	4.80	24.8
2	"	0.025	0.156	to mark	4.85	25.0
3	"	0.075	0.156	to mark	4.84	25.0
4	"	0.100	0.156	to mark	4.86	25.0
5	"	0.200	0.156	to mark	4.85	25.0
6	"	0.300	0.156	to mark	4.87	25.0
7	"	0.500	0.156	to mark	4.83	25.0
8	"	0.700	0.156	to mark	4.84	25.0

Table VIII

Aqueous-mixtures of Various Concentrations of Acetone with 9.17 x 10^{-4} M $H_3[PW_{12}O_{40}]\cdot 29H_2O$

Samples	0.1 M Buffer	Acetone (mL)	HPC (g)	D.D . Water Filled up	pH	Temperature ^0C
1	45.00 mL	0	0.156	to mark	4.80	24.0
2	"	0.025	0.156	to mark	4.83	24.0
3	"	0.075	0.156	to mark	4.84	24.0
4	"	0.100	0.156	to mark	4.84	24.0
5	"	0.200	0.156	to mark	4.83	24.0
6	"	0.300	0.156	to mark	4.85	24.0
7	"	0.500	0.156	to mark	4.88	24.0
8	"	1.000	0.156	to mark	4.85	24.0
9	"	1.500	0.156	to mark	4.85	24.0

Table IX

Aqueous-mixtures of Various Concentrations of ACN with 9.17×10^{-4} M $H_3[PW_{12}O_{40}]\cdot 29H_2O$

Samples	0.1 M Buffer	ACN (mL)	HPC (g)	D.D. Water Filled up	pH	Temperature ^0C
1	45.00 mL	0	0.156	to mark	4.86	24.8
2	"	0.025	0.156	to mark	4.86	25.7
3	"	0.075	0.156	to mark	4.83	26.0
4	"	0.100	0.156	to mark	4.84	26.0
5	"	0.200	0.156	to mark	4.84	26.0
6	"	0.300	0.156	to mark	4.81	26.0
7	"	0.500	0.156	to mark	4.85	26.0
8	"	1.000	0.156	to mark	4.86	26.0
9	"	1.500	0.156	to mark	4.88	26.0
10	"	3.000	0.156	to mark	4.95	26.0

Table X

Aqueous-mixtures of Various Concentrations of IPA with Constant Concentration of 1.1 x 10^{-3} M $Cd(NO_3)_2 \cdot 4H_2O$

Samples	0.1 M Buffer	IPA (mL)	$Cd(NO_3)_2 \cdot 4H_2O$ (g)	D.D. Water Filled up	pH	Temperature ^0C
1	45.00 mL	0	0.0163	to mark	5.04	24.2
2	"	0.100	0.0162	to mark	5.00	24.2
3	"	0.200	0.0163	to mark	5.00	25.0
4	"	0.400	0.0163	to mark	5.00	25.0
5	"	0.600	0.0163	to mark	5.00	25.0
6	"	0.800	0.0163	to mark	5.00	25.0
7	"	1.000	0.0163	to mark	5.00	25.0
8	"	5.000	0.0163	to mark	5.05	25.0

Table XI

The Reduction Current and Half-wave Potential of $Cd(NO_3)_2•4H_2O$ upon Addition of Various Concentration of IPA

Samples	0.1 M Buffer	IPA (mL)	$Cd(NO_3) \cdot 4H_2O$ (M)	Current μA	$E_{1/2}$ (mV)	Temperature ^0C
1	45.00 mL	0	0.00106	0.0360	-0.645	24.2
2	"	0.100	0.00106	0.0360	-0.645	24.2
3	"	0.200	0.00106	0.0368	-0.645	25.0
4	"	0.400	0.00106	0.0360	-0.645	25.0
5	"	0.600	0.00106	0.0359	-0.645	25.0
6	"	0.800	0.00106	0.0344	-0.645	25.0
7	"	1.000	0.00106	0.0344	-0.645	25.0
8	"	5.000	0.00106	—	-0.645	25.0

Table XII

Regression Results in Quattro Pro Program

From the Peak Heights of First-wave (μA) Versus Concentration of IPA (M) with Constant Concentration of 9.326 x 10^{-4} M $K_6[SiO_4W_{11}O_{30}CoO_6H_2]\cdot15H_2O$

IPA (mL)	IPA (M)	Peak Height Measured (µA)		Peak Height Calculated(µA)	
0.000	0.0000	0.0330		0.0336	
0.025	0.0065	0.0342		0.0337	
0.050	0.0131	0.0343		0.0338	
0.075	0.0196	0.0336		0.0338	
0.100	0.0262	0.0337		0.0339	
0.150	0.0393		0.0328		0.0321
0.200	0.0524		0.0296		0.0296
0.400	0.1047		0.0193		0.0198
0.600	0.1571		0.0088		0.0100
0.800	0.2094		0.0012		0.0002

At low concentration of IPA

Regression Output:		
Constant		0.03359
Std Err of Y Est		0.00058
R Squared		0.0591
No. of Observations		5
Degrees of Freedom		3
X Coefficient(s)	0.01222	
Std Err of Coef.	0.02816	

At high concentration of IPA

Regression Output:		
Constant		0.03947
Std Err of Y Est		0.00104
R Squared		0.99548
No. of Observations		5
Degrees of Freedom		3
X Coefficient(s)	-0.1876	
Std Err of Coef.	0.0073	

Intersection point 0.0294 (M)

Table XIII

Regression Results in Quattro Pro Program

From the Peak Heights of First-wave (µA) Versus Concentration of Acetone (M) with Constant Concentration of 9.326 x 10^{-4} M $K_6[SiO_4W_{11}O_{30}CoO_6H_2]\cdot15H_2O$

Acetone (mL)	Acetone (M)	Peak Height Measured (µA)	Peak Height Calculated(µA)
0.000	0.0000	0.02736	0.02762
0.050	0.0136	0.02784	0.02764
0.100	0.0272	0.02788	0.02767
0.200	0.0545	0.02756	0.02772
0.400	0.1090	0.02632	0.02645
0.800	0.2179	0.01996	0.01965
1.200	0.3269	0.01260	0.01286
1.500	0.4086	0.00784	0.00776

At low concentration of acetone

Regression Output:

Constant	0.02762
Std Err of Y Est	0.00030
R Squared	0.03059
No. of Observations	4
Degrees of Freedom	2
X Coefficient(s)	0.00185
Std Err of Coef.	0.00735

At high concentration of acetone

Regression Output:

Constant	0.03324
Std Err of Y Est	0.00030
R Squared	0.99908
No. of Observations	4
Degrees of Freedom	2
X Coefficient(s)	-0.0623
Std Err of Coef.	0.00134

Intersection point 0.0876 (M)

Table XIV

Regression Results in Quattro Pro Program

From the Peak Heights of First-wave (μA) Versus Concentration of ACN (M) with Constant Concentration of 9.326 x 10^{-4} M $K_6[SiO_4W_{11}O_{30}CoO_6H_2]\cdot 15H_2O$

ACN (mL)	ACN (M)	Peak Height Measured (μA)	Peak Height Calculated(μA)
0.000	0.0000	0.0257	0.0257
0.100	0.0382	0.0257	0.0258
0.200	0.0763	0.0257	0.0258
0.400	0.1526	0.0261	0.0259
0.800	0.3052	0.0260	0.0261
1.500	0.5723	0.0241	0.0243
3.000	1.1447	0.0147	0.0146
4.000	1.5262	0.0085	0.0081
5.000	1.9078	0.0012	0.0016

At low concentration of ACN

Regression Output:	
Constant	0.02571
Std Err of Y Est	0.00015
R Squared	0.55896
No. of Observations	5
Degrees of Freedom	3
X Coefficient(s)	0.00123
Std Err of Coef.	0.00063

At high concentration of ACN

Regression Output:	
Constant	0.03404
Std Err of Y Est	0.00043
R Squared	0.99871
No. of Observations	4
Degrees of Freedom	2
X Coefficient(s)	-0.017
Std Err of Coef.	0.00043

Intersection point 0.45683 (M)

Table XV

Regression Results in Quattro Pro Program

From the Peak Heights of First-wave (µA) Versus Concentration of IPA (M) with Constant Concentration of 5.227 x 10^{-4} M $K_6[SiO_4W_{11}O_{30}CoO_6H_2]\cdot 15H_2O$

IPA (mL)	IPA (M)	Peak Height Measured (μA)	Peak Height Calculated(μA)
0.000	0.0000	0.0144	0.0144
0.025	0.0065	0.0144	0.0144
0.050	0.0131	0.0143	0.0143
0.075	0.0196	0.0136	0.0137
0.100	0.0262	0.0128	0.0132
0.150	0.0393	0.0116	0.0120
0.200	0.0524	0.0112	0.0109
0.400	0.1047	0.0080	0.0064
0.600	0.1571	0.0010	0.0020

At low concentration of IPA

Regression Output:

Constant	0.01442
Std Err of Y Est	0.00004
R Squared	0.75000
No. of Observations	3
Degrees of Freedom	1
X Coefficient(s)	-0.0076
Std Err of Coef.	0.00441

At high concentration of IPA

Regression Output:

Constant	0.01539
Std Err of Y Est	0.00097
R Squared	0.96549
No. of Observations	6
Degrees of Freedom	4
X Coefficient(s)	-0.0855
Std Err of Coef.	0.00808

Intersection point 0.01249 (M)

Table XVI

Regression Results in Quattro Pro Program

From the Peak Heights of First-wave (μA) Versus Concentration of IPA (M) with Constant Concentration of 9.17×10^{-4} M $H_3[PW_{12}O_{40}]\cdot29H_2O$

IPA (mL)	IPA (M)	Peak Height Measured (μA)	Peak Height Calculated(μA)
0.000	0.000	0.030	0.030
0.025	0.007	0.030	0.030
0.075	0.020	0.030	0.030
0.100	0.026	0.029	0.029
0.200	0.052	0.023	0.023
0.300	0.079	0.016	0.016
0.500	0.131	0.003	0.003

At low concentration of IPA

Regression Output:

Constant	0.03015
Std Err of Y Est	0.00042
R Squared	0.53333
No. of Observations	4
Degrees of Freedom	2

X Coefficient(s)	-0.0306
Std Err of Coef.	0.02021

At high concentration of IPA

Regression Output:

Constant	0.03614
Std Err of Y Est	0.00027
R Squared	0.99965
No. of Observations	3
Degrees of Freedom	1

X Coefficient(s)	-0.2537
Std Err of Coef.	0.00473

Intersection point 0.02685 (M)

Table XVII

Regression Results in Quattro Pro Program

From the Peak Heights of First-wave (μA) Versus Concentration of Acetone (M) with Constant Concentration of 9.17 x 10^{-4} M $H_3[PW_{12}O_{40}]\cdot29H_2O$

Acetone (mL)	Acetone (M)	Peak Height Measured (μA)	Peak Height Calculated(μA)
0.000	0.00000	0.0242	0.02412
0.025	0.00681	0.0240	0.02409
0.075	0.02043	0.0240	0.02405
0.100	0.02724	0.0241	0.02402
0.300	0.08172	0.02320	0.02331
1.000	0.27241	0.01892	0.01866
1.500	0.40862	0.01520	0.01535

At low concentration of acetone

Regression Output:	
Constant	0.02412
Std Err of Y Est	0.00010
R Squared	0.21493
No. of Observations	4
Degrees of Freedom	2
X Coefficient(s)	-0.0035
Std Err of Coef.	0.00476

At high concentration of acetone

Regression Output:	
Constant	0.02530
Std Err of Y Est	0.00031
R Squared	0.99692
No. of Observations	3
Degrees of Freedom	1
X Coefficient(s)	-0.0243
Std Err of Coef.	0.00135

Intersection point 0.05657 (M)

Table XVIII

Regression Results in Quattro Pro Program

From the Peak Heights of First-wave (μA) Versus Concentration of ACN (M) with Constant Concentration of 9.17 x 10^{-4} M $H_3[PW_{12}O_{40}]\cdot 29H_2O$

ACN (mL)	ACN (M)	Peak Height Measured (μA)	Peak Height Calculated(μA)
0.000	0.000	0.030	0.026
0.025	0.007	0.027	0.026
0.075	0.020	0.022	0.025
0.100	0.027	0.021	0.024
0.200	0.054	0.023	0.022
0.250	0.068	0.023	0.021
0.300	0.082	0.023	0.021
1.000	0.272	0.014	0.017
3.000	0.817	0.009	0.008

At low concentration of ACN		At high concentration of ACN	
Regression Output:		Regression Output:	
Constant	0.026	Constant	0.022
Std Err of Y Est	0.003	Std Err of Y Est	0.004
R Squared	0.344	R Squared	0.809
No. of Observations	6.000	No. of Observations	3.000
Degrees of Freedom	4.000	Degrees of Freedom	1.000
X Coefficient(s)	-0.074	X Coefficient(s)	-0.017
Std Err of Coef.	0.051	Std Err of Coef.	0.008

Intersection point 0.080 (M)

Table XIX

The Results of Surface Area

For Surface Area of Keggin anion, IPA, Acetone, and ACN; and the Ratio of Total Surface Area of HPC to Total Surface Area of Organic Substrates

Substrate	Surface area $Å^2$	Total Surface in solution* x 10^{-21} $Å^2$	The total surface ratio of HPC to organic substrate at threshold values in solution
$[CoSiW_{11}O_{40}H_2]^{6-}$ $9.3 \times 10^{4-}$ M	394.1	11.04	
IPA	4.564	4.041	2.7
acetone	3.646	9.018	1.2
ACN	2.322 (1.397)	31.93 (19.21)	0.3 (0.6)
$[CoSiW_{11}O_{40}H_2]^{6-}$ $5.2 \times 10^{4-}$ M	375.8	5.916	
IPA	4.564	1.716	3.5
$[PW_{12}O_{40}]^{3-}$ $9.2\times 10^{4-}$ M	375.8	10.41	
IPA	4.564	3.691	2.8
acetone	3.646	6.203	1.7
ACN	2.322 (1.397)	5.594 (3.366)	1.9 (3.1)

* Total surface in solution is (Concentration)(Volume)(Surface area per molecule)(Avogadro #)

Table XX

Quattro Pro Results

Data of Parameters k, K_c and q

HPC	Substrate	k	K_c	q
$[CoSiW_{11}O_{40}H_2]^{6-}$				
$9.3 \times 10^{4-}$ M	IPA	35	8.4×10^3	3.9
	acetone	29	1.2×10^1	1.4
	ACN	28	7.3×10^{-1}	4.7
$5.2 \times 10^{4-}$ M	IPA	28	3.7×10^2	2.0
$[PW_{12}O_{40}]^{3-}$				
$9.2 \times 10^{4-}$ M	IPA	33	8.6×10^2	2.3
	acetone	26	1.9	0.2
	ACN	33	3.6	0.4

Table XXI

Peakfit Results

Data of Parameters k, K_R, K_c and q

HPC	Substrate	k	K_R	K_c	q
$[CoSiW_{11}O_{40}H_2]^{6-}$					
$9.3 \times 10^{4-}$ M	IPA	81	1.24	4.4×10^3	3.5
	acetone	69	1.32	7.7×10^1	2.9
	ACN	61	1.22	8.6×10^{-1}	4.6
$5.2 \times 10^{4-}$ M	IPA	50	0.85	1.5×10^4	4.0
$[PW_{12}O_{40}]^{3-}$					
$9.2 \times 10^{4-}$ M	IPA	74	1.30	2.0×10^4	3.6
	acetone	56	1.18	6.5	1.8
	ACN	54	1.00	4.8	1.1

Table XXII

Comparison of Parameters

Quattro Pro and Peakfit Results

HPC	Substrate		k	K_R	K_C	q
$[CoSiW_{11}O_{40}H_2]^{6-}$						
$9.3 \times 10^{4-}$ M	IPA	a *	81	1.24	4.4×10^3	3.5
		b**	35		8.4×10^3	3.9
	acetone	a	69	1.32	7.7×10^1	2.9
		b	29		1.2×10^1	1.4
	ACN	a	61	1.22	8.6×10^{-1}	4.6
		b	28		7.3×10^{-1}	4.7
$5.2 \times 10^{4-}$ M	IPA	a	50	0.85	1.5×10^4	4.0
		b	28		3.7×10^2	2.0
$[PW_{12}O_{40}]^{3-}$						
$9.2 \times 10^{4-}$ M	IPA	a	74	1.30	2.0×10^4	3.6
		b	33		8.6×10^2	2.3
	acetone	a	56	1.18	6.5	1.8
		b	26		1.9	0.2
	ACN	a	54	1.00	4.8	1.1
		b	33		3.6	0.4

* Peakfit results in "a" columns

** Quattro Pro results in "b" columns

I, Dinghan Lou, hereby submit this thesis to Emporia State University as partial fulfillment of the requirements for an advanced degree. I agree that the Library of the University may make it available for use in accordance with its regulations governing materials of this type. I further agree that quoting, photocopying, or other reproduction of this document is allowed for private study, scholarship (including teaching) and research purposes of a nonprofit nature. No copying which involves potential financial gain will be allowed without written permission of the author.

Signature of Author

12/15/95

Date

Polarographic Reduction of Aqueous-Isopropyl Alcohol Heteropolytungstate Mixtures

Title of Thesis

Signature of Graduate Office Staff Member

12-15-95

Date Received